UNIVERSITY OF SOUTHAMPTON

FACULTY OF PHYSICAL SCIENCES AND ENGINEERING

Electronics and Computer Science

Surface Electrode Array-based Electrical Stimulation and Iterative Learning Control for Hand Rehabilitation

by

Anna Soska

A thesis submitted in partial fulfillment
for the degree of Doctor of Philosophy

Supervisors: Professor Eric Rogers and Doctor Christopher Freeman

December 16, 2014

DECLARATION OF AUTHORSHIP

I, Anna Soska, declare the thesis entitled

Surface Electrode Array-based Stimulation and Iterative Learning Control for Hand Restoration after Stroke

and the work presented in the thesis are both my own, and have been generated by me as the result of my own original research. I confirm that:

- This work was done wholly or mainly when in candidature for research degree at the University of Southampton;
- Where any part of this thesis has previously been submitted for a degree or any other qualification at this University or any other institution, this has been clearly stated;
- Where I have consulted the published work of others, this is always clearly attributed;
- Where I have quoted from the work of others, the source is always given. With the exception of such quotations, this thesis is entirely my own work;
- I have acknowledged all main sources of help;
- Where the thesis is based on work done by myself jointly with others, I have made clear exactly what was done by others and what I have contributed myself;
- Parts of this work have been published as:
    - Soska A., Freeman C., Exell T. and Rogers E. (2013) Surface Electrode Array-based Control of the Wrist and Hand. In, IFAC International Workshop on Adaptation and Learning in Control and Signal Processing, Cean, France, 2013, 164-169
    - Exell, T., Freeman, C.T., Meadmore, K. L., Hughes, A.M., Hallewell, E. and Burridge, J.H. (2013) Optimisation of Hand Posture Stimulation Using an Electrode Array and Iterative Learning Control. *Journal of Automatic Control*, 21, (1), 1-5.
    - Soska A., Freeman C. and Rogers E. (2012) ILC for FES-based Stroke Rehabilitation of Hand and Wrist. In, IEEE Multiconference on Systems and Control (MSC 2012), Dubrovnik, Croatia, 2012, 1267-1272

UNIVERSITY OF SOUTHAMPTON

ABSTRACT

FACULTY OF PHYSICAL SCIENCES AND ENGINEERING
Electronics and Computer Science

A thesis submitted in partial fulfillment for the degree of Doctor of Philosophy

SURFACE ELECTRODE ARRAY-BASED ELECTRICAL STIMULATION AND ITERATIVE LEARNING CONTROL FOR HAND REHABILITATION

by Anna Soska

This thesis addresses the use of surface electrode arrays to regulate the stimulation applied to the hand and wrist muscles in order to induce hand movement to desired posture. Electrode array-based electric stimulation is a relatively novel and promising rehabilitation technology, due to its potential to deliver selective stimulation signal to underlying muscles via chosen elements of the arrays. A general control strategy developed in this thesis embeds optimisation methods for selection of appropriate elements of the electrode array with iterative learning control.

In iterative learning control, the patient makes repeated attempts to complete a predefined task with the aim of gradually decreasing the error between the movement performed and desired one. A number of different gradient-based methods, such as penalty method and sparse optimisation methods has been developed based on theoretical and experimental findings. These methods are used to find a sparse input vector, which is employed to select only those array elements that are critical to task completion within iterative learning control framework. Experimental results using multi-channel stimulation and 40 element surface electrode array confirm accurate tracking of selected hand postures.

Based on the experimental results and the existing literature, a new system for the hand and wrist restoration has been designed. The key element of the system is a game-based task oriented training environment designed for a wide group of patients, including patients with spasticity and hemiplegia.

Contents

Nomenclature

Ab	Abduction
Ad	Adduction Movement
ANN	The Artificial Neural Network
APB	the Abductor Pollicis Brevis
APL	Abductor Pollicis Longus
BMT	Bilateral Movement Therapy
C	The Cervical Level of spinal cord
CIMT	Constrained Induced Movement Therapy
CMC	The Carpometacarpal joint
CVA	Cerebro Vascular Accident
DIP	The Distal Interphalangeal joint
DOF	Degrees of freedom
EC	Extensor Digitorum Communis
ECR	Extensor Carpi Radialis
ECU	Extensor Carpi Ulnaris
EDM	Extensor Digiti Minimi
EI	Extensor Indicis
EMG	Electromyographic
EPB	Extensor Pollicis Brevis
EPL	Extensor Pollicis Longus
F/E	Flexion/Extension Movement

FDM Flexor Digiti Minimi

FDP Flexor Digitorum Profundus

FDS Flexor Digitorum Superficialis

FES Functional Electrical Stimulation

FPB Flexor Pollicis Brevis

ILC Iterative Learning Control

IP Interphalangeal joint

L The Lumbar level of spinal cord

LU Lumbricals

M1 Primary Motor Cortex

MCP The Metacarpophalangeal joint

MEMS Micro-Electro-Mechanical Systems

PID Proportional-Integral-Differential

PMC Premotor Cortex

PPC The Posterior Parietal Cortex

ROM Range Of Motion

S The Sacral level of spinal cord

SCI The Spinal Cord Injury

SMA The Supplementary Motor Area

T The Thoractic level of spinal cord

TBI Traumatic Brain Injury

List of Figures

List of Tables

Acknowledgements

First of all, I would like to thank my supervisors Prof. Eric Rogers and Dr. Christopher Freeman, for their help and professional support. A special gratitude I wish to express to my advisor Prof. Paul Lewin for his advice and positive feedback. I would like to also express my sincere appreciation to Dr. John Tudor, Dr. Kai Yang and Dr. Russel Torah for their help and inspiring work. I must also thank Prof. Neil White and Prof. David Shepherd for the encouraging discussions and support. Special thanks must go to Prof. Jane Burridge, Dr. Timothy Exell, Dr. Ann-Marie Hughes, Dr Katie Meadmore, Emma Hallewell and Mustafa Kutlu for finding my work so useful and inspiring! True thanks for their very hard work need to go to two brilliant electronics engineers: Simon Cole and Phuc le Dinh. And finally I would like to thank my family and friends: Daisy, Alexis, Kasia, Carol, Marek, Oli, Thanh and foremost Chris for his help and for motivating me to individual and creative thinking.

"There are only two ways to live your life. One is as though nothing is a miracle. The other is as though everything is a miracle."

. . .

A. Einstein.

. . .

To my grandmother and to all stroke survivors.

Chapter 1

Introduction

A normal functioning hand is one of the most important features for human independence. A complex neuromusculoskeletal structure of the human hand consists of many dedicated subsystems cooperated in a highly organised manner to form a powerful and precise device. The malfunction of any of its elements may result in disability and hand functional impairment. There exist many injuries that can result in the loss of hand function, such as i.e. stroke, spinal cord injuries and complications after hand surgery or hand traumatic injury such as i.e. tendon ruptures.

Generally, two major types of hand motor impairments can be distinguished: 1) a deficit in motor execution, resulting from i.e. muscle weakness or paralysis, 2) a deficit in higher-order processes of motor control, such as i.e. motor planning and motor learning. Loss of hand function following i.e. stroke, is often characterized by an inability to open the hand (Kamper et al. (2003)), due to finger extension deficit. This deficit is primarily due to a limited ability to activate the finger extensor muscles (Kamper and Rymer (2001)), crucial to appropriately grasp and release objects when interacting with the environment and therefore essential for performing everyday activities (Selzer et al. (2006)).

The human brain has the ability of developing adaptive changes and substantial cortical reorganisation at any age, i.e. through intensive and systematic task repetition. The process by which neuronal circuits are modified by repeated experience and learning is called neuroplasticity (Nudo (2003)). Studies has shown, that damage to the central nervous system results in cortical reorganisation, that varies depending on many factors. These include for example the age of a person, location and level of injury, the type and intensity of the training. Motor-learning research with subjects after i.e. stroke has shown that a high number of repetitions of task-specific activity can induce cortical changes and result in functional improvement (Miltner et al. (1998)).

The goal of the rehabilitation is to help patients regain the most independent level of functioning possible and to enable them to adjust and cope with their impairment. During traditional rehabilitation, such as physical therapy which focuses on restoring general movement or occupational therapy concentrated on the patients re-learning everyday activities such as eating, drinking and self-care skills, patients are assisted by physiotherapists in relearning their lost skills. Although these routine therapies are beneficial, they remain limited in their effectiveness. Successful rehabilitation interventions have laid stress on the importance of performing large numbers of high-intensity, repetitive motions. Unfortunately, sessions with therapists usually include only a relatively small number of exercises. Additionally, traditional therapies are expensive and difficult to manage due to the limited amount of resources compared to the number of patients. Therefore, to experience a significant recovery, patients must perform a substantial number of daily exercises at home. Unfortunately, studies have indicated patients do not perform home exercises as prescribed by therapists. For example only 31% of stroke patients actually perform home exercises as recommended.

Intensive training by repetition is more effective in combination with appropriate feedback to patients about their progress (Langhorne et al. (2009)). Additionally, research has suggested that more interactive and intuitive rehabilitation systems, i.e. systems which enhance patients‘ thinking about moving in different directions, can potentially improve the learning experience and effectiveness of therapy (Brewer et al. (2007)).

Enabling rehabilitation outside the hospital, supported by mobile technology, that motivates the patient, may reduce cost, increase intensity of therapy and shift the responsibility for good health from health professionals to patients (Lang et al. (2007)). Hence, there is a pressing need to improve the effectiveness of treatments including development of novel home-based rehabilitation systems, which are adjustable to individual needs of patients. Significant advances in electronic technology has led to development of new techniques of upper-extremity rehabilitation such as Virtual Reality (VR)-based rehabilitation and Functional Electrical Stimulation (FES). The general aim of these new techniques is to increase the effectiveness of rehabilitation, compared to traditional approaches.

VR and game applications have been recognised as novel and potentially useful technologies that can be combined with conventional rehabilitation for upper arm improvement after i.e. stroke (Saposnik and Levin, 2011). VR has potential to become a highly motivating rehabilitation environment, which also naturally embeds the ability for flexible data bases, that can provide a customized real-time data collection and storage. Explicitly using feedback, VR can be treated as a form of advanced physical therapy and has a number of recognized advantages over conventional

approaches (Burdea (2003)). These include the ability to graduate therapy and adapt automatically to a patient's (limited) functioning level, increasing patient motivation, transparent and computerized objective measures and visual presentation of progress. Appropriately designed games have the potential to motivate patients to exercise by decreasing the monotony of hundreds of repeated motions and providing performance feedback. Therefore, game-based rehabilitation system could provide more interactive and intuitive training for rehabilitation, increasing both the quality and quantity of therapy.

FES is a promising rehabilitation technique widely used to restore motor function in patients with muscle weakness, paralysis or spasticity. Re-learning skills during repeated practice of a task requires sensory feedback. However, the problem is that a significant number of i.e. stroke or spinal cord injury patients, suffer from a partial paralysis such as hemiplegia or tetraplegia and hence can hardly move. In such a case they do not receive the appropriate feedback from previous attempts needed to improve the next one. FES is able to induce functional movements in paralysed or weak limbs by delivering a series of electrical pulses to associated skeletal muscles. Existing FES-based rehabilitation systems concentrate on regaining reaching function in the arm with only a few systems in which a fine motion recovery for the wrist and hand is included. Consequently, the recovery of the hand and wrist has a delayed progression compared with the rest of the upper-limb. Patients with upper extremity paralysis typically regain motion starting from their shoulder over time gradually regaining motion in the elbow, wrist, and, at the end, the hand. The deficiency of FES-based stroke rehabilitation systems for restoration of hand and wrist function is partially due to a high complexity of hand anatomical structure and the technological limitations. The effectiveness of the FES is strongly related to the precision of stimulation in assisting functional movement (Westerveld et al. (2012)).

Commercially available large surface electrodes due to their weak selectivity and activation of several interfering muscles, are not suitable for precise control of hand and wrist. Such an activation of antagonist muscles generate movements interfering with desired ones. For example, the wrist interferes with finger flexors during grasping and finger extensors during prehension. Another problem is the variability in stimulation characteristics, which can appear due to the changes in the surface conditions of the skin and differences in positioning electrodes. Therefore, there is currently significant research into improving surface FES solutions, including the design of surface electrodes that consist of groups of array elements. The advantage of electrode arrays is that they provide the opportunity to activate an individual or a group of elements. Recent studies have shown that electrode arrays are a promising stimulation technology, that can be used to overcome standard FES shortcomings such as finding the optimum electrode placement (O'Dwyer et al. (2006)) decreasing the

muscle fatigue and increasing efficacy of use.

FES makes muscles work by causing electrical impulses to travel along nerves in a similar way as electrical impulses from the brain. If stimulation is controlled a desired movement can be made and its therapeutic effect can be enhanced when associated with the patient‘s voluntary movement (Rushton (2003)). Hence, to maximise effectiveness of FES-based stroke rehabilitation, precise control of stimulation is needed. Such a control should minimize the level of FES to promote the patient‘s maximum voluntary contribution to the movement.

One control approach that has been found to be highly effective when employed within FES-based rehabilitation (Freeman et al. (2009b)) is, Iterative Learning Control (ILC). ILC is an example of feed-forward control that has its origins Arimoto et al. (1984a) in the industrial robotics area where many tasks involve repeating the same finite duration task over and over again. Rehabilitation strategies based on repetitive task performance are an example of such processes. In order to regain for example the ability to open the hand, the patient needs to repeat the exercises multiple times. In ILC the core idea is to use information gathered on previous executions to update the control signal used for the next one and thereby sequentially improve performance. Since the original work, ILC has become an established area of control systems research and applications (Bristow et al. (2006); Ahn et al. (2007); Wang et al. (2009)). In recent years ILC algorithms from the engineering domain have been applied to upper limb stroke rehabilitation for planar and 3D tasks. The ability of model-based ILC to modify the stimulation signal in response to physiological changes, in order to achieve highly accurate tracking by exploiting the repetitive nature of the task, has been confirmed in two clinical trials with stroke patients for the most recent results see, for example (Freeman et al., 2012; Hughes et al., 2009a; Meadmore et al., 2012). These studies do not include the hand and wrist, which has limited their effectiveness.

The main focus of this thesis is therefore, to develop model-based controllers for the FES-based hand rehabilitation. The main contributions of thesis are as follows:

- An overview of the background to the research is presented in Chapter 2. The anatomical complexity of the musculoskeletal structure of the hand and wrist and the mechanisms of the neural control of movement are discussed in relation to the modern techniques of hand rehabilitation, such as i. e. electrode array-based FES. The practical considerations and constraints are discussed relating to the application of the model-based control algorithms within FES-based motor rehabilitation. The existing non-invasive technologies severely limit the application efficiacy of such complex models in practice. Thus to overcome practical limitations, a novel method for control of the hand and wrist, which uses multi-channel surface electrode array-based stimulation has been developed.

- A model, which could be clinically relevant for control of selected non-prehensile hand and wrist movements was developed and presented in Chapter 3. The proposed model incorporating extrinsic and intrinsic muscles of fingers and wrist, has been tested in simulations to investigate the ability of ILC in providing precise FES-based control of the hand opening movement. Performance when using only extrinsic muscles, that are compatible with using surface FES, are compared against using both extrinsic and intrinsic muscles. Simulation studies confirm feasibility and established efficacy of use of the dynamic hand model for the idealised case, in which the optimal selectivity of the muscles can be achieved.

- Several different control methods have been developed based on theoretical and experimental findings. These include gradient based algorithms for optimisation of electrode array-based stimulation and optimal ILC methods for control of the hand and wrist (Chapter 4). The experimental results, confirm the effectiveness of the developed general approach (Chapter 5).

- A novel system for hand and wrist restoration has been designed for a wide group of patients with neuromotor impairments, including those with hand muscle weakness, paralysis and spasticity. It comprises the ILC-based control algorithms for electrode array stimulation with a game-based training environment that provides feedback to the patient (Chapter 5). Developing an effective rehabilitation system of hand and wrist for a wide group of patients is a challenging task and a source of multidisciplinary research aspects. The discussion of the work and potential future research problems are described in Chapter 6 and the general summary and conclusions are presented in Chapter 7.

Chapter 2

Background and Related Work

2.1 Human Hand

Research in anatomy and biomechanics has shown that the human hand has a very sophisticated and complex structure, consisting of many dedicated subsystems, which cooperate in a highly organised manner to form a powerful and precise device. The hand is composed of bones connected by joints which are actuated by muscles. These elements are described in turn next.

2.1.1 Bones of the hand

The skeletal structure of the human hand consists of 27 bones constituting the wrist, palm, four fingers (index, middle, ring, little finger) and the thumb (Figure 2.1). The wrist, which connects the hand body to the forearm, is composed of eight cube-like bones arranged in two rows of four bones each. The palm (metacarpus) contains five long metacarpal bones. Fourteen phalangeal bones constitute the four fingers and the thumb. Each of the four fingers consists of three phalanges (proximal, middle and distal phalanges), while the thumb has two (proximal and distal) phalanges (Tubiana et al., 1996). The skeleton of the human hand can be treated as a complex manipulator consisting of a hierarchy of kinematic chains (the fingers). Kinematics studies the motion of bodies without consideration of the forces or moments that cause the motion. The skeleton thus defines the underlying kinematics of the hand and finger motion by constraining movement at the joints. There are four joints in each of the fingers: the Carpometacarpal (CMC) joint, placed between the carpals and metacarpal bones, the Metacarpophalangeal (MCP) joint between the metacarpals and the phalanges, the Proximal Interphalangeal (PIP) and the Distal Interphalangeal (DIP) joints which lie between the proximal and distal phalanges respectively. The thumb consists of three joints: CMC, MCP and interphalangeal (IP) joints (proximal,

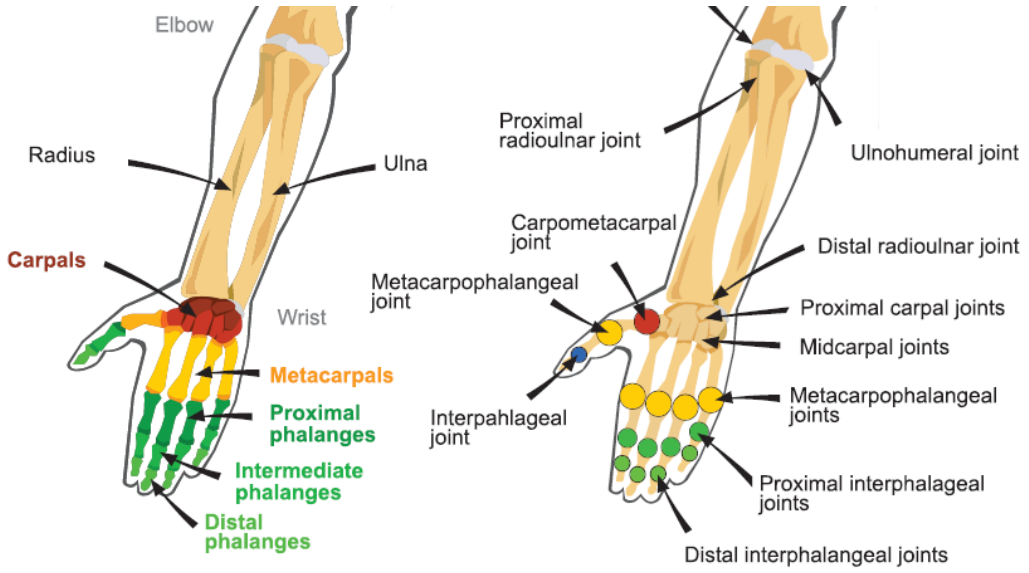

Figure 2.1: Hand bones and joints (Kowalczewski (2009)
)

intermediate and distal). The CMC joint in the thumb is considered as a saddle joint with 2 degrees of freedom (DOF), the MCP joints in the fingers and thumb are considered condyloid and hinge-like joints (respectively) each with 2 DOF, and the IP joints of the fingers and thumb are hinge joints with 1 DOF.

In summary, the hand and the wrist contains sixteen joints which afford approximately 27 degrees of freedom (five DOF for the thumb, four for each of the other fingers and the remaining six DOF define the global position and rotation of the wrist in the 3D space). There have been numerous attempts to model the kinematics of the hand by defining constraint sets on the angles of rotation of the joints Cobos et al. (2010b). The number of joints contained in the model together with the number of DOFs of each joint defines the dimensionality of the control problem. Considerable attention has been given to constructing models with reduced dimensionality Cobos et al. (2010a, 2008, 2007). The results of several studies have demonstrated that the effective dimensionality of the human hand is much less than twenty and that the wrist can be considered as a single joint with two degrees of freedom. Moreover studies have shown that 42% of the movements of the hand involve the four fingers moving together, thus in many situations the four fingers can be considered as one virtual finger Ingram et al. (2008).

The joints of unimpaired hand are able to perform the basic movements shown in Figure 2.2. These are abduction/adduction and flexion/extension for fingers. Additionally the wrist joint is capable to perform flexion/extension, abduction(ulnar deviation)/adduction (radial deviation) and circumduction movements (rotation).

- **Flexion/Extension**
  Flexion/Extension (F/E) is defined as the bending/straightening movement, that decreases/increases the angle between two bones.

- **Adduction/Abduction**
  Adduction (Ad) is a movement of the joint which brings the finger closer to the midline of the arm and hand (sagittal plane), and Abduction (Ab) is the opposite motion.

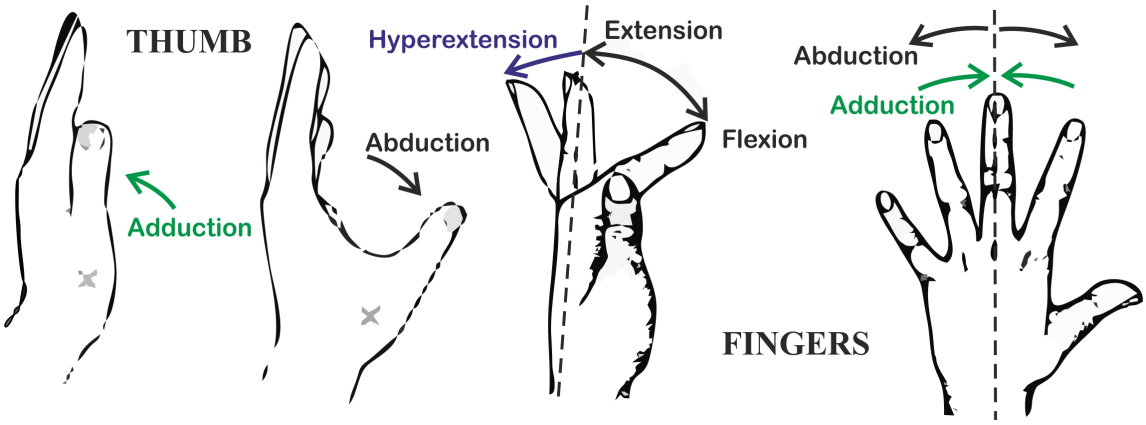

Figure 2.2: Movements of the thumb and fingers (Society for Surgery of The Hand, 1990)

The position of the fingers can be defined by the angles of the finger joints. Knowledge of the abilities and limitations of joints in the healthy hand is necessary to determine an optimal strategy to restore motor abilities in impaired patients. Range of motion (ROM) is a measurement of the distance or angle the joint can travel through over the course of its normal range of movement. ROM for each joint of the healthy hand (in degrees) is presented in Table 2.1 and Table 2.2.

Fingers (II-V)	**MCP (E/F)**	**PIP (E/F)**	**DIP (E/F)**	**MCP (Ab/Ad)**
Index (II)	0/80	0/100	10/90	13/42
Middle (III)	0/80	0/100	10/90	8/35
Ring (IV)	0/80	0/100	10/90	14/20
Little (V)	0/80	0/100	10/90	19/33

Table 2.1: ROM of the index, middle, ring and little finger joints for average unimpaired hand (in degrees) (Pitarch, 2007).

Thumb (I) Joint	Movement	ROM (in degrees)
CMC	Abduction/Adduction	60/0
	Flexion/Extension	35/25
MCP	Flexion/Extension	55/10
	Abduction/Adduction	60/0
IP	Flexion/Extension	80/15

Table 2.2: ROM of the thumb joints for average unimpaired hand (in degrees) (Pitarch, 2007).

The combination of the above discrete motions, constitute more complex movements of the hand and the wrist as a whole such as i.e.: hand opening/closing or cupping. The hand opening/closing, using the terminology introduced above can be defined as combination of extension/flexion of the fingers from their initial flexed/extended position to the final one.

2.1.2 Hand Muscles

Lying on top of the skeleton the hand contains a complex network of muscles and tendons that are used to actuate the joints position and control the movements of the hand.

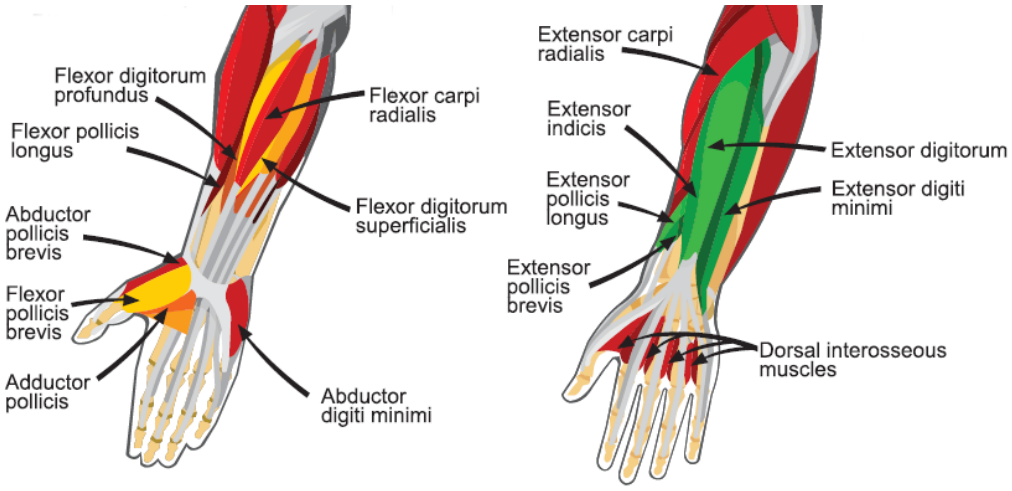

Figure 2.3: Hand muscles Kowalczewski (2009)

Tendons are tension-withstanding collagen fibers that connect the hand bones to the muscles. The muscles of the hand are divided into two groups: intrinsic muscles (listed in Table 2.3) and extrinsic muscles, listed in Table 2.4.

Muscle	**Acts upon (Joint)**	**Movement**
Flexor Digiti Minimi (FDM)	little finger	flexion
Flexor Pollicis Brevis (FPB)	Thumb (MCP)	
Lumbricals (LU)	all fingers (MCP)	
	all fingers (DIP/PIP)	extension
Dorsal Interossei (DI)	all fingers (MCP)	flexion & abduction
	all fingers (PIP/DIP)	extension
Palmer Interossei (PI)	all fingers (MCP)	flexion
	all fingers (PIP/DIP)	extension
Abductor Digiti Minimi (ADM)	Little finger (MCP)	abduction
Abductor Pollicis Brevis (APB)	thumb (CMC/MCP)	

Table 2.3: Intrinsic Muscles of the hand and the joint movements actuated by the muscles

The extrinsic muscles are located proximally in the forearm, whereas the intrinsic muscles originate solely in the hand. The muscles can be sub-classified as extensors, located on the dorsal side of the hand and forearm, and flexors located on the palmar side. Extensors are used to i.e. release objects and expand aperture, as their role is primarily to straighten the fingers.

Muscle	**Acts upon (Joint)**	**Movement**
Flexor Digitorium Superficialis (FS)	all fingers (PIP)/wrist	Flexion
Flexor Digitorium Profundus (FP)	all fingers (DIP)/wrist	
Flexor Pollicis Longus (FPL)	thumb (IP)	
Palmaris Longus (PL)	wrist	
Extensor Digitorium Communis (EC)	all fingers (all joints)/wrist	extension
Extensor Indicis (EI)	index (all joints)	
Extensor Pollicis Brevis (EPB)	thumb (MCP)	
Extensor Pollicis Longus (EPL)	thumb (IP)	
Extensor Digiti Minimi (EDM)	little finger	
Extensor Carpi Ulnaris (ECU)	wrist	extension & adduction
Extensor Carpi Radialis (ECR)	wrist	extension & abduction
Abductor Pollicis Longus	CMC/MCP	abduction

Table 2.4: Extrinsic Muscles of the hand and joint movements generated by the contraction of the muscles

The muscles involved in finger extension constitute complex network of tendons, known as digital extensor mechanism. The main muscle that powers this mechanism is the Extensor Digitorum Communis (EC). The Extensor Indicis (EI) and the Extensor Digiti Minimi (EDM) facilitate independent extension for index and little fingers

respectively. The thumb has two extrinsic extensors namely the Extensor Pollicis Brevis (EPB) and the Extensor Pollicis Longus (EPL). A group of extensors in the forearm are involved in extending the wrist. These include the Extensor Carpi Radialis (ECR), and the Extensor Carpi Ulnaris (ECU).

Fingers have two long extrinsic flexors that are connected by tendons to the phalanges on the palmar side of the hand. The deep flexor, Flexor Digitorum Profundus (FDP) is attached to the distal phalanx whereas the superficial flexor, Flexor Digitorum Superficialis (FDS), is connected to the middle phalanx.

Very precise motor control is typically accomplished with the intrinsic hand muscles, such as thenar, lumbrical and intresseous muscles. The thenar muscles group includes i.e. the Abductor Pollicis Brevis (APB) and Abductor Pollicis Longus (APL), which participate in complex movements of the thumb. Dorsal Interossei (DI) are four muscles, that act to abduct the index, middle, and ring fingers and assist in flexion at the MCP joints and extension at the IP joints of the index, middle and ring fingers. This is in contrast to the Palmer Interossei (PI), which adduct the fingers towards the middle finger, flex the fingers at the MCP joint and extend the fingers at the IP joints. In most FES systems only the extrinsic muscles are stimulated. The extrinsic muscles can provide a good estimate of the location of the fingertip in the workspace for a fixed position of the wrist (Biggs et al., 1999) and gross movements such as i.e. the movements required for grasping large objects are typically performed by the extrinsic hand muscles, as these muscles can generally generate much larger forces in comparison with intrinsic hand muscles.

2.2 Neural control of the hand

To generate a desired movement the human hand requires proper functioning of nervous system, which is responsible for complex neural control mechanisms, such as integration of sensory information (both about the world and the current state of the body) to determine the appropriate activation and coordination of selected muscles and joints. The nervous system consists of two interacting parts: peripheral and central. The central nervous system is composed of the brain and the spinal cord. Peripheral nervous system consists of all nerves leading away from and to the spinal cord, which essentially serves as a communication relay between the brain and effectors such as i.e. muscles .

At the cellular level, the core components of the nervous system are the neuron cells (neurons). **Neurons** are electrically excitable cells that have a special structure, which allows them to process and transmit information to other cells. Neurons send the

information in the form of electrochemical signals travelling along thin fibers, termed axons. The signals are passed on to other neurons at junctions called synapses. Sensory neurons are afferent nerve cells, which transmit sensory information (i.e. sight, sound, feeling, etc.) to the brain. Motor neurons (or motoneurons) are efferent nerve cells (also called effector neurons), that transmit signals from the brain via the spinal cord to the muscles to produce (effect) movement.

The mechanism by which nerve cells transmit signals and information is known as action potential or impulse. A membrane potential of the nerve cell, which is the difference in electric potential between the interior and the exterior of the cell, is regulated by the distribution of cellural ions. When neuron is not sending a signal, it is in its resting state. A nerve membrane is more permeable to potassium than to i.e. sodium ions and this unequal ionic distribution maintains a negative potential of typically 70-90 mV for resting membrane (Baker et al., 2000).

The action potential can be triggered by different stimuli, such as chemical, electrical or mechanical (e.g. stretch). The electrical stimulation of nerves depends principally on the voltage sensitivity of the nerve membrane permeability and on the frequency of impulses transmitted by a nerve fibre, the number of fibres involved and the synaptic network. The action potential can be also induced by an external stimuli, such as i.e. activation of a sensory receptor, or an externally applied electrical current (as during electrical stimulation). The generation of action potential consists of two stages, known as depolarization and re-polarization. Stimuli, regardless of their source cause an opening of sodium selective membrane channels and the beginning of an inward flow of sodium ions. This results in membrane potential being reversed from negative to a positive potential. This process is called depolarization. Immediately after depolarization, a similar amount of potassium ions from the nerve fibre interior cross the membrane until the chemical equilibrium for sodium is approached. The driving force of sodium decreases and finally stops as the membrane channels for sodium close. This process is called re-polarization. The restoration of selective potassium permeability to the membrane results in the original (potassium dominated) ionic concentration and re-establishment of the negative resting potential. The action potential, once generated, is normally self-sustaining throughout its travel along the efferent and afferent nerves (Baker et al., 2000).

The synaptic connections between neurons form complex neural networks and circuits, which are crucial in generating humans perception of the world and the voluntary and involuntary control of their bodies (Kandel et al., 2012). There exist many studies focused on developing methods for modelling of the behaviour of neuronal systems in control of basic but fundamental movements, such as i.e. flexion/extension movement in animals (Angarita-Jaimes et al., 2012). These can provide a useful insight into

understanding and classification of biological movement control and can potentially be applicable in analysis and diagnosis of neurological impairments in healthcare (Jing et al., 2012).

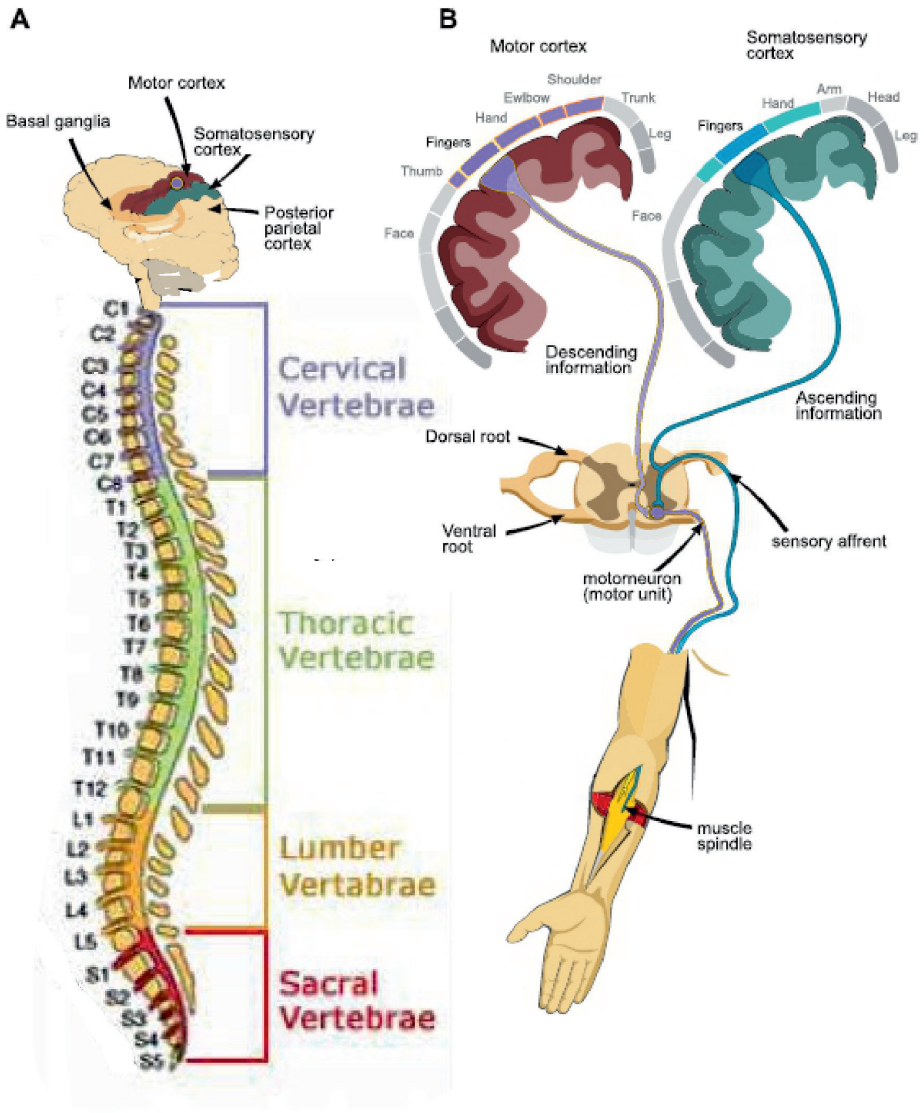

Figure 2.4: Schematic of the Nervous System adopted from (Kowalczewski, 2009) with **A.** the schematic of central nervous system, including the spinal cord levels and the main brain areas responsible for motor control and **B** the schematic of sensory and motor paths in hand movement control

Every voluntary movement performed by humans, even as simple as extending fingers during the process of hand opening to pick up an object, requires complex action of the brain. The brain contains many anatomical regions involved in motor function. One of the principal brain areas involved in voluntary movement is the primary motor cortex (M1). M1 is located in the frontal lobe of the brain. Every part of the body is

represented in M1 in a characteristic somatotopical order, which is shown in Figure 2.4 B. The amount of brain matter devoted to any particular body part is proportional to the amount of control that M1 has over that body part. For example, a larger amount of cortical space is required to control the complex movements of the hand and fingers, hence these body parts have larger representations in M1 than i.e. lower-limbs, whose muscle patterns are relatively simpler. The role of M1 is to generate neural impulses that control the execution of movement.

Other regions of the cortex involved in motor function are called the secondary motor cortices. These regions include the Premotor Cortex (PMC), the Supplementary Motor Area (SMA) and the Posterior Parietal Cortex (PPC). PPC plays a role in voluntary movements, by assessing the context in which they are being executed. PPC receives i.e. somatosensory and visual inputs and uses them to determine such aspects as the positions of the body and the object in space. It thereby produces internal models of the movement to be performed and generates motor commands, prior to the involvement of the premotor and motor cortices. PPC transmits this commands to PMC and SMA, which are involved in the planning of complex movements and in coordination two-handed movements. PMC regulates the hand posture by dictating its optimal position to the motor cortex for any given movement. SMA takes part in the planning and initiation of movements on the basis of past experience (Aizawa et al., 1991).

The signals between the brain and other parts of the body are transmitted through the spinal cord, which is build of a tubular bundle of nerves protected by the vertebral bones of the spine. Each spinal nerve runs from a specific vertebra in the spinal cord to a specific area of the body and is associated with rendering specific motor and sensory functions. Each spinal nerve is formed by the combination of nerve cells from the dorsal (also known as posterior) roots and ventral (anterior) roots of the spinal nerve. These 31 pairs of spinal nerves, are subdivided into four major regions: Cervical (C), Thoracic (T), Lumbar (L), and Sacral (S). Each region contains several segments with ventral and dorsal roots that exit or enter the spinal cord. The dorsal roots are the afferent sensory roots, that convey sensory information from the body to the brain and other regions of the spinal cord via sensory neurons. The ventral roots are the efferent motor roots, which convey motor information from the brain and spinal cord to, i.e. skeletal muscles.

Skeletal muscles are formed of a number of motor units with each motor unit consisting of a single motor neuron and all of the corresponding muscle fibers it innervates. Muscle fibres are cylindrical cells that can contract when stimulated. A single impulse in a motor neuron results in a fast, transient contraction of a single motor unit (Lynch and Popovic, 2008). To maintain a constant tension in muscles,

known as a tetanic contraction, motor neurons deliver impulses to their associated muscle fibers in a sequential asynchronous manner by recruiting adjacent motor units at different time intervals. This asynchronous recruitment ensures that the fatigue of physiologically activated muscle, a side effect of long muscle stimulation, increases slowly. The muscle fatigue reveals itself as the decreasing ability of the muscle to produce a maintained tetanic contraction of adequate power. The intensity of the resulting muscle contraction is determined by the frequency of the delivered pulses. The voluntary tetanic contraction of skeletal muscles is typically achieved at a frequency of $6 - 8$ Hz. Motor neurons can innervate any number of muscle fibers, but each fiber is only innervated by one motor neuron. When the motor neuron fires, all of its muscle fibers contract. The size of the motor units and the number of fibers that are innervated contribute to the force of the muscle contraction.

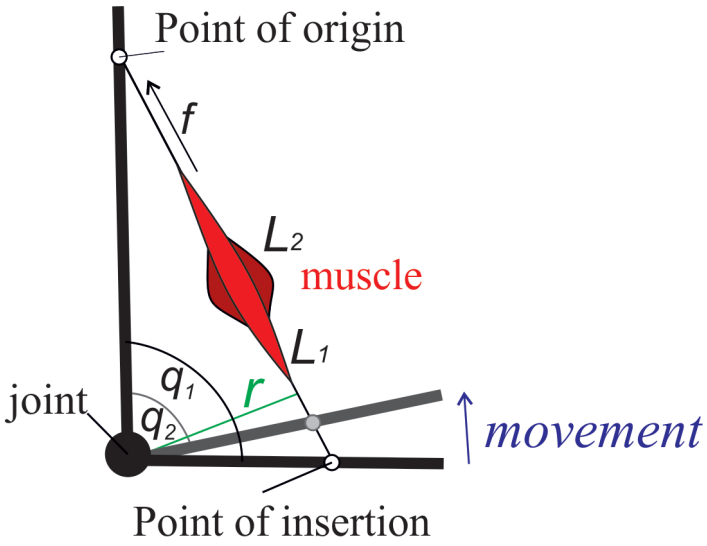

Figure 2.5: Schematic ilustration of a muscle acting on a single joint, where q_1, q_2 are the joint angles, f is the pulling force applied by the muscle, L_1, L_2 are muscle lengths and r is the moment arm of the joint-muscle system.

In the simplest case one muscle acts at a single joint. The joint can represent for example, any of the finger joints. When the muscle contracts, its length may change and produce a pulling force $\boldsymbol{f}$ (with magnitude f) that results in a torque $\boldsymbol{\tau}$ on the joint crossed by the muscle. This causes the joint angle to change by an amount $\Delta q = q_1 - q_2$ in a given time interval Δt, as illustrated in Figure 2.5, which can be observed as i.e. a finger movement.

To ensure adequate movement, the nervous system must constantly receive sensory information from the outside world and internal information about the muscle length

and force and use these informations to adjust and correct the hand's position. The hand itself provides a sensory feedback to the body, as fingertips have some of the highest concentrations of nerve endings per area in the body and are a great source of tactile feedback. The process, that initiates a voluntary motor response is just as intricate as the sensory systems, that provide, i.e. the visual, auditory or other stimuli leading to it. In fact, the brain's motor functions have many points in common with its sensory mechanisms, especially those involved in tactile sensations. Thus, the primary motor cortex and the somatosensory cortex., in the posterior portion of the frontal lobe, are adjacent to each others and the nerve fibres leaving and entering them have the same somatotopic organization.

A structure inside the muscle, that measures the length or stretch of the muscle is the muscle spindle. Information from muscle spindles and other sensory organs are directed to the cerebellum and basal ganglia. The cerebellum takes part in learning a new motor skill such as i.e. dancing or playing instrument. The cerebellum is involved in the timing and coordination of motor programs, which are generated in the basal ganglia. For the body to make any given gesture, the sequence and duration of each of the basic movements for each body segment involved must be controlled in a very precise manner. One of the cerebellum's function is to provide this control over the timing of the body's movements. In humans, the cerebellum also plays a role in analyzing the visual signals associated with movement. These signals may come either from the movement of objects within the field of vision or from the sight of the moving body segments themselves. The cerebellum appears to calculate the speed of these movements and adjust the motor commands accordingly. Errors in such calculations largely account for the poor motor control observed in patients who have suffered injuries to the cerebellum (Tortora and Derrickson, 2007).

Summarizing, a core hand motor control issue is coordination and interaction of the various components of the complex neuromusculoskeletal system of the hand to produce a desired movement (see Figure 2.4). By considering above interactions among the various neuromusculoskeletal structures, as acting in the loop, an overall understanding of the process of movement control and voluntary execution emerges. An impairment of any of the neuromuskuloskeletal elements of the hand mechanism can lead to functional disability.

2.3 Hand Injuries

There are many injuries that can result in the loss of hand function. These include but are not limited to: stroke, spinal cord injury, Traumatic Brain Injury (TBI) and complications following hand surgery or damages to the muskuloskeletal structure of

the hand, i.e due to accidents. Some of the mentioned above injuries are described next.

One of the leading causes of serious long-term disabilities is a stroke. The term stroke, generally refers to a Cerebro Vascular Accident (CVA) caused by an acute disturbance in the blood flow to the brain. Stroke can be subdivided into two major cathegories: ischemic or hemorrhagic. Ischemic stroke occurs when a supply of blood is caused by an obstruction within a blood vessel, resulting from i.e. blood clot. Hemorrhagic stroke on the other hand occurs when a vessel ruptures, i.e. due to the high blood pressure, resulting in bleeding which compresses brain tissue. In that respect hemorrhagic strokes are very similar to traumatic brain injuries and may result in a similar prognosis and pathophysiology.

Each year over 16 million people worldwide suffer from a first-ever stroke (Giroud et al., 2014). Approximately 15 % of all stroke cases belong to hemorrhagic stroke cathegory, which is associated with high mortality rates (Dennis et al., 1993). During and immediately after a stroke, in the acute phase of CVA, neurological functions are lost in the infarcted area, which may lead to a long-term disability. Statistics show, that one third of all stroke survivors are left with severe and permanent disability (Duncan et al., 2000).

The most common feature after stroke is the loss of muscle function for one or more muscles, termed paralysis. Hemiplegia, another common disability resulting from stroke, is unilateral paralysis, that can severely limit patients functional movement control. Research has shown that 80 % of acute stroke survivors lose arm and hand movement skills. Loss of hand function, following CVA, is often characterized by an inability to open the hand (Kamper et al. (2003)), due to finger extension deficit. This deficit is primarily due to a limited ability to activate the finger extensor muscles (Kamper and Rymer (2001)), crucial to appropriately grasp and release of objects when interacting with the environment and therefore essential for performing everyday activities (Selzer et al. (2006)). Other impairments following stroke, that can affect functional motor recovery of hand, are abnormal synergies, contractures and spasticity. Abnormal synergies are patterned movements, that occur due to patients' inability to appropriately control individual muscles. Common synergies are flexion and extension synergies that appear when attempting to perform a separate flexion or extension of the fingers. Approximately, 25% of stroke patients develop spasticity, which can be defined as the over-activity of monosynaptic muscle-stretch reflexes, that leads to increased resistance to a stretch. Summarizing, hand motor impairments after stroke can be divided into two major groups:

- a deficit in motor execution, resulting from i.e. muscle weakness or spasticity.

- a deficit in higher-order processes, such as motor planning and motor learning, which lead to poorly formed sensorimotor associations and to impaired motor control (Raghavan (2007)).

Another neurological injury, that can result in functional impairment of the hand is Spinal Cord Injury (SCI). SCI is basically any type of injury to the spinal cord, that interrupts the flow of electrical information between the brain and target locations i.e. skeletal muscles, typically resulting in neurological damage and long-term disability. SCI can prevent motor signals from reaching the muscles, resulting in paralysis, or sensory information from reaching the brain. In most of the developed countries, between 10 to 83 SCI cases per million per year occurs and approximately 2.5 million people live with a SCI worldwide. Nearly, 85% of SCIs reported happen in men and only about 18% affect people over 45 years old, but the average age of injury steadily increases Sekhon and Feblings (2001).

SCI can range from a small contusion, resulting in minimal motor and sensory deficits, to a full transection, with devastating motor and sensory outcomes. The motor and sensory deficits resulting from SCI are very dependent on the magnitude and the location of the injury. The injury levels, labelled by C1-S5, are assigned according to the location of the injury by the vertebra of the spinal column closest to the injury on the spinal cord (see Figure 2.4 A). If SCI occurs below the cervical area of the spinal cord it can result in paraplegia, which is paralysis of the lower extremities. Cervical injuries usually result in full or partial tetraplegia (quadriplegia), which affects the all four limbs. Depending on the severity of trauma, the injury is classified as either complete, in which nearly all movements and sensations below the level of the injury are lost, or incomplete, in which some residual movements and sensations remain. Determining the exact severity and level of injury is critical in making accurate predictions about the specific muscles and parts of the body, that may be affected. Upper-limb muscles and function can be affected by injuries of levels C5-T1 as follows (see also Figure 2.6):

- C4 results in significant loss of function at the biceps and shoulders.
- C5 results in potential loss of function at the biceps and shoulders, and complete loss of function at the wrists and hands.
- C6 results in limited wrist control (wrist extension is often affected), and complete loss of hand function.
- C7 and T1 results in lack of dexterity in the hands and fingers, but allows for limited use of arms.

Over 55% of all SCIs are cervical (Vivo et al., 1991). The most common level of injury is C5, followed by C4 and C6. Most SCIs do not involve transection of the spinal cord

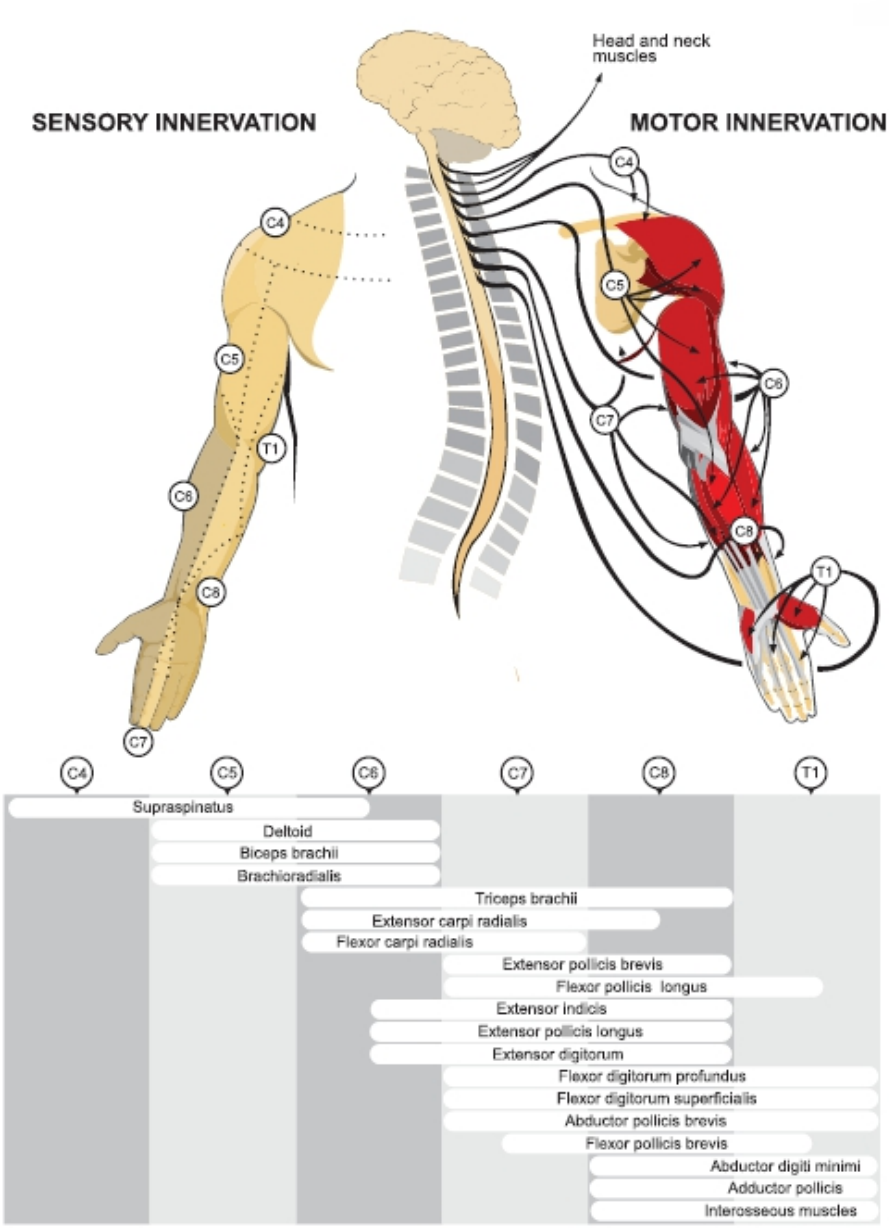

Figure 2.6: SCI regions associated with specific muscles responsible for the upper-extremity functions (Kowalczewski, 2009).

and the cord remains intact (Harvey, 2008). Other complications from SCI, similarily to stroke, include i.e. pain, muscle contractures and spasticity.

The loss of hand function can be also caused by damage or deformation of hand anatomical components such as bones, muscles or tendons, often as a result of an accident. The biological structures, that when damaged often affects proper hand function, are the tendons. The most common and difficult consequence after an injury

of the hand tendons, is the loss of the ability to fully bend (injury of flexor tendons) or straighten (damage to extensor tendons) fingers. Depending on the type of the injury, surgery can be performed to repair or graft the tendon.

Currently, tendon and nerve transfers are the accepted surgical practice for improving hand function. Many different conditions can be treated by nerve transfer surgery. Nerve transfer surgery is necessary, when a certain muscle function is lost because of a nerve injury. If a nerve is injured and cannot be repaired, then the nerve no longer sends signals to certain muscles, causing their paralysis and loss of function. In such case a surgery can be used to attempt to replace the nerve and restore the lost function.

Tendon transfer surgery may be required if a muscle function has been lost due to a disorder of the nervous system. Common nervous system disorders treated with tendon transfer surgery are i.e. SCI, stroke and traumatic brain injuries. Tendon transfer surgery may also be necessary when a muscle has ruptured and cannot be repaired. During the surgical procedure, the distal end of a functional muscle is cut and reattached at the insertion site of a nonfunctional muscle. The tendon transfer sacrifices the function at a lesser location to provide function at a more important location. Nerve transfers are conceptually similar to tendon transfers and involve cutting and connecting a healthy but less critical nerve to a more important but paralyzed nerve to restore its function.

Surgical interventions, such as nerve transfers or tendon repair or replacement give a chance for improvement of motor function in paralysed or damaged hand. However in many cases, to significantly improve motor function of the hand after those surgical procedures, long-term rehabilitation is required in post operative phases of recovery.

2.4 Hand Rehabilitation

The main purpose of rehabilitation of the hand is to reduce the level of disability and restore functional performance. The recovery of hand function is consistently rated as the highest priority among patients. A recent survey has indicated that individuals suffering from tetraplegia ranked the recovery of arm and hand function as their highest priority, far exceeding i.e. the restoration of lower-limb function. In participants opinion the regaining of hand function would most improve their life quality (Anderson, 2004). Many similar findings have been reported, with the suggestion that even partial hand function improvement can have a positive impact on independence and quality of life (Snoek et al., 2004).

Depending on the nature and cause of the loss of hand function, different rehabilitation protocols may be required. During traditional rehabilitation, such as Physical Therapy (PT) or Occupational Therapy (OT), patients are assisted by physiotherapists in relearning their lost skills. PT focuses on restoring general movement and OT concentrates on the patients re-learning activities of daily life (ADLs) such as eating, drinking and self-care skills. Hand rehabilitation programs typically concentrate on achieving following goals:

- Performing grasp and wrist fixation for grasp.
- Performing active release of grasp.
- Performing active extension and flexion for each finger with resistance.
- Alternate hand opening and closing.

These basic hand operations, are crucial in performing more complex manipulative and dexterous movements of the hand and further gradual improvement in ADLs. Humans capability to manipulate with objects of various sizes and shapes, have evolved to generate numerous types of movements while performing various ADLs. The hand movements can be divided in two separate groups:

1. Prehensile movements: Movements in which an object is seized and held partly or wholly within the compass of the hand (grasping).
2. Non-prehensile movements: Movements in which no grasping or seizing is involved. but by which objects can be manipulated by i.e. pushing or lifting motions of the hand as a whole or of the digits individually.

An example of non-prehensile movements are gestures, such as i.e. pointing or hand opening/closing. Alternate hand opening and closing are the basic non-prehensile movements, which are crucial in releasing/grasping objects. An organization of human grasping behaviour into distinct categories was a subject of many studies. In (Schlesinger, 1919) the six cathegories of prehensile movements were distinguished based on the type of objects, that hand interacts with. These are fallowing grasps: cylindrical, tip, hook, palmer, spherical, and lateral. Another categorization considered the type of tasks that need to be accomplished and divided grasps into power and precision grasps (Napier, 1956). A comprehensive organization of human grasps, which takes into accout the precision and power of grasp, as well as the shape of the object, was provided by (Cutkosky, 1989) and is shown in Figure 2.7.

Eye-hand coordination plays a key role in the effective restoration of hand function (Gao et al., 2010). This coordination is the ability to use the eyes and hands together

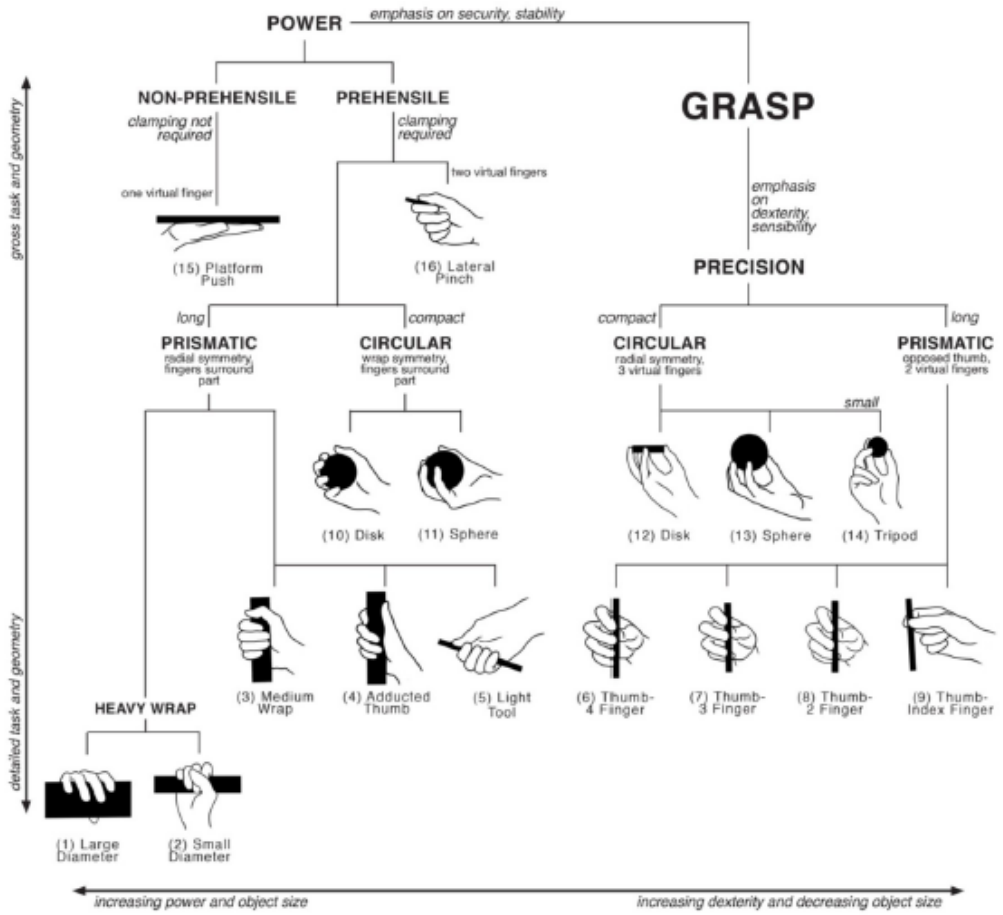

Figure 2.7: Types of grasps provided by Cutkosky (1989) are divided into power and precision grasps from left to right, and by shape and function down the taxonomy tree (Zheng et al., 2011).

to perform a particular ADL, such as i.e. handwriting. A number of techniques such as Geometric Forms or Pursuit Patterns have been employed for training of eye-hand coordination. During a rehabilitation session of this type a patient is encouraged to move one or both hands simultaneously along the specified patterns (usually geometric figures, lines). The error generated is the index that determines the level of control of the muscle to the hand and the patients‘ eye-hand coordination ability. Movement of the hand and arm is a complicated procedure and studies has indicated, that each motor cortex neuron can be assigned with a specific movement of the joints and muscles. The speed and direction of the movement as well as the muscle force is also correlated with specific neurons, however these mechanisms are still subjects of research (Moran and Schwartz, 1999).

In the 20th century it was firstly established, that even if the functions of the brain may be localized in specific areas, these regions are not confined but may change

during life, especially during the recovery after an injury (Yin et al., 2013). The process by which neuronal circuits are modified by repeated experience, learning and adaptation is termed neuroplasticity (Nudo, 2003). Neuroplasticity may be described at cellular level or in a larger-scale as cortical reorganization (Wittenberg, 2010). The fundamental concept of synaptic pruning states, that the individual connections between the different parts of the brain are constantly changing as old connections are removed and recreated. Both the physical structure and the functional organization of the brain may change during life and significant number of studies in last decades have demonstrated many physiological and anatomical examples of cortical plasticity (Nudo, 2013).

Understanding neural responses to different types of training and mechanisms of the hand control is useful in developing novel rehabilitation protocols for the restoration of hand functions lost due to neuromotor disorders. Motor training in normal individuals results in different neural changes, depending on the tasks being performed. Generally, performing more complicated tasks results in the greater cortical reorganization and increase in formation of new synapses between neurons (synaptogenesis), especially in the motor cortical regions assigned to the movement of the body parts involved in the task (Karni et al., 1995; Hund-Georgiadis and von Cramon, 1999).

2.4.1 Modern Rehabilitation Methods

The greater understanding of the mechanisms of overcoming and adaptation to neurological and motor impairments and the boom in electronic technology has lead to the development of new methods of rehabilitation, such as Constrained Induced Movement Therapy (CIMT) , Bilateral Movement Therapy (BMT) , Virtual Reality (VR)-based therapy, electrical stimulation and robot-aided therapy. The general aim of these new techniques is to increase effectiveness in delivering rehabilitation, reduce the associated costs and most importantly, produce greater functional gains in patients. Some of the modern rehabilitation approaches are described next.

CIMT derives from the learned non-use concept, which refers to a common behavioural change in patients with functional disability, in which patients prefer the use of the non-affected limb and avoid performing tasks with the impaired one (Taub, 1994). CIMT can be considered as a form of Unilateral Movement Therapy (UMT), which focuses on performing unilateral movements with impaired limb. The aim of CIMT is to force patients to use their impaired extremity during ADLs by restraining their unimpaired limb (Taub et al., 1998). Types of restraints include a sling or triangular bandage, a splint, a sling combined with a resting hand splint, a half glove and a mitt. The therapy is performed by restricting the less-affected limb for an extended period of time (usually 2 weeks) and with up to 90% of the waking hours over the course of

treatment. Successful clinical use has been reported in many studies for patients with stroke, SCI and other neurological injuries (see for example (Taub and Uswatte, 2009)).

BMT is another rehabilitation technique, in which both limbs are required to perform the same movement. This intervention operates on the principle that an unaffected limb can help restore the functions of the damaged one. The primary sensory and motor cortices for hand control are organized symmetrically, in the left and right hemispheres Rossini et al. (2003). A basic assumption supporting the concept of BMT is that symmetrical bilateral movements activate similar neural networks in both hemispheres when homologous muscle groups are simultaneously activated. Bilateral movements, therefore, may allow the activation of the undamaged hemisphere to increase activation of the damaged hemisphere and facilitate movement control of the impaired limb promoting neural plasticity. There exist studies which reported beneficial effects of BMT compared with UMT. However, due to existence of contradictory results about the actual effectiveness of BMT and UMT, there is a need for further comparison studies, that would quantify the motor improvements of both approaches (Tabak and Plummer-D'Amato, 2010; Cauraugh et al., 2010).

Traditional upper extremity rehabilitation methods such as OT or PT are labour-intensive and require extensive assistance of therapists during exercising the tasks. One recently emerged rehabilitation approach which can be an alternative to traditional rehabilitation methods is robot-aided therapy. Many systematic reviews of robotic technologies used for upper extremity rehabilitation exist and provide evidence in support of the hypothesis that the therapeutic robot devices are clinically beneficial in neurorehabilitation (Loureiro et al., 2011; Krebs et al., 2008).

In therapeutic training, robots are able to assist, enhance, evaluate and document (Riener et al., 2005). Robot-assisted therapy can be treated as a modern form of support to patients in performing repetitive, high-intensity and task-specific treatment in an interactive manner. Existing rehabilitation robots can help patients in performing their movement by either passive support of the movement such as i.e. anti-gravitational support (Sanchez et al., 2006) or by active application of forces to the affected limb. Additionally, robot-aided therapies allow for precise recording of movements and hence can potentially be used to provide the precisely controlled and objective monitoring and evaluation of patients progress. The information about patients progress (feedback) can be conveyed to patients by i.e. utilising visual cues displayed on a computer screen and converting repetitive movement practice into an engaging task such as i.e. a game. Visual cues can also be used to control feedback to the patients about exercise performance and to potentially address psychosomatic factors, which can influence the therapy (Loureiro et al., 2013), i.e. can increase a

motivation to actively participate in training exercises (Nef et al., 2007).

A significant number of different robotic devices have been proposed for upper extremity rehabilitation, which include

- custom-built robots designed specifically for the specific tasks, such as i.e. the MIT-Manus designed for the hand (Masia et al., 2006)
- adaptation of commercially available robots to rehabilitation as in MIME therapy which uses the Puma-560 robot (Lum et al., 2005)
- adapting arm-support devices to the rehabilitation purposes such as i.e. the T-Wrex (Sanchez et al., 2006) or ARMEO (Meadmore et al., 2012)

Unfortunately, most of existing robot devices commercially used in rehabilitation are very costly additionally many robotic treatments reduce the patients required effort and produce movements without the contribution of the patient. Thus, there is currently a need for future development of robot-aided rehabilitation systems, which would alleviate this deficiencies. These include designing of modern low-cost, interactive robot-aided systems, which could enhance patients voluntary contribution to the movement. This can be potentially achieved by combining robot-aided therapeutic devices with other modern interventions, such as VR (Loureiro et al., 2009) and electric stimulation. This comprehensive approach, which combines different modern rehabilitation interventions is currently an emerging direction in neurorehabilitation studies.

2.4.2 Game technologies and VR in motor rehabilitation

VR can be described as a high-end user-computer interface or an immersed in a world, interactive system that can be both autonomous and responsive to users actions. The user is connected to the VR system as part of the input/output loop, allowing individuals to provide input to the virtual environment and experience the result of that input. To place the user within a loop of real-time simulation, VR systems require an output device or visual interface (flat screen or head mounted display) and input devices for interaction (mouse, joystick, data glove) and tracking (camera, kinect, leap motion).

In the last few years there has been a major effort to develop new VR-based rehabilitation systems (Holden, 2005; Rose et al., 2005) and to assess their general effectiveness (Broeren et al., 2007). These include an active research focused on investigating a number of implicit or explicit assumptions on how VR-based rehabilitation technology can promote a functional recovery and on understanding the mechanisms of the recovery. These include attempts to explain a variety of

multidisciplinary aspects of effective rehabilitation, such as i.e. psychological factors focused on patients self-motivation or biological mechanisms of cortical reorganization (Kalra and Ratan, 2007). Several VR-based systems for upper limb rehabilitation have been developed and tested worldwide following diverse methods and therapy concepts. Examples of these are: systems used to train reaching movements through imitation of a virtual instructor (Holden and Dyar, 2002; Piron et al., 2005) or with the use of haptics (Broeren et al., 2007), systems to train general upper limb movements by mental rehearsal and the imitation of movements of the non-paretic arm (Gaggioli et al., 2004).

Substantial research has been focused on developing VR-based technology to increase the self-motivation and exercise adherence in patients. Research has shown that the effectiveness of retraining of sensorimotor function is influenced by the quantity, duration, and intensity of practice (Merians et al., 2009a,b). Problem of low exercise adherence is a significant hurdle to overcome, especially in the presence of high-intensity training and a long-term disability. Self-motivation and activity enjoyment have been reported to be crucial in long-term exercise adherence. Providing a treatment that is fun and motivating whilst simultaneously enhances motor performance, can improve exercise adherence and functional outcomes of rehabilitation.

Video game consoles and video games can be labelled as home-based VR systems, which are interactive, immersive, and provide the user with a sense of presence within a virtual environment. Many studies have investigated the problem of effective application of games for the purpose of rehabilitation. A review of the properties and effectiveness of VR and gaming technologies in the context of needs of patients suggests this to be a very promising and active research area (Saposnik and Levin, 2011). Many application of VR and game-based systems to improve hand and finger function in people with variety of neurological impairments, such as i.e. stroke (Brewer et al., 2008) or cervical level SCI (Szturm et al., 2008) have shown positive outcomes.

Game-based rehabilitation systems include the ability to manipulate motivational factors, which have an impact on recovery by demanding focus and attention. When patients focus on a game than their exercises become more enjoyable, motivating, and are more likely to be maintained over the many trials needed to induce plastic changes in the nervous system (Wood et al., 2003). Moreover, appropriately designed game can motivate users to intensive training by providing them with a sense of achievement even if they cannot perform many functional tasks in the real world, i.e. at the early stage of recovery. Additionally, the use of games in rehabilitation provides new possibilities for improving therapy, such as those centred on social interactions and values, which could reduce the sense of isolation and depression related complications (Loureiro et al., 2010).

The increasing use of low-cost game consoles at homes lead to application of commercially available games in rehabilitation and resulted in the rapid expansion of this area of research. A number of studies has examined the potential of using commercial games with motion-based input devices such as the Sony Playstation 2 and Nintendo Wii (Deutsch et al., 2008). In Loureiro et al. (2010) a usability study for Nintendo Wii console games in rehabilitation was conducted for varying degrees physical ability and cognitive function, based on patients opinion questionnaire. Nine acute subjects undergoing rehabilitation played a variety of games included in the Wii Sports and Wii Play game packs, which are suitable for different types of training. These include games such as bowling, tennis, shooting and air hockey suitable for practicing unilateral movements and games such as golf, boxing and baseball which are suitable for BMT. The participants all suffered from neurological injuries which ranged from CVA, TBI to SCI and other more rare conditions, for more details see (Loureiro et al., 2010). Impairments included weakness, reduced ROM and limited motor skills, pain, sensory loss, and cognitive deficits, such as reduced concentration and memory or/and slowed information processing. The results have shown 100% of the participants enjoyed playing on the Nintendo Wii and 89 % of them reflected that the game-based therapy should be a regular part of their treatment sessions. 33 % of the subjects required therapist help to perform the movement, i.e. to stabilise the arm or use both hands. Although the main responses of participating in the study subjects were definitely positive, it was concluded that certain aspects of the Wii therapy require improvement, such as i.e. development of a custom-made hardware and software which would be more suitable for specific needs of patients with different levels of disabilities.

The commercial console games are principally aimed at patients in the later stages of recovery, as they were designed for users with a full range of motion. Consequently, they are not suitable for the majority of paralysed patients, who are at the early stage of their recovery (Flynn et al. (2007)). Therefore, the majority of research has focused on development of dedicated games, that can be used by wider group of patients, some of which are listed in Table (2.5).

Comprehensive and reproducible assessment of hand function is crucial for prescription of appropriate treatment program and further evaluation of its effectiveness. Subjective evaluations of hand function by a therapists form the basis of clinical assessments, but these evaluations tend to be performed in non-standardized ways, and therefore depend on the training and skills of the clinicians involved. Therefore, home-based rehabilitation systems need to include reliable and objective self-assessment and testing methods to quantify effect of therapy and provide clear and understandable feedback to the patients.

Research	**Game description**
Colombo et al. (2007)	simple game in which the patient tried to move a coloured circle from an initial position to a goal position using a robotic device designed for arm rehabilitation
Huber et al. (2008)	haptic glove based games in which users scare away butterflies, play the piano, and squeeze virtual pistons to improve the player's finger flexion and extension.
Broeren et al. (2008)	several games for use with a pen-like haptic device that patients could position in 3D.
Burke et al. (2009)	a physics-based orange catching game and a whack-a-mouse game, both controlled with magnetic sensors and a vibraphone game which used a Wii remote as a pointing device

Table 2.5: Example of games developed for stroke rehabilitation

The therapy should be adjustable according to ongoing assessment over the course of the treatment program to ensure optimal benefits to the patient. The traditional assessment of hand function includes evaluation of ROM, testing of the strength of intrinsic and extrinsic muscles and evaluation of motor and sensory functions. ROM can be a useful index, which if appropriately incorporated with modern VR-based rehabilitation system, can become clear and motivating information to patients about their progress.

An appropriately designed game can be a fundamental element of a modern VR-based rehabilitation system, addressing the most important aspects of effective hand restoration. Game-based rehabilitation system can couple the advantages of modern and quantitative assessment methods and feedback, to make the rehabilitation process motivating and intensive for the patient. It can be also a modern dynamic training environment, that can be adjustable to the patients rate of recovery and performance.

Summarizing, VR integrates our understanding of rehabilitation with advanced interactive multi-media technology, which can improve and enhance the therapeutic effect, by i.e. delivering individualized and motivating to the patients therapy. Additionally, VR-based rehabilitation systems can be directly placed in patients home via a tele-rehabilitation approach to enable them increased contact with both medical professionals and other patients. These can increase patients autonomy during training and decrease the requirement of constant surveillance. Moreover, VR game-based tele-rehabilitation brings new comprehensive possibilities for monitoring and evaluation of therapy, i.e. by coupling modern and standard clinical evaluation methods with social element of exchanging patients personal experiences. This could

provide complementary data to the patients and clinicians about the effectiveness of the therapy on the both individual and global scales.

2.5 Functional Electrical Stimulation

Functional Electrical Stimulation (FES) is a rehabilitation technique widely used to restore motor function of patients with muscle weakness or paralysis. FES has theoretical support from neurophysiology and motor learning research. A body of clinical evidence exists to confirm its effectiveness in motor control recovery (Pomeroy et al., 2006). FES is able to induce functional movements in paralysed or weak limb, by delivering a series of electric pulses to associated skeletal muscles.

FES is effective only when the peripheral nervous system is intact. Damage to the peripheral nerve causes muscle degeneration. Such muscles with changed characteristic become harder to stimulate. Therefore FES is more likely to be effective therapy for injuries such as i.e. stroke, moderate spinal cord injury or traumatic brain injury.

2.5.1 FES Techniques

A wide range of existing FES technologies, use different types of electrodes to stimulate the motor units. Generally, FES can be categorized into two major types of stimulation:

- Invasive stimulation, which uses implanted electrodes such as: epimysial electrodes (placed on the surface of the muscle), intramuscular electrodes (placed within a muscle), and cuff electrodes (wrapped around the nerve that innervates the muscle)
- Non-invasive surface stimulation, which uses self-adhesive electrodes or electrodes arrays, that can be both placed on the surface of the skin.

In all types of electrical stimulation the muscle is stimulated by placing two electrodes: active and return, which are attached in the manner that reduces the amount of stimulation required to produce a given contractile force. The active electrode is usually placed as close as possible to the major motor point, which is a point at which a motor nerve enters a muscle. The return electrode is usually located near the muscle tendon.

The main disadvantages of the invasive methods is the surgical character of the application. Electrode placement needs to be very precise, which can be difficult to evaluate during the surgery. Additionally, the use of wire connections requires keeping the entry site for the wire free from infection and avoiding electrode wire breakage

during the relative movement between the muscle and the skin. Moreover the impermeable electrodes can cause permanent damage to the nerve tissue.

Surface (or transcutaneous) FES can be an effective alternative for the invasive techniques of electrical stimulation, however, there exist many factors, that can affect the stimulation efficiency and its practical application. These factors include electrode type (size and electrode placement), a selection of the stimulation signal parameters and control of the stimulation.

There exist different FES parameters that can be used to produce an effective motor response in paralysed or weak limb. These are: Pulse strength (amplitude) and duration (pulse width), pulse repetition rate (stimulation frequency), On-off time, Ramp time, Waveform. The tension produced in electrically stimulated muscle depends on the intensity and frequency of stimulation. The stimulation intensity is a function of the total charge transferred to the muscle, which depends on the pulse amplitude, duration, and frequency in addition to the shape of the pulse train Lynch and Popovic (2008). FES recruits motor units in a non-physiological synchronous manner, stimulating all of the motor units at the same time. Therefore, FES stimulation requires a much higher frequency ($20 - 40$ Hz) to achieve tetanic contraction. This can result in rapid muscle fatigue.

At the electrode-tissue interface the stimulation signal generated between electrodes causes a current of ions to flow and penetrate through the tissues underneath the skin that includes muscles (motor points) and nerves. One electrode has more negative charge than the other. The polarity of the electrode depends on the type of stimulation signal polarity. In stimulation with monophasic signal one of the electrodes is negative in polarity (cathode electrode) and the other is positive in polarity (anode or indifferent electrode). In case of bi-phasic signal polarity at each electrode alternates from positive to negative or vice-versa. Ions in the region will migrate towards or away from the electrodes according to their charge. This movement of ions occurs in the extracellular fluid and through the nerve and causes a depolarisation of the nerve membrane. If the current is large enough, an action potential is produced.

In order to induce an action potential, external electrical stimuli must be of adequate intensity and of sufficient duration to equal or exceed the threshold of excitability of the cell membrane. Nerves have a lower threshold than muscle and thus electrical activation of peripheral nerves can induce muscular contraction by the normal physiological mechanism. Critical to whether a given stimulus causes an action potential or not is the impedance between the electrodes and the skin, the orientation, size and placement of the electrodes and the stimulation signal type. The best stimulation location of the electrode is over the selected muscle motor point (Baker

et al., 2000).

The sizes of the stimulation electrodes have direct effect on the current density. When the electrode size decreases the current density increases and vice versa. Small electrodes produce high current densities, with moderate stimulation amplitudes, which may be uncomfortable or even painful and can limit the effectiveness of stimulation. Pain impedes a further increase of the stimulation current and hence no higher forces or torques can be produced. Additional factor which also influence the perceived comfort during stimulation is the area of the stimulation. The optimum size of electrode depends on the muscle stimulated and location of the stimulation, defined by the position of the electrodes (stimulation sites) (Lyons et al. (2004)).

Locating the optimal stimulation sites is critical to the effective application of surface stimulation. Usually the best stimulation site is the nearest to the muscle motor point, which provides the greatest amount of motor excitation with the minimal intensity of stimulation. Generally, the correct positions of the electrodes resulting in desired movements have to be found manually. This is time-consuming and relies heavily on the skill and experience of the therapist. Hence, there is currently significant research interest in improving surface FES solutions, including the design and application methods for surface electrodes that consist of groups of array elements.

2.5.2 Electrode Array-based FES

Array electrodes consist of multiple elements which can be activated (individually or in a chosen combination) to form a virtual electrode of arbitrary size and location. The signal is transmitted to the specific muscles or area of the muscle, which are located directly underneath the active elements. The position and size of the active region (virtual electrode) can be automatically modified. Recent studies have shown that electrode arrays are a promising stimulation technology, that can be used to overcome standard FES problems such as manual finding of the optimal electrode placement, decreasing resulting muscle fatigue and increasing overall function (Popovič and Popovič (2009)). The advantage of electrode arrays is that they provide the opportunity to distribute the stimulation signal through an automatic selection of appropriate individual or a group of active elements.

Studies have also indicated that electrode arrays have the potential to improve muscle activation and selectivity (Westerveld et al., 2012), compared with standard FES electrodes and can automatize the finding a location and size of the active stimulation region. Additionally, this technology can eliminate the problem of repeated reattachment of electrodes, as the electrode array once attached to the hand, can be automatically set to obtain many different optimal configurations O'Dwyer et al.

(2006) for a variety of movements and muscles. Methods to assess and automatically select the optimal configuration of the multipad electrodes is currently an emerging and active area of research. A range of these are discussed next.

In O'Dwyer et al. (2006) a system consisting of an analogue de-multiplexer and an electrode array, that used one channel of stimulation was developed. A key element of the system was an algorithm, which selected from the array of electrodes a single best electrode to provide the optimal orthotic performance for the subject. Ideal orthotic performance was defined as a hand posture, which satisfies certain criteria for the mechanical attributes of a reaching motion. The criteria were defined by: wrist extension of 15 ± 5 degrees, finger flexion which is below a threshold of 25% of the maximum finger flexion angle and hand adduction/abduction angles which were below a threshold of 25% of the maximum angle. A tests with healthy subjects confirmed the effectiveness of the system.

Schill et al. (2009) developed an automatic approach of electrode array optimisation for active wrist joint stabilisation in tetraplegic SCI patients. The method of automatic selection of the appropriate single elements (pads) of electrode array consisted of 9 pads and the level of the stimulation was based on two criteria: the magnitude criterion and the dynamic criterion. In the first step, a reference movement of the wrist joint was generated manually and recorded using bending sensors. A set of evaluation movements was generated through application of different activation patterns to the electrode array. Two different modes were implemented for generating an activation signal, the single mode and the combined mode. In the single mode all electrodes were activated sequentially one by one. In the combined mode a combination of 2 elements of electrode array was activated to generate and record movements. To find the best electrode configuration for a given reference movement, the magnitude and dynamic criteria were applied to the recorded data. Each evaluation time series was generated by the use of either a single electrode or a combination of two elements from the electrode array. Approximately, 30 2-elements combinations were investigated. These were then compared with the reference movement in order to find an electrode configuration which resulted in movements that best fitted the reference. The best electrode configuration was obtained directly from the best matching time series. The approach was not tested in clinical trials with patients.

Popovič and Popovič (2009) developed an algorithm for automatic determination of elements of the electrode array for the functional activation of finger flexors and extensors. The goal of the optimization procedure was to select elements of electrode array, which when activated, resulted in position of the selected fingers (index and ring fingers) and the wrist of individuals with tetraplegia that are minimally different from the fingers position measured in healthy individuals during palmar and lateral grasps.

The flexion/extension of the PIP and MCP joints of index and ring fingers and adduction/abduction, extension/flexion of the wrist and pronation/supination of the forearm were measured by goniometers. The algorithm was based on the selection of eight elements of electrode array that, when activated would result in the minimum aggregate error, defined as follows:

$$\Delta_{ij} = \frac{1}{7}\sqrt{\left(\frac{\Delta_{IPIP}}{\phi_{IPIP}}\right)^2 + \left(\frac{\Delta_{IMCP}}{\phi_{IMCP}}\right)^2 + \left(\frac{\Delta_{RPIP}}{\phi_{RPIP}}\right)^2 + \left(\frac{\Delta_{RMCP}}{\phi_{RMCP}}\right)^2 + \left(\frac{\Delta_{Ext/Flx}}{\phi_{Ext/Flx}}\right)^2 + \left(\frac{\Delta_{Add/Abd}}{\phi_{Add/Abd}}\right)^2 + \left(\frac{\Delta_{Pron/Sup}}{\phi_{Pron/Sup}}\right)^2} \tag{2.1}$$

where ij determines the position of one a single pad in electrode array and Δ_{IPIP}, Δ_{IMCP} (index finger), Δ_{RPIP}, Δ_{RMCP} (ring finger), $\Delta_{Ext/Flx}$, $\Delta_{Add/Abd}$ (wrist) and $\Delta_{Pron/Sup}$ (arm) are the differences between the maximum joint angles $\phi_{IPIP}, ..., \phi_{Pron/Sup}$ measured during activation of an individual element ij of electrode array and the target join angle in healthy individuals. The assumption behind the algorithm was based on the findings that the electrical field in the body tissues is quasistatic and hence the superposition principle can be applied. The method minimized the aggregate error for static maximal values of selected joints of the hand and wrist for hand opening (extension) and hand closing (flexion). The procedure was applied for the dorsal and volar sides of electrodes independently, using four channel stimulator. The method was tested on 6 subjects with tetraplegia. The values of selected hand and wrist joints for selected by the method elements of electrode array for all test subjects, were similar to the target joint angles collected from healthy individuals (Popovìc and Popovìc, 2009).

Maleševìc and Popović (2010) developed a procedure of classification of muscle twitch response during low-frequency electrical stimulation via consecutive activation of elements within 16-elements electrode array. The twitch response, recorded by mounted on hand Micro-Electro-Mechanical Systems (MEMS) accelerometers, was chosen due to its relatively quick and reliable occurrence following single stimulation impulse, correlated with muscle force elicited during continuous stimulation. Derived method was capable to automatically detect elements of electrode array which, when stimulated, resulted in wrist or fingers flexion/extension and generation of different and characteristic wave shapes of acceleration. The method used optimization algorithm which employed Artificial Neural Network (ANN) to detect the correlation between each element of electrode array and the muscle activated beneath. The tests were designed to measure the influence of the stimulation point on the twitch response in the hand, with a minimal number of sensors. The recordings were used to train the neural network to distinguish between following types of movements: wrist flexion, finger flexion or none. This initially developed approach was meant not to provide quantitative measure of finger/wrist movement but to find a simple but reliable method for calibration of electrode array, using only one MEM sensor and a signal waveform shape as supplementary information for ANN-based decision making. The method was tested on 3 unimpaired subjects and showed that the developed

classification method achieved high-degree from approximatelly 80 % to 93% accurate results.

The above ANN-based classification method, was further extended and applied in optimal selection of appropriate elements of electrode array Maleševič and Popovič (2010). The method was extended two the case, where 2 additional accelerometers were placed on the middle and ring finger, in order to analyse the influence of differnt sensor locations on the accuracy of developed ANN-based classification algorithm. The ANN was trained using the characteristic acceleration wave shapes acquired during wrist and finger flexion/extension movements, measured by MEMS sensors and goniometers. The methods were tested on 6 unimpaired participants with electrode array consisted of 16 elements. The ANN procedure resulted in intrasubject classification of high accuracy for each participant which ranged from 81% $\pm$ 8% (3 ± 1 pads incorrectly chosen) to 93% $\pm$ 5% (1 element classified incorrectly).

2.5.3 FES Control Strategies

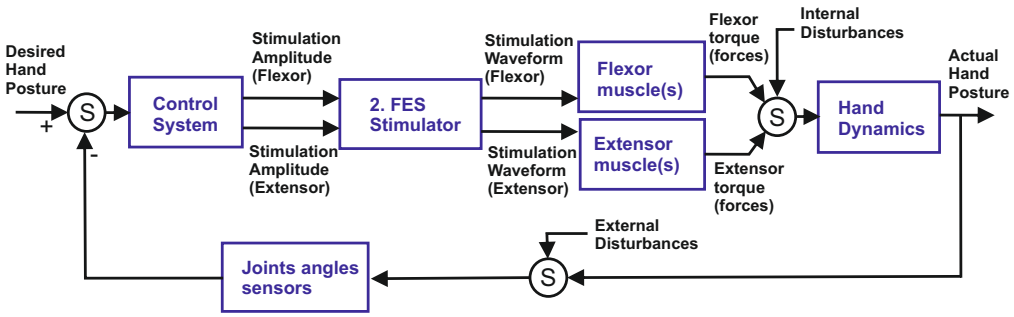

Figure 2.8: Example of FES schematic for hand and wrist rehabilitation.

In system engineering terms the musculoskeletal system can be considered as a plant to be controlled. In this analogy the muscles are actuators and the electrical pulses driving the actuators are control signals. The posture of the hand is typically defined by the angles of the hand joints. By calculating the appropriate electrical stimulation signal a desired output posture/trajectory can be followed.

There exist two main control strategies, that can be employed in FES-based control of the hand and wrist. These are: open-loop control and closed-loop control, that typically employs a model of the system. Open-loop control is the method of control, which does not rely on the presence of sensors giving information on the plant. Open-loop controllers therefore do not adjust the input according to performance, and have no knowledge of the plant trajectory. In a closed-loop control system, the system output is monitored by a sensor and the data is fed to a controller which adjusts the

control as necessary to maintain the desired system output. The control affects the system output, which in turn is measured and looped back to alter the control. A closed-loop control scheme for the hand and wrist is shown in Figure 2.8.

Determining the control signal is a challenging problem, mainly due to the complexity of the musculotendon structure of the hand and wrist. Regulating angles or torques of hand joints with FES involves controlling a highly coupled system since each joint is actuated by at least two muscle groups, i.e. these comprising either flexor/extensor or adductor/abductor muscles. Furthermore most of the hand muscles are either bi-articular or multi-articular, which means they actuate simultaneously two or more joints respectively.

The controller provides the control signals needed to obtain a muscle force that produces a desired movement. Hence, the movement can be controlled indirectly by modulating the stimulation parameters. Variations in these affect the stimulus applied to the tissues, determining the physiological response. Therefore, to achieve the precise control of the motion, the identification of input-output response of the muscle is significant for use in model-based control approaches. There are several empirical models that reproduce the input-output response of a muscle. The most popular muscle model commonly used in FES control is the Hill model (Hill (1938)).

The Hill model describes the output force as the product of three independent experimentally measured factors: the force-length property, the force-velocity property, and the non-linear activation dynamics of the stimulation input. The actuation dynamics operate under the condition that the muscle has a constant length (isometric condition), and are almost always represented by a Hammerstein structure. Such a model comprises a static non-linearity in series with linear dynamics. The static non-linearity represents the static gain relation between stimulus activation level and the steady-state output torque, when the muscle is held at a fixed length and is termed the Isometric Recruitment Curve (IRC). The linear dynamics refers to the muscle contraction dynamics and in combination with IRC gives the overall torque generated by the muscle Le et al. (2010).

Open-Loop Controllers

The most widely used FES controllers, due to their simplicity, have an open-loop architecture. There exist a number of commercial FES systems for the hand and wrist, primarily based on this control technique.

The Bionic Glove (Prochazka, 1997) is a fingerless glove that electronically senses wrist position and uses it to trigger a logical on-off signal to provide FES control of

finger/thumb muscles. The degree of wrist angle allows the user to select their grasp or hand opening posture. The glove has three channels of electrical stimulation acting on the Flexor Pollicis Longus, Flexor Digitorum Superficialis, Flexor Pollicis Brevis and Adductor Pollicis. Practical tests involving nine impaired patients showed a significant increase in average grip force for palmar and lateral grasp (Prochazka, 1997; Popovic, 1999).

The NESS H200 system (Hendricks et al., 2001) contains inbuilt electrodes worn on the upper arm. This system provides a simple interface, that allows the user to select seven different stimulation patterns in order to assist hand grasp. The control unit applies suitable stimulation allowing the fingers and thumb to move while reaching, grasping and pinching. The effectiveness of the device was tested clinically with eighteen stroke patients, who exhibited upper body dysfunction (Hendricks et al., 2001). Although the results showed increased motor function, especially in patients with moderate motor defects, the beneficial impact of the device was not clear.

Another type of FES system is triggered using position/force sensors in response to a command supplied by the user. The commercial system (**Freehand**) (Taylor et al., 2002), uses proportional control with a reference given by shoulder position sensing to regulate grip force for lateral and palmer grasp. It hence requires user feedback to achieve force control. The system uses implanted electrodes to ensure better selectivity over the muscle activation. The Freehand was tested with nine users and the results confirmed similar advantages in hand grasp function to the previously described commercial devices (Taylor et al., 2002).

Another control technique is based on using Electromyographic (EMG) signals recorded from muscles. The EMG signals can be recorded from unimpaired users and replayed during FES grasp control of injured patients, thereby providing an open-loop reference. Alternatively, they are measured directly from the impaired user to provide a direct command input for FES control of impaired limb. In (Hart et al. (1998)) proportional control using wrist position together with EMG signals from the wrist have been used to provide grasp and release control. This study has shown wrist control is not affected by movements undertaken during reaching tasks and the function of the wrist is easy to re-learn by participants. The use of EMG control in practical applications is limited by the availability and range of usable muscles, in addition to distortion caused by the artefacts produced by the stimulated muscle. Additionally, signals associated with paralysed muscle can be weak and unreliable to record.

Closed-Loop Controllers

Relatively little research has considered closed-loop or model-based control of the hand, This deficiency may be partially explained by the anatomical complexity of the human hand. One of the few existing model-based control approaches, existing in the literature is a multi-channel Proportional-Integral-Differential (PID) controller proposed by (Watanabe (2003)). This PID controller uses the error between the desired input and the actual measured output to generate a control signal for the plant. The controller acts on two degrees of freedom in the wrist joint, measured with a two-axis goniometer. To achieve wrist movement four muscles were stimulated using surface electrodes: Extensor Carpi Radialis (ECR), Extensor Carpi Ulnalis (ECU), Flexor Carpi Radialis (FCR) and the Flexor Carpi Ulnaris (FCU). The controller was tested on five neurologically intact patients and showed promising results.

Advanced feedforward control architectures, that use adaptive ANN have been also applied to FES of the hand and/or wrist. In (Fujita et al. (1998)) work aiming to establish the feasibility of using an ANN learning controller for generating hand posture stimulus is presented. The training data for a three-layered neural network were obtained using a 3D magnetic position sensing system of FES hand motion. The controller demonstrated the ability to cope with the non-linearity of the system. The disadvantage of using ANN controllers is the need of extensive training and the training procedure often not possible in real-time, which is required especially in case of clinical trials with stroke patients. Additionally there is no simple relationship between the learned weights of the neural network and the plant parameters, as the operation of the trained network has a hidden structure. This precludes stability and convergence analysis.

2.6 Iterative Learning Control

Iterative learning control (ILC) is an example of a feed-forward control approach, that can be an effective alternative for ANN controllers. ILC is a control methodology developed for uncertain dynamic systems that operate in a repetitive manner over a fixed time interval. ILC can improve the transient response and tracking performance of such systems by learning from past actions. The concept of ILC emerged extensively with publications of Arimoto et al. (1984a), that introduced firstly the Derivative-type ILC and Proportional-type ILC (P-type ILC) afterwards Arimoto et al. (1984b). Henceforward, ILC has remained a very active area of research and this has led to development of many new and advanced ILC schemes. These include: PID type algorithms, robust, adaptive, predictive and optimal ILC schemes, as well as approaches such as a fuzzy - based ILC , Neural Network - based ILC and Fuzzy

Neural Network -based ILC for both linear and nonlinear systems. ILC algorithms has been widely implemented on industrial robot manipulators, certain types of medical equipment and within manufacturing. Originating from the field of robotics, ILC still attracts significant research interest in both theoretical and experimental domains Bristow et al. (2006).

The main concept of ILC is to iteratively find an input sequence such that the output of the system is as close as possible to a desired output, using information gathered from past trial(s). The state space representation of a general nonlinear discrete-time time-invariant control system has following form:

$$\begin{aligned} \boldsymbol{x}_k(t+1) &= \mathbf{f}[\mathbf{x}_k(t), \boldsymbol{u}_k(t)] \\ \mathbf{y}_k(t) &= \mathbf{h}[\mathbf{x}_k(t)] \end{aligned} \tag{2.2}$$

where $k = 1, 2, \ldots$ is the trial index, $t \in [0, 1, 2, ..., N-1]$ is the sample number and $\mathbf{x}_k(t)$, $\boldsymbol{u}_k(t)$ and $\mathbf{y}_k(t)$ are the state, input and output vectors respectively on the k^{th} trial.

Let $\boldsymbol{y_d}(t)$ denotes the desired (reference) trajectory and $\boldsymbol{e_k}(t) = \boldsymbol{y_d}(t) - \boldsymbol{y_k}(t)$ is the error on k^{th} trial. The principal design idea behind ILC is to make the tracking error signal converge to zero as the number of trials goes to infinity.

P-type

In the simples P-type ILC, controller learns from the error of the current trial (k) and produces the input for the next trial (k+1) in the form:

$$\boldsymbol{u}_{k+1}(t) = \boldsymbol{u}_k + \boldsymbol{L}\boldsymbol{e}_k(t) \tag{2.3}$$

where L denotes the learning gain.

Phase-Lead ILC

Instead of using the instant error, Phase-Lead ILC can anticipate the error at advance time step λ, that can be varied to accommodate changes in the system. The phase lead control update law is following:

$$\boldsymbol{u}_{k+1}(t) = \boldsymbol{u}_k(t) + \boldsymbol{L}\boldsymbol{e}_k(t+\lambda) \tag{2.4}$$

where $\boldsymbol{u_k}$ and $\boldsymbol{u}_{k+1}$ are the control inputs of the current and next trial respectively, t is the sample number, L is proportional learning gain and λ is the phase-lead in samples. The term $Le_k(t+\lambda)$ is the core novel feature of ILC as it uses data that is not causal in the standard systems sense. In particular, ILC at sample instant p allows the use of information at future values of p, where this is possible because this term uses

information generated on the previous trial. If such a term is not possible then it can be shown that the ILC can be expressed as a standard feedback control scheme.

2.6.1 Optimal ILC Algorithms

Optimisation is a process of determining the best solution for varieties of problems. Optimal ILC attempts to find solution to a control problem using certain optimisation criterion, termed cost function. Usually the cost function provides some description of the tracking error, which supposed to be minimized by the controller. Standard ILC cost function can be expressed as:

$$\min_{\boldsymbol{u}} \|\mathbf{y}_d - \boldsymbol{g}(\boldsymbol{u})\|^2 \tag{2.5}$$

where $\boldsymbol{g}(\boldsymbol{u}) = \boldsymbol{y}$ is the output of the system

Gradient-based ILC

The gradient-based ILC algorithm ILC update law is following

$$\boldsymbol{u}_{k+1} = \boldsymbol{u}_k + \alpha \boldsymbol{g}'\left(\boldsymbol{u}_k\right)^T \boldsymbol{e}_k \tag{2.6}$$

where the derivative $\boldsymbol{g}'(\boldsymbol{u}_k)$ is equivalent to the system linearisation around $\boldsymbol{u}_k$ and is represented by the $pN \times mN$ matrix

$$\boldsymbol{g}'(\boldsymbol{u}_k) = \begin{bmatrix} \frac{\partial \boldsymbol{g}_1}{\partial \boldsymbol{u}_k(0)} & \frac{\partial \boldsymbol{g}_1}{\partial \boldsymbol{u}_k(1)} & \cdots & \frac{\partial \boldsymbol{g}_1}{\partial \boldsymbol{u}_k(N-1)} \\ \frac{\partial \boldsymbol{g}_2}{\partial \boldsymbol{u}_k(0)} & \frac{\partial \boldsymbol{g}_2}{\partial \boldsymbol{u}_k(1)} & \cdots & \frac{\partial \boldsymbol{g}_2}{\partial \boldsymbol{u}_k(N-1)} \\ \vdots & \vdots & \ddots & \vdots \\ \frac{\partial \boldsymbol{g}_N}{\partial \boldsymbol{u}_k(0)} & \frac{\partial \boldsymbol{g}_N}{\partial \boldsymbol{u}_k(1)} & \cdots & \frac{\partial \boldsymbol{g}_N}{\partial \boldsymbol{u}_k(N-1)} \end{bmatrix} \tag{2.7}$$

Note, that local tracking of an arbitrary reference is only possible if $\boldsymbol{g}'()$ has full row rank which also implies $m \leq p$ since the convergence within is $P(\boldsymbol{I} - \alpha \boldsymbol{g}'(\boldsymbol{u}_{\text{inf}})\boldsymbol{g}'(\boldsymbol{u}_k)^T)) < 1$.

Newton method-based ILC

As the name suggests, Newton method-based ILC is based on the Newton algorithm used in non-linear optimization. Translating the Newton algorithm to the considered ILC problem leads to the following ILC update in the case where $\boldsymbol{g}'()$ is square and full rank

$$\boldsymbol{u}_{k+1} = \boldsymbol{u}_k + \boldsymbol{g}'(\boldsymbol{u}_k)^{-1} \boldsymbol{e}_k \tag{2.8}$$

Calculating the inverse and derivative is computationally expensive, so writing equation (2.8) as

$$\boldsymbol{u}_{k+1} = \boldsymbol{u}_k + \boldsymbol{z}_{k+1} \tag{2.9}$$

converts the problem to that of solving the equation $\boldsymbol{z}_{k+1} = \boldsymbol{g}'(\boldsymbol{u}_k)^{-1}\boldsymbol{e}_k$, or

$$\boldsymbol{e}_k = \boldsymbol{g}'(\boldsymbol{u}_k)\boldsymbol{z}_{k+1} \tag{2.10}$$

In this way calculation of the inverse is avoided. Further details appear in Lin et al. (2006a).

Point to point ILC

The application of ILC in the area of point-to-point motion control offers the potential to benefit from the ability to learn from experience gained over previous trials of the task. Point-to-point ILC is a technique applied to tracking tasks which require the plant output to reach given points at selected time instants, without the specification of intervening reference points Freeman et al. (2011b) and Freeman et al. (2011a). The method of Freeman et al. (2011a) is applied for plant output specified at a fixed number, M, of sample instants given by $N_1, N_2, \ldots, N_M$, where $M \leq N$. Let the prescribed values of the output at these instants be $\mathbf{u}_1, \mathbf{u}_2, \ldots, \mathbf{u}_M$, where $\mathbf{u}_i \in \mathbb{R}^p$. The gradient method may be applied to such point-to-point constraints simply by exchanging (2.5) for

$$\min_u \|\bar{\boldsymbol{y}}_d - \boldsymbol{\Phi}\boldsymbol{g}(\boldsymbol{u})\|_2^2 \tag{2.11}$$

where the $pM \times pN$ matrix $\boldsymbol{\Phi}$ has block-wise components

$$\Phi_{i,j} = \begin{cases} \boldsymbol{I}_p & j = N_i, \quad i = 1, 2 \ldots M \\ \mathbf{0}_p & \text{otherwise} \end{cases} \tag{2.12}$$

where $\boldsymbol{I}_p$ and $\mathbf{0}_p$ are the $p \times p$ identity and zero matrices respectively, and the hand configurations at the M points of interest are contained in the vector

$$\bar{\mathbf{y}}_{\mathbf{d}} = \begin{bmatrix} \mathbf{y}_1^T & \mathbf{y}_2^T & \cdots & \mathbf{y}_M^T \end{bmatrix}^T \quad \in \mathbb{R}^{pM} \tag{2.13}$$

The gradient descent iterative solution to (3.56) is

$$\boldsymbol{u}_{k+1} \;=\; \boldsymbol{u}_k + \beta \left(\boldsymbol{\Phi}\boldsymbol{g}'(\boldsymbol{u}_k)\right)^T (\bar{\boldsymbol{y}}_d - \boldsymbol{\Phi}\boldsymbol{g}(\boldsymbol{u}_k)) \tag{2.14}$$

which in the ILC framework, using experimentally recorded data $\boldsymbol{q}_k$, is

$$\boldsymbol{u}_{k+1} \;=\; \boldsymbol{u}_k + \beta \left(\boldsymbol{\Phi}\boldsymbol{g}'(\boldsymbol{u}_k)\right)^T (\bar{\mathbf{y}}_d - \boldsymbol{\Phi}\mathbf{y}_k) \tag{2.15}$$

It is possible to show that the feasibility space is enlarged compared with the standard tracking framework. In particular $\mathbf{\Phi}$ can be selected to ensure $\mathbf{\Phi} \boldsymbol{g}'()$ has full row rank and hence guarantee feasibility. Given an underactuated setup, conditions can be derived for the existence of a feasible tracking task by reducing the point-to-point times Freeman et al. (2011a).

2.6.2 ILC in Stroke Rehabilitation - Previous Research

ILC can be applied to processes that are required to repeat the same finite duration task over and over again. One form of stroke rehabilitation is to ask the patient to make an attempt to complete a task, such as reaching out over a table top to a cup, with FES assistance. During each attempt, the error between a prescribed path and that actually generated by the patient can be measured and then used in the rest time to update the FES signal to be applied on the next attempt. A critical objective is that if the patient is improving with each attempt then the level of voluntary effort should increase and the applied stimulation decrease. In ILC the core idea is to use information gathered on previous executions to update the control signal used for the next one and thereby sequentially improve performance. Dou et al. (1999) has confirmed that ILC schemes can effectively react to time-varying effects of the muscle fatigue which comprises a major component of the non-linearity in the system and reject repeatable uncertainties and disturbances. Previous ILC systems for the upper-limb were focused on restoration of arm movements.

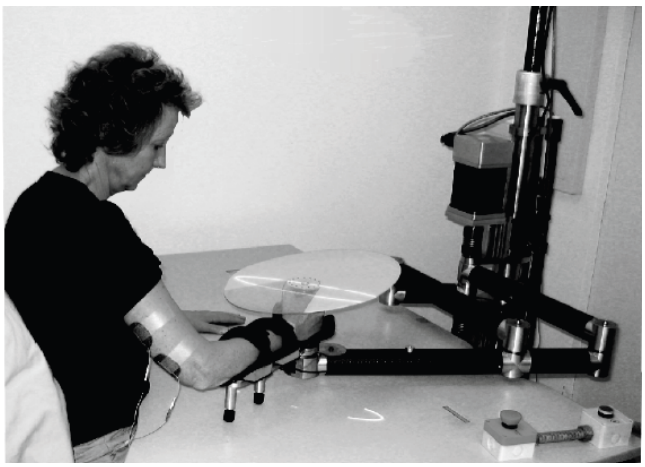

Figure 2.9: Planar arm movements rehabilitation system

ILC mediated by Functional Electrical Stimulation has been used in robotic-assisted rehabilitation of the upper-limb after a stroke, to produce two different systems, each with successful clinical trials. Freeman et al. (2009b) presented results of the application of Phase-Lead and Newton method-based ILC to control the stimulation

level used to assist hemiplegic patients in completion of planar reaching tasks. The planar rehabilitation system used in the clinical trials is shown in Figure 2.9. The

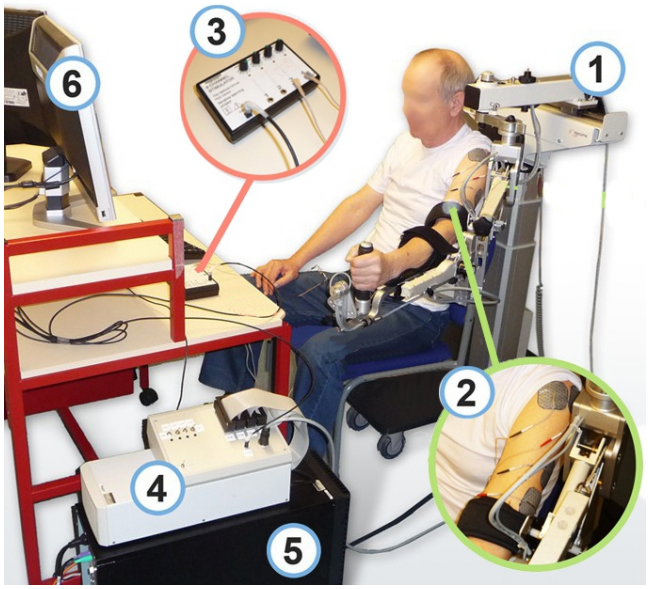

Figure 2.10: 3D Arm rehabilitation system for stroke patients. The system includes a mechanical robotic unweighting system used to support patient's arm - ARMEO (1), FES hardware (2,3), control system and user software including custom -made virtual reality module (4,5,6).

training procedure was based on tracking elliptical trajectories in a repetitive mode. During the clinical trials, patients were asked to track a spot of light by moving a vertical rod over a flat board. If they tracked the target well, then on the next attempt the stimulation support was reduced, and if not it was increased. Treatment consisted of performing a selection of 27 treatment tasks, comprising three different trajectories, each with three levels of reach extension in one of three oriented directions. The clinical trials have shown promising results of arm function improvement after only 18 treatment sessions (Hughes et al. (2009b)). To increase the accuracy of performance, dynamic models of the arm were developed (Freeman et al. (2009a)). This was the first use of advanced model-based electrical stimulation controllers in clinical trials, that was precise enough to support the hypothesis based on Hebbian learning, that FES applied co-incidentally with voluntary movement could enhance the motor learning Freeman et al. (2008).

Cai et al. (2011) presented results of the subsequent research programme in which Phase-Lead and Newton-methods based ILC algorithms were used to assisted 3D movements of the patient's arm to deliver effective treatment. Research confirmed the efficacy of the 3D arm rehabilitation system (Meadmore et al. (2012)). The system is shown in Figure 2.10.

The next step in recovering the use of the upper extremity is the relearning of hand functions. Design of appropriate control algorithms is a key element of any FES-based rehabilitation system. ILC algorithms were chosen for this purpose, as they were recognized to be an effective FES control method for the arm. However, the use of ILC controllers for the hand and wrist to adjust stimulation parameters during task performance, in order to assist the patient's intention as accurately as possible remains a challenging open research question. The next step is therefore to investigate the possibility of using ILC for FES control of hand and wrist and ultimately incorporate the control procedures into the FES-based rehabilitation system.

Chapter 3

The Hand Model and ILC

The hand can be considered as a mechanical system and it is possible to apply mechanical principles to study it. In this context, it involves two elements: muscles serve as the motor to provide driving force, and tendons, bones, and joints transmit the motor's driving force (Valero-Cuevas et al., 2003). The overal structure is arranged around skeletal joints and links. The complexity of the human hand makes the construction of accurate models a very challenging task. However the usefulness and necessity of using such models in many different science disciplines and problems, makes hand modelling an extremely active research area. Hand models arise in areas such as surgery (Esteki and Mansour, 1997), biomechanics, robotics Miller et al. (2005); Deshpande et al. (2009), and computer graphics Sueda et al. (2008).

The diversity of existing hand models results from consideration of many different factors such as: model application, level of complexity, and anatomical accuracy. Generally, hand models can be modelled in terms of three main aspects: kinematics, dynamics, and shape. In control analysis, only the two first aspects, kinematics and dynamics, are of principal importance. Kinematic models describe the motion position, velocity and acceleration of bodies and systems without consideration of the forces that cause the motion. Conversely, dynamics focuses on the causes of the motion (Spong and Vidyasagar, 1989). Biomechanical models are characterized by their great complexity and anatomical accuracy, building on kinematic hand model based on the underlying skeleton structure of the hand. This consists of a hierarchical arrangement of bones which combine to form a complete musculoskeletal model (Albrecht et al., 2003; Tsang et al., 2005). Musculoskeletal modeling has been a mainstream topic of biomechanics research worldwide over the last three decades. This class of model requires the intensive use of multibody system dynamics analysis tools integrated with an understanding of which aspects of the underlying biological model are most important. The control problem under consideration in this thesis requires use of an anatomically accurate model, containing muscles and tendons.

This chapter provides an overview of the development of hand model. A variety of models with different level of kinematic and dynamic complexity (2D and 3D case) was analysed over the course of the study. Since this model will be used in clinical tests with patients, rather then purely for the purposes of simulation, care was taken to develop simplest possible model that integrates realistic anatomical and physiological aspects alongside a standard kinematic and dynamic representation of a multi-body system.

3.1 The 2D hand and wrist model

The 2D hand and wrist model suitable for clinical use includes a single composite finger, representing the combined action of four fingers, wrist and neglects the thumb orientation. The finger and wrist are modelled as 3-link rigid body system, consisting of 3 active revolute joints, as shown in Figure 3.1. This provides an approximate representation of the hand since 42% of the functional movements of the hand involve the four fingers moving together (Ingram et al., 2008). Link 1 represents the II-V Metacarpal bones connected by the wrist joint, Link 2 represents proximal phalanges and Link 3 represents middle and distal phalanges of the finger.

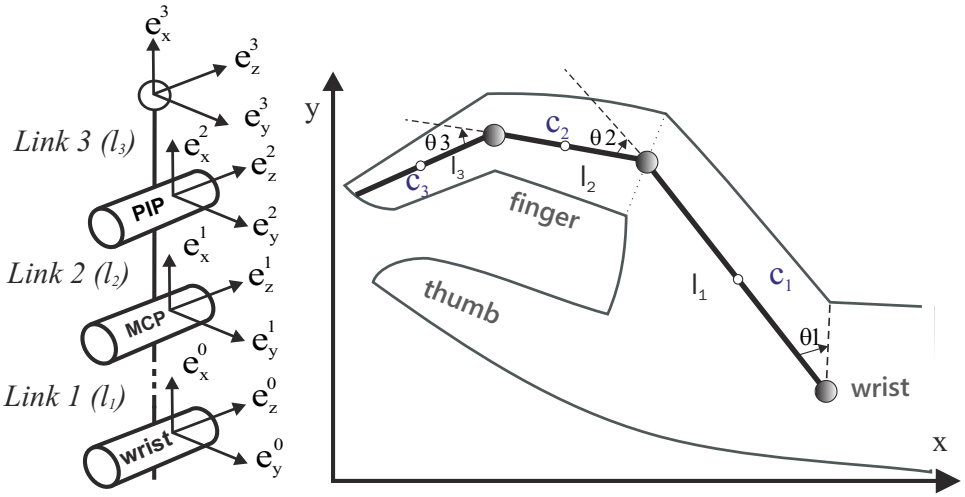

Figure 3.1: Planar hand model

The kinematic model of the hand together with the coordinate frames is shown in Figure 3.1. The x-, y- and z-directions of the i^{th} frame in a right-handed Cartesian coordinate system are denoted by $\mathbf{e}_x^i$, $\mathbf{e}_y^i$ and $\mathbf{e}_z^i$ respectively. The coordinate frame $\mathbf{e}^0$, $\mathbf{e}^1$, $\mathbf{e}^2$ are located in each joint of the hand (wrist, MCP and PIP joints respectively) as shown in Figure 3.1. The $\mathbf{e}^3$ has origin at the tip of the virtual finger. The angles θ_1, θ_2 and θ_3 represent the three rotations of the metacarpal bones about wrist and proximal and middle phalanges about MCP and PIP joints respectively.

In general, frame i can be expressed in frame $i+1$ coordinates by means of the rotation matrix ${}^{i}\mathbf{T}_{i+1}$

$$\mathbf{e}^{i} = {}^{i}\,\mathbf{T}_{i+1}\mathbf{e}^{i+1} \tag{3.1}$$

and the rotation matrices for $i = 0, 1, 2, 3$ assume the form

$${}^{i}\mathbf{T}_{i+1} = \begin{bmatrix} \cos(\theta_{i+1}) & -\sin(\theta_{i+1}) & 0 \\ \sin(\theta_{i+1}) & \cos(\theta_{i+1}) & 0 \\ 0 & 0 & 1 \end{bmatrix} \tag{3.2}$$

By extension, to go from frame i to frame $i+2$ a multiplication of the rotation matrices can be used

$$\mathbf{e}^{i} = {}^{i}\,\mathbf{T}_{i+1}\ {}^{i+1}\mathbf{T}_{i+2}\ \mathbf{e}^{i+2} \tag{3.3}$$

and to go from frame $i+1$ to frame i the inverse of the rotation matrices is applied

$$\begin{aligned} \mathbf{e}^{i+1} &= {}^{i+1}\mathbf{T}_{i}\ \mathbf{e}^{i} \\ \mathbf{e}^{i+1} &= \left({}^{i}\mathbf{T}_{i+1}\right)^{-1}\ \mathbf{e}^{i} \end{aligned} \tag{3.4}$$

These transformations are now used to obtain a dynamic model of the system.

Equations of motion

The dynamic model is formulated using the Lagrange method. The Lagrange‘s equation of motion for a non-conservative system is given by:

$$\frac{d}{dt}\left(\frac{\partial L}{\partial \dot{\mathbf{q}}}\right) - \frac{\partial L}{\partial \mathbf{q}} = \mathbf{Q}^{\mathbf{NC}} \tag{3.5}$$

where $\boldsymbol{q}$ denotes the generalized coordinates of the system:

$$\mathbf{q} = [\theta_1, \theta_2, \theta_3] \tag{3.6}$$

and L is the Lagrangian defined as the difference between kinetic energy (K) and potential energy (V):

$$L = K - V \tag{3.7}$$

The term $\boldsymbol{Q^{NC}}$ represents the component due to non-conservative forces such as damping and externally applied torque. Substituting (3.7) into (3.5) gives:

$$\frac{d}{dt}\left(\frac{\partial K}{\partial \dot{\mathbf{q}}}\right) - \frac{\partial K}{\partial \mathbf{q}} + \frac{\partial V}{\partial \mathbf{q}} = \mathbf{Q}^{\mathbf{NC}} \tag{3.8}$$

The kinetic energy can be expressed in terms of the mass matrix $\mathbf{M}(\mathbf{q})$:

$$K = \frac{1}{2}\dot{\mathbf{q}}^{\mathbf{T}}\mathbf{M}(\mathbf{q})\dot{\mathbf{q}} \tag{3.9}$$

The first derivative of kinetic energy K with respect to $\boldsymbol{q}$ can be rewritten as

$$\frac{\partial K}{\partial \mathbf{q}} = \frac{1}{2}\begin{bmatrix} \dot{\mathbf{q}}^{\mathbf{T}}\frac{\partial \mathbf{M}}{\partial \mathbf{q_1}}\dot{\mathbf{q}} \\ \vdots \\ \dot{\mathbf{q}}^{\mathbf{T}}\frac{\partial \mathbf{M}}{\partial \mathbf{q_n}}\dot{\mathbf{q}} \end{bmatrix} \tag{3.10}$$

The first derivative of kinetic energy K with respect to $\dot{\boldsymbol{q}}$ can be expressed as

$$\frac{\partial K}{\partial \dot{\mathbf{q}}} = \frac{\partial}{\partial \dot{\mathbf{q}}}\left[\frac{1}{2}\dot{\mathbf{q}}^{\mathbf{T}}\mathbf{M}(\mathbf{q})\dot{\mathbf{q}}\right] = \mathbf{M}(\mathbf{q})\dot{\mathbf{q}} \tag{3.11}$$

Substituting (3.9),(3.10) and (3.11) into (3.8) yields

$$\mathbf{M}(\mathbf{q})\ddot{\mathbf{q}} + \underbrace{\dot{\mathbf{M}}(\mathbf{q})\dot{\mathbf{q}} - \frac{1}{2}\frac{\partial}{\partial \mathbf{q}}\left[\dot{\mathbf{q}}^{\mathbf{T}}\mathbf{M}(\mathbf{q})\dot{\mathbf{q}}\right]}_{\mathbf{C}(\mathbf{q},\dot{\mathbf{q}})} + \underbrace{\frac{\partial V(\mathbf{q})}{\partial \mathbf{q}}}_{\mathbf{G}(\mathbf{q},\dot{\mathbf{q}})} = \mathbf{Q}^{\mathbf{NC}} \tag{3.12}$$

Equation (3.12) can be expressed in more compact form

$$\boldsymbol{M}(\boldsymbol{q})\ddot{\boldsymbol{q}} + \boldsymbol{C}(\boldsymbol{q},\dot{\boldsymbol{q}}) + \boldsymbol{G}(\boldsymbol{q},\dot{\boldsymbol{q}}) = \mathbf{Q}^{\mathbf{NC}} \tag{3.13}$$

where $\boldsymbol{M}(\boldsymbol{q})$ is the inertia matrix, $\boldsymbol{C}(\boldsymbol{q},\dot{\boldsymbol{q}})$ denotes the centrifugal and Coriolis forces, $\boldsymbol{G}(\boldsymbol{q},\dot{\boldsymbol{q}})$ is the vector of the gravitational forces and $\mathbf{Q}^{\mathbf{NC}}$ vector of non-conservative forces.

Kinetic energy

The kinetic energy of a single rigid body can be described by

$$T = \frac{1}{2}m\dot{\mathbf{r}}^{T}\dot{\mathbf{r}} + \frac{1}{2}\boldsymbol{\omega}^{T}\mathbf{I_O}\cdot\boldsymbol{\omega} \tag{3.14}$$

The first term of the right hand side relates to the translational kinetic energy of the rigid body, where m is its mass and $\dot{\mathbf{r}}$ is the velocity of the center of mass ($\mathbf{r}$ is the position of the center of mass). The second term represents the rotational kinetic energy of the rigid body, where rotation is about a fixed point O. The angular velocity vector $\boldsymbol{\omega}$ represents all the rotations from the base frame to the body-fixed frame. The tensor $\mathbf{I_O}$ is the mass moment of the inertia tensor of the rigid body with respect to the point of rotation.

The kinetic energy of a system composed of multiple bodies is the sum of the kinetic

energy of each body. Thus kinetic energy of the three-link hand equals

$$T = \frac{1}{2}\sum_{i=1}^{3} m_i \dot{\mathbf{r}}_i^T \dot{\mathbf{r}}_i + \frac{1}{2}\sum_{i=1}^{3} \boldsymbol{\omega}_i^T \mathbf{I}_{\mathbf{O}i} \boldsymbol{\omega}_i \tag{3.15}$$

where m_i is a mass of $i-th$ link, $i = 1, 2, 3$, $\mathbf{I_{O1}}$ is the mass moment of inertia tensor of the metacarpal bone with respect to the wrist joint and $\mathbf{I_{O2}}$, $\mathbf{I_{O3}}$ are the mass moment of inertia tensor of the proximal and middle+distal phalanges (denoted by link 3) with respect to the MCP and PIP joints respectively. Each link is considered as a cylinder about the local x-axis , hence the mass moment of inertia can be expressed using the following formulae:

$$I_x = m r_c^2 \tag{3.16}$$

$$I_y = I_z = \frac{m r_c^2}{4} + \frac{m l_c^2}{12} \tag{3.17}$$

where m is the mass, r_c the radius and l_c the length of the cylinder. Firstly, the mass moment of inertia tensor with respect to the centre of mass is determined. The mass moment of inertia tensors with respect to the center of mass are expressed as

$$\mathbf{I_{CM1}} = \mathbf{e}^{1^T} \begin{bmatrix} I_1 & 0 & 0 \\ 0 & I_2 & 0 \\ 0 & 0 & I_2 \end{bmatrix} \mathbf{e}^1 \quad , \quad \mathbf{I_{CM2}} = \mathbf{e}^{2^T} \begin{bmatrix} I_3 & 0 & 0 \\ 0 & I_4 & 0 \\ 0 & 0 & I_4 \end{bmatrix} \mathbf{e}^3$$

$$\mathbf{I_{CM1}} = \mathbf{e}^{3^T} \begin{bmatrix} I_5 & 0 & 0 \\ 0 & I_6 & 0 \\ 0 & 0 & I_6 \end{bmatrix} \mathbf{e}^3 \tag{3.18}$$

Secondly, the Parallel Axes Theorem (3.19) is used to calculate the mass moment of inertia tensors with respect to the point of rotation.

$$\mathbf{I}_O = \mathbf{I}_{CM} + m\left(\mathbf{r}^T\mathbf{r}\mathbf{I} - \mathbf{r}\mathbf{r}^T\right) \tag{3.19}$$

with $\mathbf{I}$ the identity tensor. The resulting mass moment of inertia about each of the joints (wrist, MCP and PIP) for the three links respectively are

$$\mathbf{I_{O1}} = \mathbf{e}^{1^T} \begin{bmatrix} J_1 & 0 & 0 \\ 0 & J_2 & 0 \\ 0 & 0 & J_2 \end{bmatrix} \mathbf{e}^1 \quad , \quad \mathbf{I_{O2}} = \mathbf{e}^{2^T} \begin{bmatrix} J_3 & 0 & 0 \\ 0 & J_4 & 0 \\ 0 & 0 & J_4 \end{bmatrix} \mathbf{e}^3$$

$$\mathbf{I_{O3}} = \mathbf{e}^{3^T} \begin{bmatrix} J_5 & 0 & 0 \\ 0 & J_6 & 0 \\ 0 & 0 & J_6 \end{bmatrix} \mathbf{e}^3 \tag{3.20}$$

with $J_1 = I_1$, $J_2 = I_2 + m_1 c_1^2$,$J_3 = I_3$, $J_4 = I_4 + m_2 c_2^2$, $J_3 = I_3$, and $J_6 = I_6 + m_3 c_3^2$.

The position vectors are:

$$\begin{aligned} \mathbf{r}_1 &= [c_1 \quad 0 \quad 0]\boldsymbol{e}^1 \\ \mathbf{r}_2 &= [l_1 \quad 0 \quad 0]\boldsymbol{e}^1 + [c_2 \quad 0 \quad 0]\boldsymbol{e}^2 \\ \mathbf{r}_3 &= [l_1 \quad 0 \quad 0]\boldsymbol{e}^1 + [l_2 \quad 0 \quad 0]\boldsymbol{e}^2 + [c3 \quad 0 \quad 0]\boldsymbol{e}^3 \end{aligned} \tag{3.21}$$

The velocity vectors can be determined by calculating the derivatives of the position vectors

$$\dot{\mathbf{r}}_i = \frac{d\mathbf{r}_i}{dt} \tag{3.22}$$

The vectors of angular velocity equal

$$\boldsymbol{\omega}_1 = \dot{\theta}_1 \mathbf{e}_z^1 \tag{3.23}$$

$$\boldsymbol{\omega}_2 = \boldsymbol{\omega}_1 + \dot{\theta}_2 \mathbf{e}_z^2 \tag{3.24}$$

$$\boldsymbol{\omega}_3 = \boldsymbol{\omega}_2 + \dot{\theta}_3 \mathbf{e}_z^3 \tag{3.25}$$

Potential energy

The potential energy of a system is the sum of the internal energy (for example elastic energy) and the potential energy of the conservative external forces V

$$V = \sum_{i=1}^{M} \int_0^{y^i} K_i(y) y dy - \sum_{j=1}^{N} m_j \mathbf{g}^T \mathbf{r}_j \tag{3.26}$$

where M is the number of springs, $K_i(y)$ the nonlinear stiffness function of spring i and y^i the elongation of the spring. The gravitational acceleration vector is denoted by $\mathbf{g}$. In the case considered we can assume that the only conservative external force is the gravity force and that the muscle groups which actuate each joint produce a stiffness that can be represented by a spring with zero elongation at the initial position $\theta_{0,i}$ and with a stiffness k_i, $i = 1, 2, 3$. In the simplest case, the potential energy of the hand equals

$$V = \sum_{i=1}^{3} \left[\frac{1}{2} k_i (\theta_{0,i} - \theta_i)^2 - m_i \mathbf{g}^T \mathbf{r}_i \right] \tag{3.27}$$

with the gravitational acceleration vector $\mathbf{g}$ aligned with the axis $-\mathbf{e}_z^1$. However during purely horizontal movement of the hand the gravity can be neglected.

Generalized non-conservative forces

The generalized non-conservative forces consist of all externally applied non-conservative forces and moments, together with, all forces and moments due to damping and friction.

$$\mathbf{Q}^{NC} = \sum_{i=1}^{n_F} \left(\frac{d\mathbf{a}_i}{d\mathbf{q}} \right) \mathbf{F}_i^{NC} + \sum_{j=1}^{n_M} \left(\frac{d\theta_j}{d\mathbf{q}} \right) \boldsymbol{\omega}^T(\theta_j) \mathbf{M}_j^{NC} \tag{3.28}$$

where n_F, m_N represent the number of applied non-conservative forces and moments respectively. In addition, $\mathbf{a_i}$ is the absolute position vector of the point at which $\mathbf{F}_i^{NC}$ is exerted, θ_j the rotational parameters and $\boldsymbol{\omega}(\theta_j)$ a column vector containing the directions of rotation.

The hand model consists of revolute joints, thus only generalized non-conservative moments appear. In each direction of rotation viscous friction and a driving torque are considered ($n_M = 3$). In the simplest case, the vector of non-conservative moments can be written in the form

$$\mathbf{M}^{NC} = \underbrace{\begin{bmatrix} \tau_1 \\ \tau_2 \\ \tau_3 \end{bmatrix}}_{\boldsymbol{\tau}} - \underbrace{\begin{bmatrix} b_1\dot{\theta}_1 \\ b_2\dot{\theta}_2 \\ b_3\dot{\theta}_3 \end{bmatrix}}_{\mathbf{F}} \tag{3.29}$$

where $\mathbf{F}$ is the vector of friction with b_i the viscous friction coefficient and $\boldsymbol{\tau}$ represents the vector of applied torque.

Combining (3.13), (3.28) and (3.29), the dynamic model of the human hand can be rewritten into the form

$$\mathbf{M}(\mathbf{q})\ddot{\mathbf{q}} + \mathbf{C}(\mathbf{q}, \dot{\mathbf{q}}) + \mathbf{F}(\mathbf{q}, \dot{\mathbf{q}}) + \mathbf{G}(\mathbf{q}, \dot{\mathbf{q}}) = \boldsymbol{\tau} \tag{3.30}$$

where $\boldsymbol{\tau}$ is the vector of moments produced through application of FES to muscles of the hand, and $\boldsymbol{F(q, \dot{q})}$ is the vector of frictional components acting about each joint.

(Freeman et al., 2009b). The elements of the symmetric inertia matrix are

$$\begin{aligned}
m_{11} =& m_1c_1^2 + m_2l_1^2 + m_2c_2^2 + 2m_2l_1c_2\cos\theta_2 + m_3l_1^2 \\
&+m_3l_2^2 + 2m_3l_1l_2\cos\theta_2 + 2m_3l_1c_3\cos(\theta_2+\theta_3) \\
&+2m_3l_2c_3\cos\theta_3 + m_3c_3^2 + J_1 + J_2 + J_3 \\
m_{12} =& m_2(c_2^2 + l_1c_2\cos\theta_2) + m_3l_2^2 + m_3c_3^2 + m_3l_1l_2\cos\theta_2 \\
&+m_3l_1c_3\cos(\theta_2+\theta_3) + 2m_3l_2c_3\cos\theta_3 + J_2 + J_3 \\
m_{13} =& m_3c_3^2 + m_3l_1c_3\cos(\theta_2+\theta_3) + m_3l_2c_3\cos\theta_3 + J_3, \\
m_{22} =& m_2c_2^2 + m_3l_2^2 + m_3c_3^2 + m_3l_2c_3\cos\theta_3 + J_3, \\
m_{23} =& m_3c_3^2 + m_3l_2c_3\cos\theta_3 + J_3 \\
m_{33} =& m_3c_3^2 + J_3
\end{aligned} \tag{3.31}$$

The elements of $\mathbf{C}(\mathbf{q}, \dot{\mathbf{q}})$ are

$$\begin{aligned}
c_{11} =& -[m_3c_3l_1s_{23} + m_3c_3l_2\sin\theta_3](2\dot{\theta_1}\dot{\theta_3} + 2\dot{\theta_2}\dot{\theta_3} + \dot{\theta_3^2}) \\
&-[(m_2l_1c_2 + m_3l_1l_2)\sin\theta_2 + m_3l_1c_3s_{12}](2\dot{\theta_1}\dot{\theta_2} + \dot{\theta_2^2}) \\
c_{21} =& [(m_2c_2l_1 + m_3l_1l_2)\sin\theta_2 + m_3c_3l_2s_{23}]\dot{\theta_1^2} \\
&- m_3c_3l_2\sin\theta_3(2\dot{\theta_1}\dot{\theta_3} + 2\dot{\theta_2}\dot{\theta_3} + \dot{\theta_3^2}) \\
c_{31} =& [m_3c_3l_2\sin\theta_3 + m_3c_3l_1s_{23}]\dot{\theta_1^2} \\
&+ m_3c_3l_2\sin(2\dot{\theta_1}\dot{\theta_2} + \dot{\theta_2^2})
\end{aligned} \tag{3.32}$$

where $s_{ij} = \sin(\theta_i + \theta_j)$. The vector of moments produced through application of FES is $\boldsymbol{\tau}$, and $\boldsymbol{F(q, \dot{q})}$ is the vector of frictional components acting about each joint, with the form

$$\boldsymbol{F(q, \dot{q})} = \begin{bmatrix} k_1(\theta_{0,1} - \theta_1) - b_1\dot{\theta}_1 \\ k_2(\theta_{0,2} - \theta_2) - b_2\dot{\theta}_2 \\ k_3(\theta_{0,3} - \theta_3) - b_3\dot{\theta}_3 \end{bmatrix} \tag{3.33}$$

where b_1, b_2 and b_3 are the viscous friction coefficients and $\boldsymbol{\tau}$ represents the vector of applied torque. It has been assumed that the muscle groups which actuate each joint produce a stiffness that may be represented by a spring with zero elongation at the initial position $\theta_{0,1}$, $\theta_{0,2}$ and $\theta_{0,3}$ and with stiffness coefficients k_1, k_2 and k_3.

Electrically stimulated muscles of the hand generate pulling forces causing the finger/thumb movement. Kinetic functions of the musculotendon units in the fingers, however, are especially difficult to evaluate due to their anatomical complexity and multiarticular character. However, moment arms at the different joints will differ, determining the relative effect of stimulation at each joint.

Each human finger has at least 6 muscles and 7 in the case of the index finger. The strength of the finger depends on the anatomical structure and the maximum effort of

each individual muscle involved (Brook et al., 1995). Moreover, muscles of fingers act through a complex tendon network, (the extensor mechanism). The network, firstly approximated by Winslow as a longitudinally symmetric tendon rhombus, was modified in subsequent research (Sancho-Bru et al., 2001; Valero-Cuevas et al., 2007).

The anatomical structure of fingers takes as inputs muscular actions and produces as outputs motions and forces. Many of the muscles/tendons within the finger span more than one joint, which means the muscle forces to joint torque relationship becomes more complicated. The tension along the muscle or tendon remains the same, even as it changes direction when crossing different joints. However, its moment arms at the different joints will differ, determining its relative effect at each joint in terms of actuating torque. The transformation from positive muscle forces $\boldsymbol{f}$ to the lower - dimensional net joint torques $\boldsymbol{\tau}$ at the finger joints can be defined as in (Valero-Cuevas, 2009)

$$\boldsymbol{\tau} = \mathbf{R}(\mathbf{q})\mathbf{f} = \begin{bmatrix} r_{11} & \dots & r_{1j} \\ \vdots & \ddots & \vdots \\ r_{i1} & \dots & r_{ij} \end{bmatrix} \begin{bmatrix} f_1 \\ \vdots \\ f_j \end{bmatrix} \tag{3.34}$$

where $\mathbf{R}(\mathbf{q})$ is matrix of moment arms where each entry is the signed scalar moment arm value that transforms a positive muscle force into torques at the various joints it crosses. Most techniques for estimating moment arm values rely on kinematic measurements, such as correlation between the tendon excursion and the resultant joint rotation (Brook et al., 1995), or the geometric distance between the tendon action line and the joint estimated using medical imaging techniques (Wilson et al., 1999).

Calculation of moment arm values

The r_{ij} element of the moment arm matrix can be evaluated by differentiating the excursion (displacement) E of the j^{th} tendon with respect to the i^{th} joint angle

$$r_{ij} = \frac{\partial E_j(q_i)}{\partial q_i} \tag{3.35}$$

Several dynamic muscle models of the finger have been developed to describe the kinetic functions of finger-muscle tendons. Landsmeer (Landsmeer, 1955) laid the foundation of later studies on spatial relationships between tendons and muscles and their associated joints in the hand. This paper proposed three different models of tendon-joint displacement relationships for flexion/extension of the finger. Although there is a lack of quantitative information in his studies, Landsmeer‘s models provided a basis for much future research. Determining exact muscle or tendon forces for dynamic modelling is extremely difficult. There exists the difficulty of measuring the

exact forces in the different tendons and muscles as various forces come into action at different points to produce a particular movement. Most of models use inverse dynamics to examine the muscle force coordination patterns that generate the observed movements (Brook et al., 1995) or fingertip force patterns (Sancho-Bru et al., 2001). Additionally, existing models are only valid for certain hand configurations (Chao et al., 1976; Roloff et al., 2006; Sghaier et al., 2007).

3.2 Musculotendon system

The musculoskeletal structure of the finger and wrist included in the model is shown in Figure 3.2. The wrist joint is assumed to be actuated by three extensor muscles: Extensor Communis (EC), Extensor Carpi Radialis Longus (ECR) and Extensor Carpi Ulnaris (ECU). The muscles of the finger act through a complex tendon network, termed the extensor mechanism. The network is approximated by a longitudinally symmetric tendon rhombus, consisting of active and the passive tendons, as shown in Figure 3.2.The proposed finger model is based on the biomechanical model given in (Theodorou et al., 2011). The extensor mechanism of the finger includes 5 active tendons, driven by independently controlled muscles: the Flexor Digitorum Profundus (FDP), the Extensor Digitorum Communis (EC), the Ulnar and Radial Interosseous (UI and RI), the Lumbrical muscle (LU), and 3 passive tendons: the Radial Band (RB) the Ulnar Band (UB) and the Extensor Slip (ES).

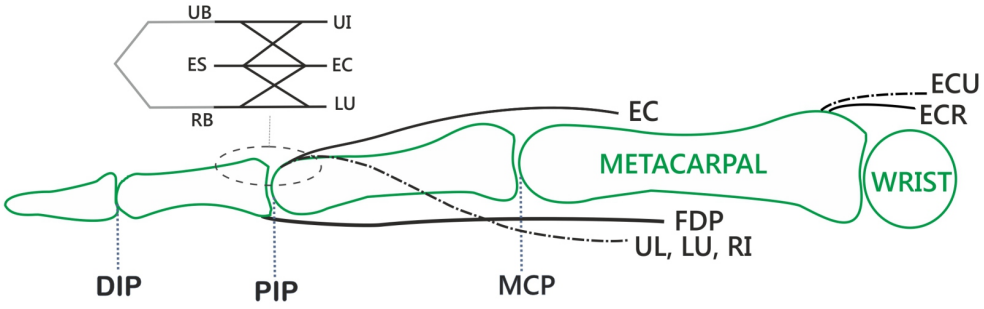

Figure 3.2: The network of the finger tendons (Vigouroux et al., 2006)

For the flexor muscle FDP, III. Landsmeer's model shown in Figure 3.3 is used (Landsmeer, 1955), where excursion is given by

$$E^{tendon} = \theta d^{tendon} + 2y^{tendon}\left(1 - \frac{\theta/2}{\tan(\theta/2)}\right) \tag{3.36}$$

where d^{tendon} is the distance from the straight part of the tendon towards the long axis and θ is the corresponding angle rotation. The term y^{tendon} corresponds to the distance

from the end of the straight part towards the joint centre. This distance is measured along the axis of the bone.

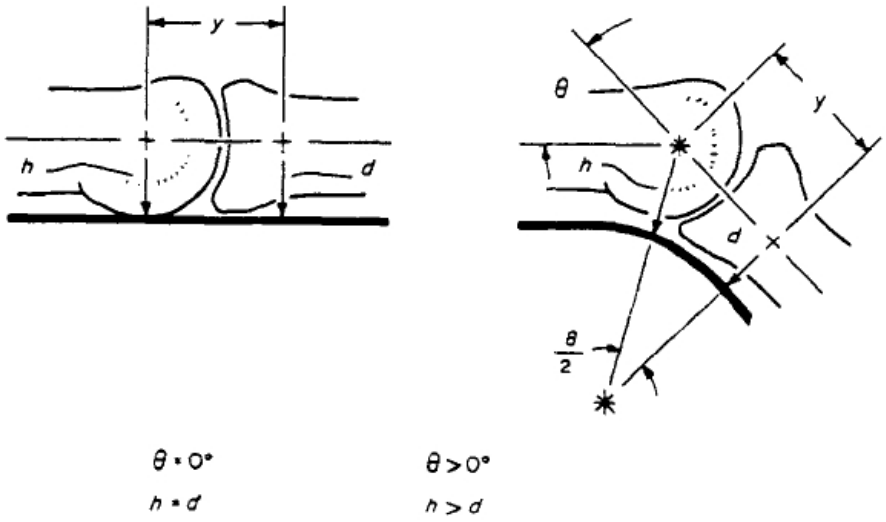

Figure 3.3: The III Landsmeer model of the finger (Armstrong and Chaffin, 1978)

The remaining tendons are modelled as second order polynomial approximation of (3.36)

$$(b^{tendon} + h_{tendon}\theta)\theta \tag{3.37}$$

where b^{tendon} and h^{tendon} are constants.

The tendon excursion of the EC is a function of the wrist and MCP with the addition of the displacement, transformed to the PIP joint through the extensor mechanism

$$E^{EC} = -r_1^{EC}\theta_1 - r_2^{EC}\theta_2 + L(E_1, E_2, E_3) \tag{3.38}$$

where

$$E_1 = E^{ES}, \quad E_2 = E^{UB}, \quad E_3 = E^{RB} \tag{3.39}$$

and $L(E_1, E_2, E_3)$ is the excursion function defined as

$$L(E_1, E_2, E_3) = \sum_{i=1}^{3} w_i E_i = 0, \quad w_i > 0 \quad \forall j = 1, 2, 3 \tag{3.40}$$

The excursions of remaining tendons in the considered case are expressed as functions of finger extension/flexion angles θ_2 and θ_3. They are as follows

$$\begin{aligned}
E^{FDP} &= \sum_{i=2}^{3} \theta_i^{FDP} + 2y_i^{FDP}\left(1 - \frac{\theta_i/2}{\tan(\theta_i/2)}\right) \\
E^{ES} &= -r^{ES}\theta_3 \\
E_{RB} &= -(b^{RB} + h^{RB}\theta_3)\theta_3 \\
E_{UB} &= -(b^{UB} + h^{UB}\theta_3)\theta_3 \\
E^{RI} &= (b^{RI} + h^{RI}\theta_2)\theta_2 + E^{UB} \\
E^{UI} &= (b^{UI} + h^{UI}\theta_2)\theta_2 + E^{UB} \\
E^{LU} &= (b^{LU} + h^{LU}\theta_2)\theta_2 + E^{RB} - E^{FDP} \\
E^{ECU} &= (b^{ECU} + h^{ECU}\theta_1)\theta_1 \\
E^{ECR} &= (b^{ECR} + h^{ECR}\theta_1)\theta_1
\end{aligned} \tag{3.41}$$

Hence, applying (3.35), each column of moment arm matrix $\mathbf{R}(\mathbf{q})$ represents the moment arm vector corresponding to each muscle, yielding

$$\mathbf{R}(\mathbf{q}) = \left[\mathbf{R}^{FDP}, \mathbf{R}^{LU}, \mathbf{R}^{UI}, \mathbf{R}^{RI}, \mathbf{R}^{EC}, \mathbf{R}^{ECR}, \mathbf{R}^{ECU}\right] \tag{3.42}$$

Here the moment arm vectors for FDP is

$$\mathbf{R}^{FDP} = \begin{bmatrix} 0 \\ d_1^{FDP} + y_1^{FDP}\left(\frac{\sin(\theta_2)-\theta_2}{2\sin^2(\theta_2)}\right) \\ d_2^{FDP} + y_2^{FDP}\left(\frac{\sin(\theta_3)-\theta_3}{2\sin^2(\theta_3)}\right) \end{bmatrix} \tag{3.43}$$

and the moment arm vector for LU is given by

$$\mathbf{R}^{LU} = \begin{bmatrix} 0 \\ b^{LU} + 2h^{LU}\theta_2 - R_{\theta_2}^{FDP} \\ -b^{RB} - 2h^{RB}\theta_3 - R_{\theta_3}^{FDP} \end{bmatrix} \tag{3.44}$$

The moment arm vector for UI is

$$\mathbf{R}^{UI} = \begin{bmatrix} 0 \\ b^{UI} + 2h^{UI}\theta_2 \\ -b^{UB} - 2h^{UB}\theta_3 \end{bmatrix} \tag{3.45}$$

and the moment arm vector for EC has the form

$$\mathbf{R}^{EC} = \begin{bmatrix} -r_1^{EC} \\ -r_2^{EC} \\ -w_1 r^{ES} + w_2 R_{\theta_3}^{UB} + w_3 R_{\theta_3}^{RB} \end{bmatrix} \tag{3.46}$$

where

$$R_{\theta_3}^{UB} = -(b^{UB} + 2h^{UB}\theta_3) \tag{3.47}$$

$$R_{\theta_3}^{RB} = -(b^{RB} + 2h^{RB}\theta_3) \tag{3.48}$$

The moment arm vector for ECR equals

$$\boldsymbol{R}^{ECR} = \begin{bmatrix} b^{ECR} + 2h^{ECR}, & 0, & 0 \end{bmatrix}^T \tag{3.49}$$

and the moment arm vectors for ECU is

$$\boldsymbol{R}^{ECU} = \begin{bmatrix} b^{ECU} + 2h^{ECU}, & 0, & 0 \end{bmatrix}^T \tag{3.50}$$

Using relation (3.34), the torque at each joint can now be calculated as a function of the force in each muscle and the current joint angle vector. Each element of the muscle force vector $\mathbf{f}(\mathbf{u}, \mathbf{q}, \dot{\mathbf{q}})$ comprises the moment produced through the application of FES signal $u_j(t)$ to the j^{th} stimulated muscle, with

$$\boldsymbol{u} = \begin{bmatrix} u_1 & \cdots & u_m \end{bmatrix}^T \tag{3.51}$$

As discussed in (Le et al., 2010), the most prevalent form of muscle representation is a Hill-type model of the form

$$f_i\left(u_i(t), q_i, \dot{q}_i\right) = h_i(u_i, t) \times F_{m,i}(q_i, \dot{q}_i), \quad i = 1, \cdots, m \tag{3.52}$$

The term $F_{m,i}(q_i, \dot{q}_i)$ models the multiplicative effect of the muscle length q_i and muscle velocity $\dot{q}_i$ on the active torque developed by the muscle and here for simplicity it is assumed, that $F_{m,i}(q_i, \dot{q}_i) \approx 1$. The term, $h_i(u_i, t)$ is a Hammerstein structure incorporating a static non-linearity, $h_{IRC,i}(u_i)$, representing the isometric recruitment curve, cascaded with linear activation dynamics, $h_{LAD,i}(t)$ These typically are second order, and in the considered case are modelled as a second order critically damped system with a natural frequency ω_n, and will be represented by the state-space model matrices $\mathbf{M}_{A,i}$, $\mathbf{M}_{B,i}$, $\mathbf{M}_{C,i}$. The complete model is presented in the appendix A.

3.3 FES control of hand and wrist using Newton method-based ILC

Often physical systems must be considered in the presence of constraints. The FES-based system, is an example of system with input constraints as it is required to generate only suitable electrical pulse signals to activate appropriate muscles in the hand and wrist. The activated muscles contract developing muscle forces, that combine to produce a desired movement/torque of the musculoskeletal system. Different

stimulation parameters can be used as controlled variables, i.e. the current/voltage amplitude or the duration of the stimulus pulses (pulse-width). In the considered case, the pulse-width parameter was chosen to be the input of the system, since it provides a more consistent response across subjects, requires a smaller charge per stimulus pulse, and allows for greater selectivity of recruitment. The practical values of pulse-width, that can be safely applied during the trails on human subjects, are within a range $[0, 300\mu s]$.

To take the design constraints as discussed into account, the point-to-point Newton method-based ILC with input constraint is used. The algorithm is applied to the hand and wrist system in simulation to investigate feasibility and performance capabilities prior to its future experimental use.

System description

From (3.30) the relationship between stimulation and joint angles can be expressed in state-space form as

$$\begin{aligned}\dot{\mathbf{x}}(t) &= \begin{bmatrix} \dot{\mathbf{q}} \\ \mathbf{M}(\mathbf{q})^{-1}\mathbf{X}(\mathbf{q},\dot{\mathbf{q}}) \\ \mathbf{M}_{A,1}x_1 \\ \vdots \\ \mathbf{M}_{A,p}x_p \end{bmatrix} + \begin{bmatrix} \mathbf{0} \\ \mathbf{0} \\ \mathbf{M}_{B,1}h_{\mathrm{IRC},1}(u_1) \\ \vdots \\ \mathbf{M}_{B,p}h_{\mathrm{IRC},p}(u_p) \end{bmatrix} \\ &:= \mathbf{f}\left(\mathbf{x}(t), \mathbf{u}(t)\right) \\ \mathbf{q}(t) &= \begin{bmatrix} \mathbf{I} & \mathbf{0} & \cdots & \mathbf{0} \end{bmatrix} \mathbf{x}(t) := \mathbf{h}\left(\mathbf{x}(t)\right)\end{aligned} \tag{3.53}$$

where $\mathbf{x} = [\mathbf{q}^T,\ \dot{\mathbf{q}}^T,\ x_1\ \cdots\ x_j]^T$ and $\mathbf{X}(\mathbf{q},\dot{\mathbf{q}})$ has i^{th} row

$$\mathbf{R}_i(\mathbf{q})\mathbf{M}_{C,i}x_i\ F_{m,i}(\mathbf{q},\dot{\mathbf{q}}) - \mathbf{C}_i(\mathbf{q},\dot{\mathbf{q}}) + \mathbf{F}_i(\mathbf{q},\dot{\mathbf{q}}) \tag{3.54}$$

Hence, the ILC is an iterative approach, it can be formulated in the discrete-time domain. The discretised nonlinear stimulated hand and wrist system (3.53) has form (for details see the appendix A)

$$\begin{aligned}\mathbf{x}_k(t+1) &= \mathbf{f}[\mathbf{x}_k(t), \boldsymbol{u}_k(t)] \\ \mathbf{q}_k(t) &= \mathbf{h}[\mathbf{x}_k(t)]\end{aligned} \tag{3.55}$$

where $k = 1, 2, \ldots$ is the trial number, $t \in [0, 1, 2, ..., N-1]$ is the sample number and $\mathbf{x}_k(t)$, $\boldsymbol{u}_k(t)$ and $\mathbf{q}_k(t)$ are the state, input and output vectors respectively on the k^{th} trial. To replace (3.55) with a set of algebraic equations in $\mathbb{R}^N$, define the shifted input

and output vectors as

$$\begin{aligned} \boldsymbol{u}_k &= [\boldsymbol{u}_k(0)^T, \boldsymbol{u}_k(1)^T, \ldots, \boldsymbol{u}_k(N-1)^T]^T \quad \in \mathbb{R}^{mN} \\ \mathbf{q}_k &= [\mathbf{q}_k(1)^T, \mathbf{q}_k(2)^T, \ldots, \mathbf{q}_k(N)^T]^T \quad \in \mathbb{R}^{pN} \end{aligned}$$

and the relationship between the input and output time-series can be expressed by the following algebraic functions

$$\begin{aligned} \mathbf{q}_k(1) &= \mathbf{h}(\mathbf{x}_k(1)) = \mathbf{h}(\boldsymbol{f}(\mathbf{x}_k(0), \boldsymbol{u}_k(0))) \\ &= \boldsymbol{g}_1(\boldsymbol{x}_k(0), \boldsymbol{u}_k(0)) \\ &\vdots \\ \mathbf{q}_k(N) &= \boldsymbol{h}(\boldsymbol{x}_k(N)) = \boldsymbol{h}(\boldsymbol{f}(\boldsymbol{x}_k(N-1), \boldsymbol{u}_k(N-1))) \\ &= \boldsymbol{g}_N(\boldsymbol{x}_k(0), \boldsymbol{u}_k(0), \boldsymbol{u}_k(1), \ldots, \boldsymbol{u}_k(N-1)) \end{aligned}$$

Hence the system (3.53) can be represented as

$$\mathbf{q}_k = \boldsymbol{g}\left(\boldsymbol{u}_k\right), \quad \boldsymbol{g}(\cdot) = \left[\boldsymbol{g}_1(\cdot)^T, \boldsymbol{g}_2(\cdot)^T, \ldots, \boldsymbol{g}_N(\cdot)^T\right]^T$$

To control hand posture it is necessary to specify the desired joint positions at a fixed number, $M \leq N$, of sample instants given by $1 \leq n_1 < n_2 < \cdots < n_M \leq N$. Let the prescribed joint positions at these instants be

$$\mathbf{q}^* = [\mathbf{q}^*(0)^T, \mathbf{q}^*(1)^T, \ldots, \mathbf{q}^*(M-1)^T]^T \quad \in \mathbb{R}^{pM}$$

ILC can be considered an iterative numerical solution to the problem of finding a control input which solves

$$\min_{\mathbf{u}} J(\mathbf{u}) \quad \text{subject to} \quad \Lambda\mathbf{u} \preceq \mathbf{b}, \qquad J(\mathbf{u}) = \|\mathbf{q}^* - \Phi\mathbf{g}(\mathbf{u})\|_2^2 \tag{3.56}$$

Here $J(\mathbf{u})$ is the point-to-point error norm, and the $pM \times pN$ matrix Φ has block-wise entries

$$\Phi_{i,j} = \begin{cases} I_p & j = n_i, \quad i = 1, 2 \ldots M \\ 0_p & \text{otherwise} \end{cases} \tag{3.57}$$

where I_p and 0_p are the $p \times p$ identity and zero matrices respectively. Due to the requirement that each FES input is bounded, $u_m \leq u_i \leq u_M$, it is necessary to apply vector inequality constraints on the system input of the form $\Lambda\mathbf{u} \preceq \mathbf{b}$, where $\Lambda = [-I, I]^T$ and $\mathbf{b} = [u_m \ldots u_m, u_M \ldots u_M]^T$.

Temporarily neglecting the constraint, the iterative solution of the ILC optimisation problem via the Newton method is

$$\begin{aligned}\mathbf{u}_{k+1} &= \mathbf{u}_k - \nabla^2 J\left(\mathbf{u}_k\right)^{-1} \nabla J\left(\mathbf{u}_k\right) \\ &= \mathbf{u}_k + \left(\Phi \mathbf{g}'(\mathbf{u}_k)\right)^{\dagger} \left(\mathbf{q}^* - \Phi \mathbf{g}(\mathbf{u}_k)\right)\end{aligned} \tag{3.58}$$

where $\mathbf{g}'(\mathbf{u}_k) = \frac{\delta \mathbf{g}(\mathbf{u}_k)}{\delta \mathbf{u}}$, and in the ILC framework $\mathbf{q}^* - \Phi \mathbf{g}(\mathbf{u}_k)$ is replaced with the experimental point-to-point error $\mathbf{e}_k = \mathbf{q}^* - \Phi \mathbf{q}_k$. The descent direction term in (3.58) is the solution $\bar{\mathbf{u}}$ to

$$\min_{\bar{\mathbf{u}}} \|\bar{\mathbf{u}}\|_2^2 \qquad \text{subject to} \quad \Phi \mathbf{g}'(\mathbf{u}_k)\bar{\mathbf{u}} = \mathbf{e}_k \tag{3.59}$$

and hence applying the constraint $\Lambda \mathbf{u}_{k+1} \preceq \mathbf{b}$, which translates to $\Lambda \bar{\mathbf{u}} \preceq \mathbf{b} - \Lambda \mathbf{u}_k$, (3.56) is solved using

$$\mathbf{u}_{k+1} = \mathbf{u}_k + \Delta \mathbf{u}_k \tag{3.60}$$

with $\Delta \mathbf{u}_k$ the solution to

$$\min_{\bar{\mathbf{u}}} \|\bar{\mathbf{u}}\|_2^2 \qquad \text{subject to} \quad \begin{cases} \Phi \mathbf{g}'(\mathbf{u}_k)\bar{\mathbf{u}} &= \mathbf{e}_k \\ \Lambda \bar{\mathbf{u}} &\preceq \mathbf{b} - \Lambda \mathbf{u}_k \end{cases}$$

From (Freeman et al., 2011b) this is solved by applying the gradient method to

$$\min_{\mathbf{u}} \|\mathbf{q}^* - \Phi \mathbf{q}_k - \Phi \mathbf{g}'(\mathbf{u}_k)\mathbf{u}\|_2^2 \qquad \text{subject to} \quad \Lambda \mathbf{u} \preceq \mathbf{b} - \Lambda \mathbf{u}_k$$

using the barrier method, with corresponding update

$$\mathbf{u}_{j+1} = \mathbf{u}_j + \alpha \left(\Phi \mathbf{g}'(\mathbf{u}_k)\right)^T \left(\mathbf{e}_k - \Phi \mathbf{g}'(\mathbf{u}_k)\mathbf{u}_j\right) - \frac{1}{\tau_j} \Lambda^T \mathbf{d} \tag{3.61}$$

applied to the plant $\Phi \mathbf{g}'(\mathbf{u}_k)$, where the elements of $\mathbf{d}$ are given by $d_i = 1/(b_i - \mathbf{\Lambda}_i^T(\mathbf{u}_j + \mathbf{u}_k))$. This is performed multiple times between trial k and $k+1$ in order to generate the decent term $\Delta \mathbf{u}_k$ in (3.60). The parameter τ_j is increased at each inter-trial update j in order to reach the hard constraint, as described in (Freeman et al., 2011b). Note that no large matrix calculations are required within (3.61) since $\boldsymbol{w} = \mathbf{g}'(\mathbf{u}_k)\boldsymbol{v}$ corresponds to the linear time-varying system

$$\begin{aligned}\tilde{\boldsymbol{x}}(t+1) &= \boldsymbol{A}(t)\tilde{\boldsymbol{x}}(t) + \boldsymbol{B}(t)\boldsymbol{v}(t) \\ \boldsymbol{w}(t) &= \boldsymbol{C}(t)\tilde{\boldsymbol{x}}(t) + \boldsymbol{D}(t)\boldsymbol{v}(t) \qquad t = 0, \ldots, N-1\end{aligned}$$

where

$$\begin{aligned}\boldsymbol{A}(t) &= \left(\frac{\partial \mathbf{f}}{\partial \boldsymbol{x}}\right)_{\mathbf{u}_k(t), \boldsymbol{x}_k(t)}, \quad \boldsymbol{B}(t) = \left(\frac{\partial \mathbf{f}}{\partial \mathbf{u}}\right)_{\mathbf{u}_k(t), \mathbf{x_k}(\mathbf{t})} \\ \boldsymbol{C}(t) &= \left(\frac{\partial \mathbf{h}}{\partial \boldsymbol{x}}\right)_{\mathbf{u}_k(t), \boldsymbol{x}_k(t)}, \quad \boldsymbol{D}(t) = \left(\frac{\partial \mathbf{h}}{\partial \boldsymbol{u}}\right)_{\mathbf{u}_k(t), \boldsymbol{x}_k(t)}\end{aligned}$$

Similarly the term $\boldsymbol{w} = (\boldsymbol{g}'(\boldsymbol{u}_k))^T \boldsymbol{v}$ equates to the system

$$\tilde{\boldsymbol{x}}(t+1) = \boldsymbol{A}^T(t)\tilde{\boldsymbol{x}}(t) + \boldsymbol{C}^T(t)\boldsymbol{v}(N-1-t)$$
$$\boldsymbol{w}(N-1-t) = \boldsymbol{B}^T(t)\tilde{\boldsymbol{x}}(t) + \boldsymbol{D}^T(t)\boldsymbol{v}(N-1-t)$$

Convergence and robustness properties are given in (Freeman et al., 2011b), and in particular, convergence to zero error requires that $\Phi\mathbf{g}'(\mathbf{u}_k)$ has full row rank. This thereby allows point-to-point locations to be chosen to recover feasibility in the presence of a high coupled interaction matrix $\mathbf{R}(\mathbf{q})$.

3.4 Simulation Evaluation

The point-to-point ILC based control approach was tested in simulation using the previously described model of the wrist and hand. The complete model and values of the model parameters used in the simulation are presented in the appendix A. The clinically relevant task considered during simulation was to move the hand from initial flexed position defined by $\boldsymbol{q_0}$ to the final reference (extended) position $\boldsymbol{q}^*$. These can be treated as approximate representation of the hand opening movement, crucial during performing basic hand operations such as grasping and realising objects. To investigate the general behaviour of the system and performance of the algorithm, a number of simulations was performed for tracking a variety of different final positions. These can be interpreted as control of alternate hand opening with different apertures in order to grasp objects of different sizes.

The extrinsic muscles are generally more compatible with surface FES compared with intrinsic ones. Hence, to investigate a feasibility of surface FES two separate cases were considered

1. stimulation is applied to all muscles,
2. only extrinsic muscles are stimulated

Practical stimulation limits ($u_m = 0$, $u_M = 300\mu$) were applied, which represent standard range of pulse width values with u_M denoting a maximal stimulation that can be safely applied to the muscle. Simulation studies have indicated, that a wide variety of point-to-point movements can be achieved via extrinsic muscle stimulation, however this type of stimulation requires higher levels of stimulation signal. The movement from initial position $\boldsymbol{q}_0 = [2.1, 1.6, 1.05]$ to the final reference position $\boldsymbol{q}^* = [1.57, 0.47, 0.21]$ defined in radians was chosen as a representative one from a set of those considered in simulation studies. This movement can be an approximate representation of a relaxation movement of i.e. spastic hand from its initially flexed position to the final straighten one.

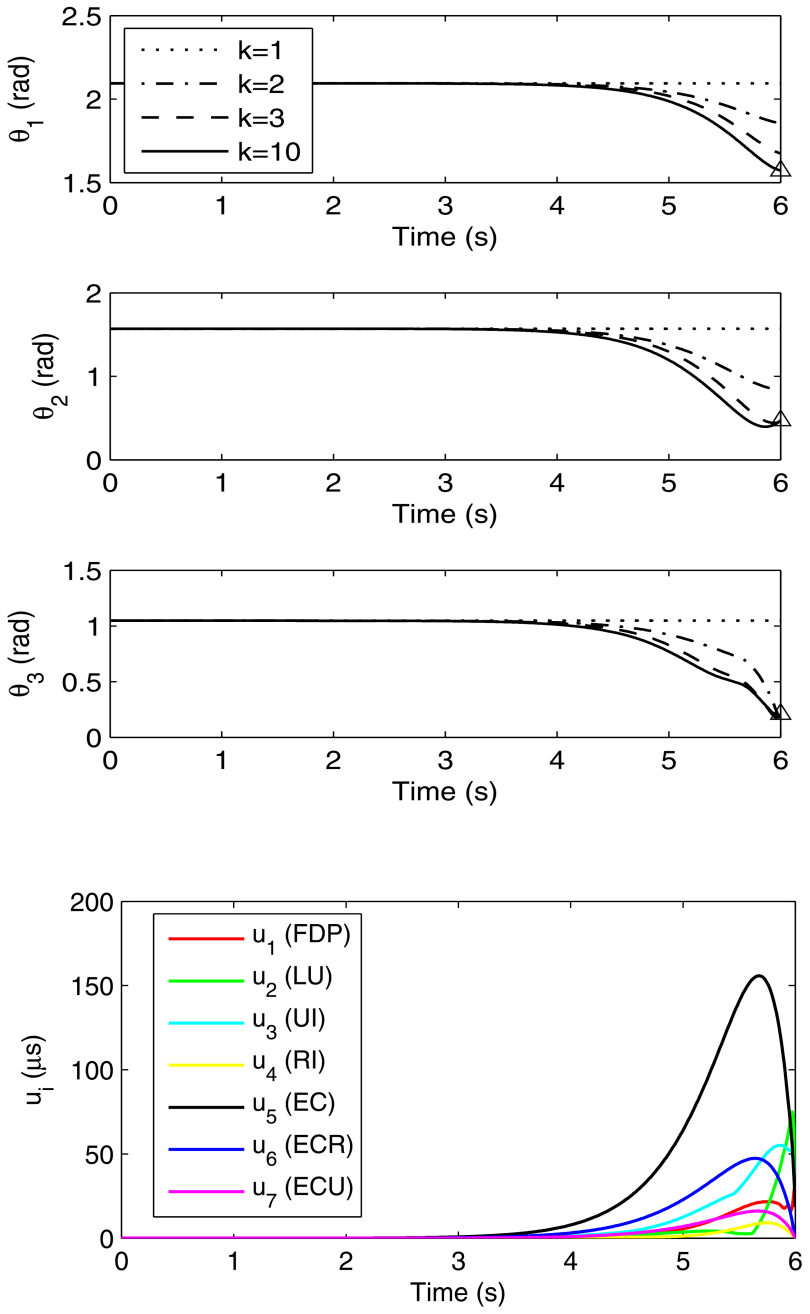

Figure 3.4: Stimulation of extrinsic and intrinsic muscles using Newton method-based point-to-point ILC with inequality constraint. First three figures show output trajectories on four different k trials ($k = 1, k = 2, k = 3, k = 10$) and the 4th Figure shows input values on the last $k = 10$ trial.

Figures 3.4 and 3.5 show joint trajectories over 10 trials, together with FES inputs on the final trial. As shown in Figures 3.6 and 3.7, error convergence for both types of stimulation shows high accuracy achieved in a small number of trials.

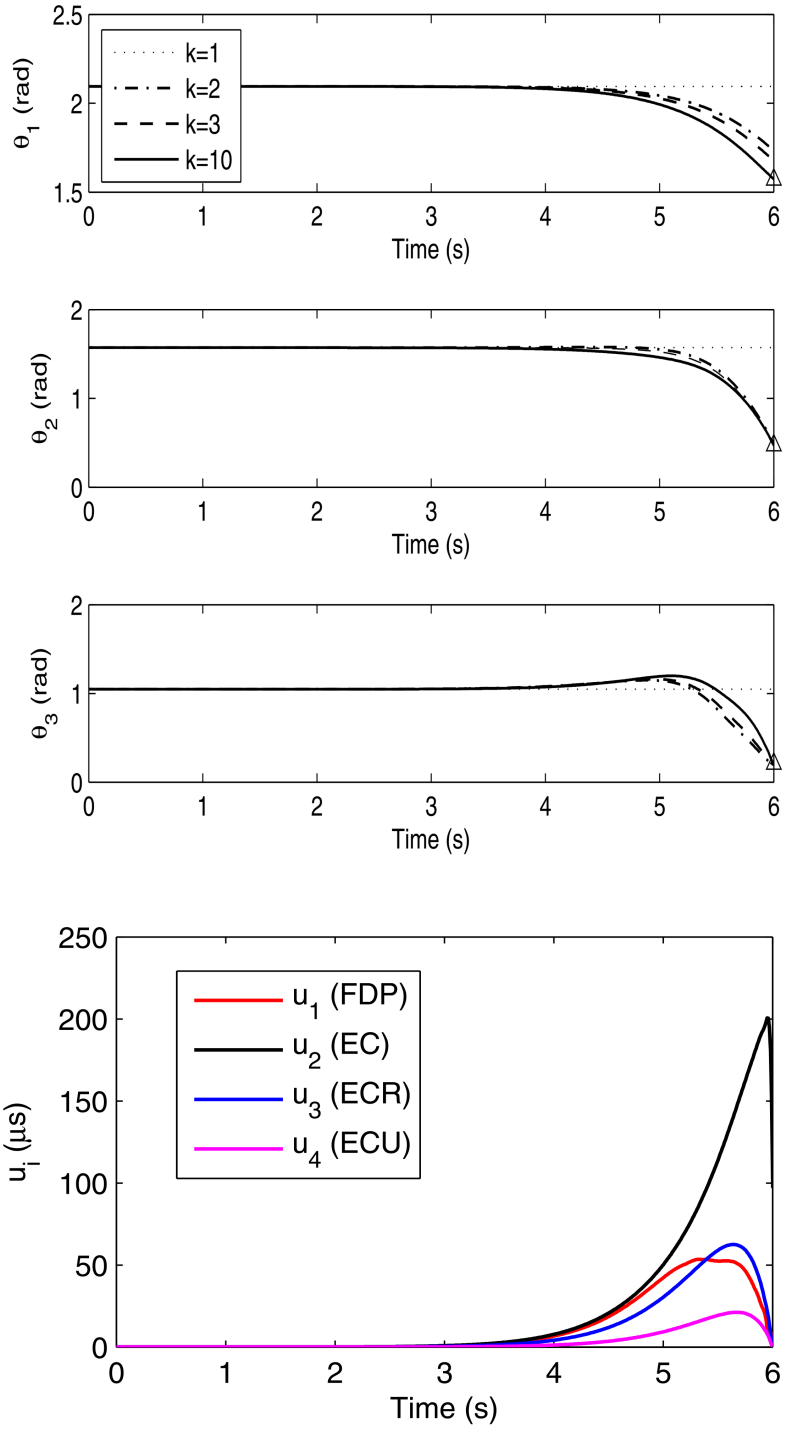

Figure 3.5: Stimulation of extrinsic muscles using Newton method-based point-to-point ILC with inequality constraint. First three figures show output trajectories on four different k trials ($k = 1, k = 2, k = 3, k = 10$) and the 4th Figure shows input values on the last trial ($k = 10$).

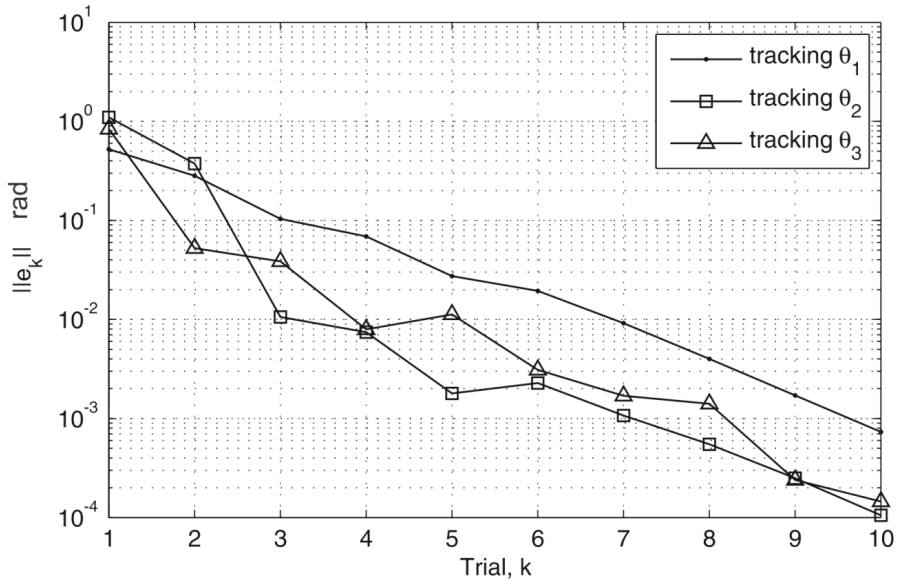

Figure 3.6: Stimulation of extrinsic and intrinsic muscles using Newton method-based point-to-point ILC: error norm.

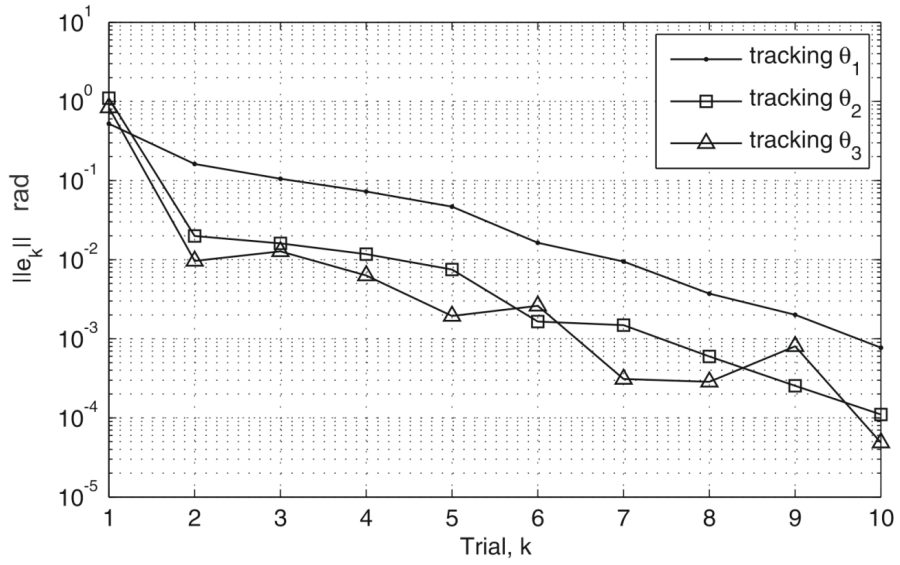

Figure 3.7: Stimulation of extrinsic muscles using Newton method-based point-to-point ILC with inequality constraint: error norm.

The results, hence, confirm effectiveness of ILC-based method for control of non-prehensile movements (such as hand opening), when only extrinsic muscles are stimulated. However, simulation studies have indicated that stimulation of extrinsic muscles results in increased input norms and hence likelihood of increased muscle fatigue, especially for the EC muscle.

3.5 Summary and discussion

Although simulation studies have established the feasibility of model-based ILC of the hand and wrist using FES of extrinsic muscles, the practical use of the considered model of the hand and wrist is strongly related to the selectivity of stimulation. In case of surface stimulation the selectivity depends of the size and appropriate placement of the electrodes. Although, research has provided evidences, that it is possible to selectively stimulate different fingers (Westerveld et al., 2012), this is most likely the result of stimulation of individual muscle parts through individual nerve branches. In this case i.e., the contraction of different branches of EC can induce extension of separate fingers. Thus to be able to apply the proposed model-based control for this type of a selective stimulation, additional knowledge of the subject‘s model and its properties is required.

Clearly the complexity and number of muscles in the model must align with those muscles likely to be actuated through the proposed surface stimulation. The model however extends beyond what is likely to be achievable, which allows scope for future application, using implanted electrodes or more precise electrode arrays. However, proposed model can be easily modified (i.e. by removing/adding muscles) once the selectivity of stimulation is established experimentally. The choice of the model depends on the selectivity of the task, i.e. cylindrical release requires less selectiveness than assisting the pinch grip or other more complex manual tasks. These are the factors, that require further research and examination in order to efficiently use the model-based control of hand and wrist in practice. Some of these aspects of the overall problem are discussed in the next chapter.

Chapter 4

Surface Electrode Array based Control of the Wrist and Hand

Surface Electrode Array (SEA)-based electrical stimulation is a non-invasive method of muscle activation, that uses adhesive electrodes placed on the surface of the patient skin above the location of the desired muscles. In SEA-based stimulation movement in a paralysed or weak limb is induced by sending a series of electrical pulses to associated skeletal muscles through activation of chosen elements of electrode array. Activated elements constitute a stimulation pattern. The optimal stimulation pattern is a map that determines which electrode or combination of electrodes must be activated to achieve a desired movement Schill et al. (2009). The movement is controlled by modulation of the control input $\boldsymbol{u}$. In the multi-channel case, separate stimulation signals can be passed through selected elements of electrode array, see Figure 4.1.

SEA-based electrical stimulation has the potential to be an effective technique for stroke rehabilitation of the upper-limb. However, the effectiveness of the method is strongly related to the precision and accuracy of the stimulation. The precision of stimulation is associated with the accurate selection of the optimal stimulation pattern and with the selectivity of stimulation (Westerveld et al., 2012). These are essential for functionality and ease of application. The specific character of SEA-based control of the human hand and wrist, makes the design process a difficult task compared with the control of mechanical systems, where the main difficulties arise from the biomechanical nature of the system. This requires that the additional patient-oriented factors such as patient response and safety issues are taken into account during the process of controller design and implementation.

Small electrodes are able to more precisely target muscles for selective activation than larger electrodes (Westerveld et al., 2012), potentially inducing more precise

movements of the fingers and wrist if the stimulation signal is appropriately controlled.

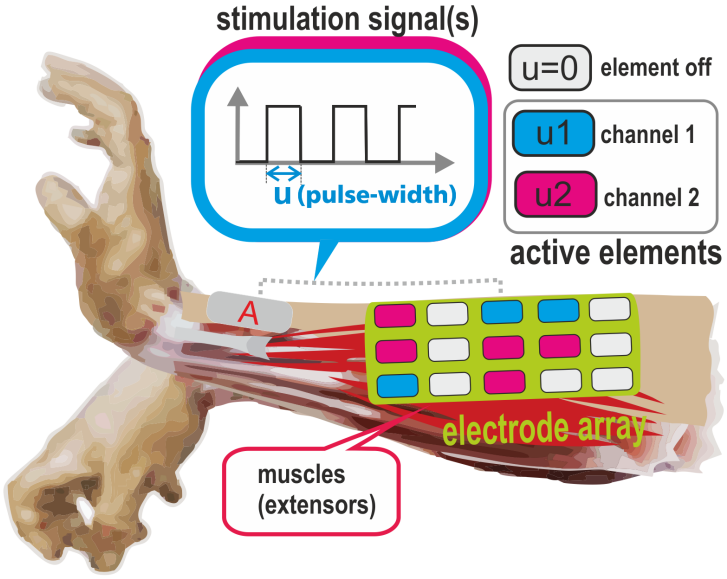

Figure 4.1: Surface Electrode Array Stimulation - schematic of technique

For smaller electrodes there is a higher possibility of occuring deviation in electrode location during the movement. Additionally, a larger number of smaller electrodes is required to span all the area of the target muscles, compared with larger electrodes used for the same purpose. This increases the search space for optimisation algorithms, making the problem of selecting optimal stimulation patterns more difficult task.

Another recognised problem, that can limit practical use of SEA-based technologies is the activation of sensory receptors on the skin surface during the stimulation process. The sensation of stimulation and level that can trigger the pain vary from one subject to another. Single element stimulation can cause irritation and discomfort or even pain sensation, if the stimulation intensity increased above a certain limit Lyons et al. (2004). Generally the smaller single element the lower the level of the stimulation that triggers the pain sensation.

To overcome this problem a group of single array elements was selected to emulate the single elements of the electrode array and were used in the optimization procedure. This emulated single array element is termed a “virtual element” of the electrode array. Each type of “virtual element” can be defined by its size (the number of single electrode array elements) and the spatial configuration of the single elements used.

4.1 System and Problem Description

In the most general case the problem of how to select the stimulation level applied to each element of electrode array is based on representing the hand and wrist as a non-linear dynamic system. Consider m elements and p joint angles and at time t define the input and output vectors

$$\boldsymbol{u}(t) = \begin{bmatrix} \boldsymbol{u}_1(t) \\ \vdots \\ \boldsymbol{u}_m(t) \end{bmatrix} \in \mathbb{R}^m, \qquad \boldsymbol{y}(t) = \begin{bmatrix} \boldsymbol{y}_1(t) \\ \vdots \\ \boldsymbol{y}_p(t) \end{bmatrix} \in \mathbb{R}^p \tag{4.1}$$

To model the relationship between stimulation inputs and joint angle outputs, the non-linear discrete-time system

$$\begin{aligned} \boldsymbol{x}(t+1) &= \boldsymbol{f}\left(\boldsymbol{x}(t), \boldsymbol{u}(t)\right) \\ \boldsymbol{y}(t) &= \boldsymbol{h}\left(\boldsymbol{x}(t)\right), \qquad\qquad \boldsymbol{x}(0) = x_0 \end{aligned} \tag{4.2}$$

model is assumed over the sample times $t = 0, 1, \ldots, N-1$ with state vector $x \in \mathbb{R}^r$. Here $f(\cdot)$ and $h(\cdot)$ are assumed to be continuously differentiable with respect to t and the total time duration is $T = (N-1)T_s$.

An equivalent analysis description uses the supervectors

$$\boldsymbol{u} = \begin{bmatrix} \boldsymbol{u}(0) \\ \vdots \\ \boldsymbol{u}(N-1) \end{bmatrix} \in \mathbb{R}^{mN}, \ \boldsymbol{y} = \begin{bmatrix} \boldsymbol{y}(1) \\ \vdots \\ \boldsymbol{y}(N) \end{bmatrix} \in \mathbb{R}^{pN} \tag{4.3}$$

to give $\mathbf{y} = \boldsymbol{g}(\boldsymbol{u})$ where

$$\boldsymbol{g}(\cdot) = \begin{bmatrix} \boldsymbol{g}_1(\cdot)^T & \cdots & \boldsymbol{g}_N(\cdot)^T \end{bmatrix}^T \tag{4.4}$$

with elements

$$\begin{aligned} \boldsymbol{g}_i(\boldsymbol{x}(0), \boldsymbol{u}(0), \boldsymbol{u}(1), \ldots, \boldsymbol{u}(i-1)) &= \boldsymbol{h}(\boldsymbol{x}(i)) \\ &= \boldsymbol{h}(\boldsymbol{f}(\boldsymbol{x}(i-1), \boldsymbol{u}(i-1))), \\ &= \boldsymbol{h}(\boldsymbol{f}(\boldsymbol{f}(\boldsymbol{x}(i-2), \boldsymbol{u}(i-2)), \boldsymbol{u}(i-1))), \\ &\vdots \\ &= \boldsymbol{h}(\boldsymbol{f}(\boldsymbol{f}(\cdots \boldsymbol{f}(\boldsymbol{x}(0), \boldsymbol{u}(0)), \cdots, \boldsymbol{u}(i-2)), \boldsymbol{u}(i-1))), \end{aligned} \tag{4.5}$$

over $i = 1, \ldots N$. In this formulation $\boldsymbol{g}(\cdot)$ represents the hand and wrist response to applied stimulation.

The general problem of tracking a desired reference $y_d(t)$, alternatively expressed by the supervector

$$\boldsymbol{y}_d = \begin{bmatrix} \boldsymbol{y}_d(0) \\ \vdots \\ \boldsymbol{y}_d(N-1) \end{bmatrix} \quad \in \mathbb{R}^{pN} \tag{4.6}$$

requires the construction of a sequence of stimulation inputs, $\{\boldsymbol{u}_k\}_{k=0,1,\ldots,\infty}$ such that

$$\lim_{k\to\infty} \|\boldsymbol{y}_d - \boldsymbol{g}(\boldsymbol{u}_k)\| = 0, \qquad \lim_{k\to\infty} \|\boldsymbol{u}_d - \boldsymbol{u}_k\| = 0 \tag{4.7}$$

where $\boldsymbol{u}_d$ is a fixed input signal given by

$$\boldsymbol{u}_d = \begin{bmatrix} \boldsymbol{u}_d(0) \\ \vdots \\ \boldsymbol{u}_d(N-1) \end{bmatrix} \quad \in \mathbb{R}^{mN}. \tag{4.8}$$

and $||\cdot||$ denotes an appropriate norm.

Selecting the sampling time that exceeds the steady-state response time of the system and setting $N = 1$ ($T = T_s$), giving

$$\boldsymbol{u} = \boldsymbol{u}(0), \quad \boldsymbol{y} = \boldsymbol{y}(1), \quad \boldsymbol{g}(\cdot) = \boldsymbol{g}_1(\cdot) \tag{4.9}$$

This equates to the'steady-state' tracking problem is a special case of the full dynamic problem. Although the algorithms described in this chapter can address both cases, the former requires far shorter identification tests to produce a models needed in the algorithms which follow. Consider an operating point, $\boldsymbol{u_a}$, given by

$$\boldsymbol{u_a} = \begin{bmatrix} u_{a,1} & \cdots & u_{a,m} \end{bmatrix}^T \in \mathbb{R}^m \tag{4.10}$$

Then it is possible to represent the linearized system about $\boldsymbol{u} = \boldsymbol{u}_a$ as

$$\begin{aligned} \boldsymbol{g}'(\boldsymbol{u}_a) = \left.\frac{\partial \boldsymbol{g}}{\partial \boldsymbol{u}}\right|_{\boldsymbol{u}=\boldsymbol{u}_a} &= \begin{bmatrix} \left.\frac{\partial g_{1,1}}{\partial u_1}\right|_{u=u_a} & \cdots & \left.\frac{\partial g_{1,1}}{\partial u_m}\right|_{u=u_a} \\ \vdots & \ddots & \vdots \\ \left.\frac{\partial g_{1,p}}{\partial u_1}\right|_{u=u_a} & \cdots & \left.\frac{\partial g_{1,p}}{\partial u_m}\right|_{u=u_a} \end{bmatrix} \\ &= \begin{bmatrix} \left.\frac{\partial y_1}{\partial u_1}\right|_{u=u_a} & \cdots & \left.\frac{\partial y_1}{\partial u_m}\right|_{u=u_a} \\ \vdots & \ddots & \vdots \\ \left.\frac{\partial y_p}{\partial u_1}\right|_{u=u_a} & \cdots & \left.\frac{\partial y_p}{\partial u_m}\right|_{u=u_a} \end{bmatrix} \in \mathbb{R}^{p\times m} \end{aligned} \tag{4.11}$$

4.2 Identifying the System about an Operating Point

Suppose it is desired to identify the linearized system about $\boldsymbol{u} = \boldsymbol{u}_p = \mathbf{0}$ using experimental data. Then the procedure is to set the stimulation to zero on all channels except u_i, and slowly increase u_i whilst measuring y. Strictly the derivative at $u_i = 0$ should be estimated, as shown in Figure 4.2 and this produces a whole set of

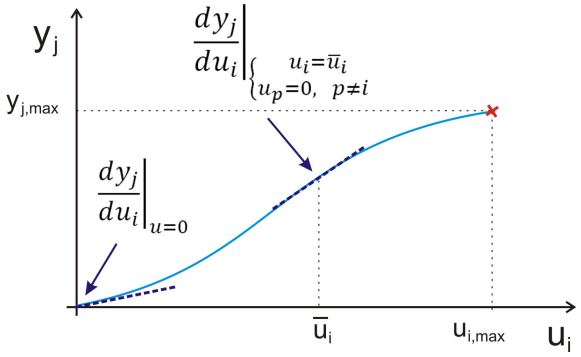

Figure 4.2: Linearization points for u_i with $u_p = 0$, $p \neq 0$.

linearization points for u_i. They can hence be averaged to produce a representative model that is more valid within a region about $u_i = 0$. If the maximum stimulation is $u_{i,max}$, giving rise to a monotonic increase in y_j, with maximum value $y_{j,max}$, then the average value of $\frac{\partial y_j}{\partial u_i}$ is

$$\frac{1}{u_{i,max}} \int_0^{y_{j,max}} \frac{\partial y_j}{\partial u_i} \mathrm{d}u_i = \frac{y_{j,max}}{u_{i,max}} \tag{4.12}$$

i.e. the average value equates to the simple ratio of output to applied input. If $u_{i,max}$ is small, (4.12) provides an approximate value of $\left.\frac{\partial y_j}{\partial u_i}\right|_{u=0}$.

The alternative is to not average, but to produce a set of linearized models at different operating points, $\bar{u}_i$, where each $\bar{u}_i$ produces a column vector

$$\left.\frac{\partial y}{\partial u_i}\right|_{\begin{cases} u_i = \bar{u}_i \\ u_p = 0, \;\; p \neq i \end{cases}} \tag{4.13}$$

To produce a consistent linearized system $g'(\cdot)$, the above can only be combined with other columns that are linearized about zero. Hence if there are M linearization points for each input (including zero), then this procedure produces M^m models.

Identifying the System about an Arbitrary Operating Point by Averaging

To reliably calculate the linearized system about $\boldsymbol{u} = \boldsymbol{u}_a$ using experimental data, a slow ramp is applied to each input u_i over the set of inputs

$$S_i = \Big\{ \; u_{a,i} - \tfrac{u_{i,width}}{2}, \quad u_{a,i} - \tfrac{u_{i,width}}{2} + \Delta u_i, \\ u_{a,i} - \tfrac{u_{i,width}}{2} + 2\Delta u_i, \quad \cdots, \quad u_{a,i} + \tfrac{u_{i,width}}{2} \; \Big\}$$

whilst the other inputs are fixed at $u_j = u_{a,j}$. The response of the j^{th} output, y_j^i, is shown in Figure 4.3. The required estimate of $\frac{\partial y_j}{\partial u_i}\Big|_{u=u_a}$ is then calculated by averaging

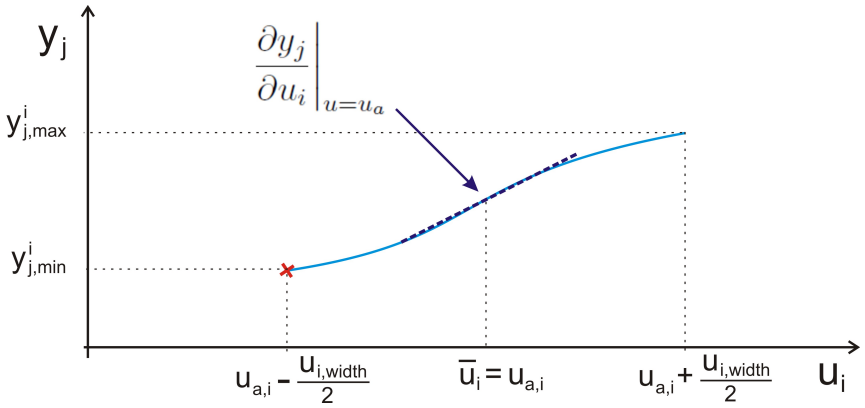

Figure 4.3: Linearization points about u_a.

provided $u_{i,width}$ is sufficiently small. The result is given by

$$\frac{\partial y_j}{\partial u_i}\bigg|_{u=u_a} \approx \frac{1}{u_{i,width}} \sum_{u_i \in S_i} \frac{\partial y_j}{\partial u_i} \Delta u_i = \frac{y^i_{j,max} - y^i_{j,min}}{u_{i,width}} \tag{4.14}$$

Applying the above to all outputs, yields

$$\begin{bmatrix} \frac{\partial y_1}{\partial u_i}\Big|_{u=u_a} \\ \vdots \\ \frac{\partial y_p}{\partial u_i}\Big|_{u=u_a} \end{bmatrix} = \frac{\partial y}{\partial u_i}\bigg|_{u=u_a} \approx \frac{y^i_{max} - y^i_{min}}{u_{i,width}} \tag{4.15}$$

where

$$y^i_{max} = \begin{bmatrix} y^i_{1,max} \\ \vdots \\ y^i_{p,max} \end{bmatrix} \in \mathbb{R}^p, \quad y^i_{min} = \begin{bmatrix} y^i_{1,min} \\ \vdots \\ y^i_{p,min} \end{bmatrix} \in \mathbb{R}^p \tag{4.16}$$

Each test hence populates the i^{th} column of (4.11).

4.3 ILC Applied to Array Element Selection

The problem of finding a stimulation profile, $\boldsymbol{u}$, which produces the required posture, $\boldsymbol{y}_d$, can be expressed as

$$\textbf{minimize} \;\; f(\boldsymbol{u}), \quad f(\boldsymbol{u}) = \|\boldsymbol{y}_d - \boldsymbol{g}(\boldsymbol{u})\|_2^2 \tag{4.17}$$

subject to constraints on $\mathbf{u}$. A general algorithm to solve this problem is proposed as follows :

Step 1. Set $k = 0$ and set the initial input to $\boldsymbol{u}_0 = \mathbf{0}$.

Step 2. Apply $\boldsymbol{u}_k$ to the system experimentally and record $\boldsymbol{y}_k$. Calculate the error $\boldsymbol{e}_k = \boldsymbol{y}_d - \boldsymbol{y}_k$.

Step 3. Linearize the system about the operating point input $\boldsymbol{u}_k$ to obtain the linear model $\boldsymbol{g}'(\boldsymbol{u}_k)$.

Step 4. Using the model of the previous step, update the control input using any linear gradient based ILC approach, i. e. Gradient ILC, Newton-based ILC.

Step 5. Increment k and go to step 2.

The process of linearization followed by input updating is used by a broad class of nonlinear minimization algorithms, which use experimental data collected during the trials of the underlying repetitive process to minimize an objective function. Here, to solve the problem of minimising the tracking error norm, the implementation of the process within ILC framework is developed.

As an example, inverse ILC in the update step 4 of above procedure is now considered. This corresponds to 'Newton method-based ILC' Lin et al. (2006b), one technique in the wide class of gradient-based algorithms, which has well defined convergence criteria (see, for example, Ortega and Rheinboldt (1970)). It has also been used in unconstrained and constrained ILC Freeman (2012) approaches.

Newton-method based ILC

The new input can be calculated applying Newton method based ILC in step 4 as follows:

$$\boldsymbol{u}_{k+1} = \boldsymbol{u}_k + \boldsymbol{v}_k^* \tag{4.18}$$

where $\boldsymbol{v}_k^*$ is the solution to the following problem:

$$\textbf{minimize} \;\; f_k(\boldsymbol{v}), \quad f_k(\boldsymbol{v}) = \left\|\boldsymbol{e}_k - \boldsymbol{g}'(\boldsymbol{u}_k)\boldsymbol{v}\right\|_2^2 \tag{4.19}$$

Without constraints, the solution to (4.19) will be non-unique if $\boldsymbol{g}'(\boldsymbol{u}_k)$ does not have full row rank (which will be the case if, for example, $m > p$). To avoid this problem, (4.19) can be augmented as

$$\begin{aligned} \textbf{minimize} \quad & \|\boldsymbol{v}\|_2^2 \\ \textbf{subject to} \quad & \boldsymbol{e}_k = \boldsymbol{g}'(\boldsymbol{u}_k)\boldsymbol{v} \end{aligned} \tag{4.20}$$

which has the solution

$$\boldsymbol{v}_k^* \;=\; \left(\left(\boldsymbol{g}'(\boldsymbol{u}_k)\right)^T \boldsymbol{g}'(\boldsymbol{u}_k)\right)^{-1} \left(\boldsymbol{g}'(\boldsymbol{u}_k)\right)^T \boldsymbol{e}_k = \left(\boldsymbol{g}'(\boldsymbol{u}_k)\right)^\dagger \boldsymbol{e}_k \tag{4.21}$$

Constraints are required to ensure that the experimentally applied stimulation signal $\boldsymbol{u_k}$ is practically achievable. When the FES stimulator supports multi-channel stimulation and the number of channels is not less than the number of elements of the electrode array, the only constraint is due to the control input limits and the control problem can be solved using, i.e. the Newton method based ILC with boundary input constraints as described in previous chapter.

A challenging problem occurs, when the number of channels available is less than the number of elements in the electrode array. In such a case, finding an optimal stimulation pattern can be considered as an integer programming problem, or a sparse optimisation problem due to the presence of additional constraints. The different approaches to solve this optimisation problem are described next.

Limited number of stimulation levels - penalty method approach

In the case when n-number of stimulation levels is available, the stimulation signal must satisfy

$$u_{k,i} \in \mathcal{U}_n, \qquad \forall\, k \tag{4.22}$$

$$0 \leq \mathcal{U}_{n,j} \leq 300, \qquad j = 1, 2, \cdots, n \tag{4.23}$$

where $\mathcal{U}_n$ is a set with n non-zero distinct elements with $\mathcal{U}_{n,j}$ denoting the j^{th} element. Here n is the number of channels supported by the hardware. The problem (4.19) is hence replaced by

$$\begin{aligned} &\textbf{minimize} && \|\boldsymbol{v}\|_2^2 \\ &\textbf{subject to} && \begin{cases} \boldsymbol{e}_k = \boldsymbol{g}'(\boldsymbol{u}_k)\boldsymbol{v}, \\ v_i \in \{\tilde{u}_1 - u_{k,i},\ \tilde{u}_2 - u_{k,i},\ \ldots\ \tilde{u}_n - u_{k,i}\}, \\ -u_{k,i} \leq v_i \leq 300 - u_{k,i} \end{cases} \end{aligned} \tag{4.24}$$

This last problem can be solved in simulation between experimental trials. Hence the inequality constraint can be removed since the applied solution will always satisfy it through appropriate selection of $\mathcal{U}_n$. It is shown in (Freeman, 2012) that repeated application of gradient ILC (an implementation of the gradient descent algorithm) to the problem (4.19), converges to a solution which solves (4.20). It is hence necessary to apply the gradient descent algorithm to the problem

$$\begin{aligned} &\textbf{minimize} && \boldsymbol{f}_k(\boldsymbol{v}), \quad \boldsymbol{f}_k(\boldsymbol{v}) = \left\|\boldsymbol{e}_k - \boldsymbol{g}'(\boldsymbol{u}_k)\boldsymbol{v}\right\|_2^2 \\ &\textbf{subject to} && v_i \in \{\tilde{u}_1 - u_{k,i},\ \tilde{u}_2 - u_{k,i},\ \ldots\ \tilde{u}_n - u_{k,i}\} \end{aligned} \tag{4.25}$$

whilst also ensuring the solution, $\boldsymbol{v}_k^*$, satisfies the constraint. This then is used in step 4 to produce the next input, via $\boldsymbol{u}_{k+1} = \boldsymbol{u}_k + \boldsymbol{v}_k^*$.

To solve (4.25) first substitute for the optimized variable to give

$$\begin{aligned} &\textbf{minimize} && \tilde{\boldsymbol{f}}_k(\tilde{\boldsymbol{v}}), \quad \tilde{\boldsymbol{f}}_k(\tilde{\boldsymbol{v}}) = \left\|\boldsymbol{e}_k - \boldsymbol{g}'(\boldsymbol{u}_k)(\tilde{\boldsymbol{v}} - \boldsymbol{u}_k)\right\|_2^2 \\ &\textbf{subject to} && \tilde{v}_i \in \{\tilde{u}_1,\ \tilde{u}_2,\ \ldots\ \tilde{u}_n\} \end{aligned} \tag{4.26}$$

This problem can be solved using gradient descent optimization by introducing a suitable penalty function. Accordingly, the problem (4.26) becomes

$$\begin{aligned} \textbf{minimize} \qquad \tilde{\boldsymbol{f}}_k(\tilde{\boldsymbol{v}}), \quad \tilde{\boldsymbol{f}}_k(\tilde{\boldsymbol{v}}) &= \left\|\boldsymbol{e}_k - \boldsymbol{g}'(\boldsymbol{u}_k)(\tilde{\boldsymbol{v}} - \boldsymbol{u}_k)\right\|_2^2 \\ &\quad + \tau \sum_i^m \varphi(\tilde{v}_i), \end{aligned} \tag{4.27}$$

where τ is a penalty multiplier for values not in the set $\mathcal{U}_n$, and $\varphi(\tilde{v}_i)$ is the penalty term for the i^{th} variable. Different forms of the discrete penalty function are possible, and here the sine-function form (Shin et al., 1990) is employed and a suitable form is

$$\varphi(\tilde{v}_i) = \sin\left(\frac{2\pi\left(\tilde{v}_i - \frac{1}{4}(\tilde{u}_{j+1} + 3\tilde{u}_j)\right)}{\tilde{u}_{j+1} - \tilde{u}_j}\right) + 1, \quad \tilde{u}_j \leq \tilde{v}_i \leq \tilde{u}_{j+1} \tag{4.28}$$

The scalar multiplier τ is initially zero and is increased gradually to ensure that the converged solution satisfies the constraint in (4.26) that $\tilde{v}_i \in \{\tilde{u}_1, \ \ldots \ \tilde{u}_n\}$. Application of the gradient algorithm to (4.27) gives

$$\boldsymbol{\tilde{v}_{l+1} = \tilde{v}_l + \left(g'(u_k)\right)^T \left(e_k - g'(u_k)(\tilde{v}_l - u_k)\right) + \tau_l \chi_l} \tag{4.29}$$

where $\tilde{v}_0 = u_k$. Now the vector $\boldsymbol{\chi_l}$ has elements

$$\begin{aligned} \chi_{l,i} &= \frac{\partial\varphi(\tilde{v}_i)}{\tilde{v}_i}, \qquad\qquad \tilde{u}_j \leq \tilde{v}_i \leq \tilde{u}_{j+1} \\ &= \frac{2\pi}{(\tilde{u}_{j+1} - \tilde{u}_j)} \cos\left(\frac{2\pi\left(\tilde{v}_{l,i} - \frac{1}{4}(\tilde{u}_{j+1} + 3\tilde{u}_j)\right)}{\tilde{u}_{j+1} - \tilde{u}_j}\right) \end{aligned} \tag{4.30}$$

The solution obtained after sufficient inter-trial iterations of (4.29), $\tilde{v}_k^*$, is used to obtain the new input $u_{k+1} = \tilde{v}_k^*$.

4.4 Selection using Virtual Elements

Virtual elements (VEs) potentially provide more effective and practical base units of stimulation. These can simply be incorporated into the previous approach by redefining the underlying stimulation elements to be constructed of multiple array elements. The inherent non-linearity of the system means that more accurate results will be produced by extending the number of possible input elements, so that the same element appears in multiple independent input units. This does not violate the assumption of local linearity since linearization is based on a single operating point, and the subsequent input increase treats the input elements as independent. Each input is termed a 'virtual element' since it no longer encompasses a single array element, but a set of elements that can be overlapped. This approach embeds richer model information, and can be analysed using the approaches of Section 4.3.

Suppose the electrode array is rectangular with m_v vertical elements and m_h horizontal elements, and hence $m = m_v \times m_h$. The requirement that the elements comprising each virtual element be adjacent to each other reduces the number of placements and

hence size of the input vector. The following virtual element dimensions are considered

$$\begin{array}{lll} \boldsymbol{u}^{1hv} & \in \mathbb{R}^{(m_v \times m_h)} & \text{virtual = real elements} \\ \boldsymbol{u}^{2v} & \in \mathbb{R}^{(m_h \times (m_v-1))} & \text{2 vertical VEs} \\ \boldsymbol{u}^{2h} & \in \mathbb{R}^{((m_h-1) \times m_v)} & \text{2 horizontal VEs} \\ \boldsymbol{u}^{2hv} & \in \mathbb{R}^{((m_h-1) \times (m_v-1))} & \text{2 horizontal + 2 vertical VEs} \end{array} \tag{4.31}$$

These inputs are assumed to be independent and can be combined under the assumption of local linearity. Hence the augmented input vector is given by

$$\boldsymbol{u} = \begin{bmatrix} \boldsymbol{u}^{1hv} \\ \boldsymbol{u}^{2v} \\ \boldsymbol{u}^{2h} \\ \boldsymbol{u}^{2hv} \end{bmatrix} \in \mathbb{R}^{(2(m_h(m_v-1)+(m_h-1)m_v)+1)} \tag{4.32}$$

and (4.11) in this case can be written as

$$\begin{aligned} \boldsymbol{g}'(\boldsymbol{u}_a) &= \left.\frac{\partial \boldsymbol{g}}{\partial \boldsymbol{u}}\right|_{\boldsymbol{u}=\boldsymbol{u}_a} \in \mathbb{R}^{p \times (2(m_h(m_v-1)+(m_h-1)m_v)+1)} \\ &= \left[\left.\frac{\partial \boldsymbol{g}}{\partial \boldsymbol{u}^{1hv}}\right|_{\boldsymbol{u}=\boldsymbol{u}_a} \left.\frac{\partial \boldsymbol{g}}{\partial \boldsymbol{u}^{2v}}\right|_{\boldsymbol{u}=\boldsymbol{u}_a} \left.\frac{\partial \boldsymbol{g}}{\partial \boldsymbol{u}^{2h}}\right|_{\boldsymbol{u}=\boldsymbol{u}_a} \left.\frac{\partial \boldsymbol{g}}{\partial \boldsymbol{u}^{2hv}}\right|_{\boldsymbol{u}=\boldsymbol{u}_a}\right] \\ &= \begin{bmatrix} \left.\frac{\partial y_1}{\partial u^{1hv}}\right|_{u=u_a} \left.\frac{\partial y_1}{\partial u^{2v}}\right|_{u=u_a} \left.\frac{\partial y_1}{\partial u^{2h}}\right|_{u=u_a} \left.\frac{\partial y_1}{\partial u^{2hv}}\right|_{u=u_a} \\ \vdots \quad\quad \vdots \quad\quad \vdots \quad\quad \vdots \\ \left.\frac{\partial y_p}{\partial u^{1hv}}\right|_{u=u_a} \left.\frac{\partial y_p}{\partial u^{2v}}\right|_{u=u_a} \left.\frac{\partial y_p}{\partial u^{2h}}\right|_{u=u_a} \left.\frac{\partial y_p}{\partial u^{2hv}}\right|_{u=u_a} \end{bmatrix} \end{aligned} \tag{4.33}$$

where, for example,

$$\begin{bmatrix} \left.\frac{\partial y_1}{\partial u^{1hv}}\right|_{u=u_a} \\ \vdots \\ \left.\frac{\partial y_p}{\partial u^{1hv}}\right|_{u=u_a} \end{bmatrix} = \begin{bmatrix} \left.\frac{\partial y_1}{\partial u_1^{1hv}}\right|_{u=u_a} & \cdots & \left.\frac{\partial y_1}{\partial u_{m_v \times m_h}^{1hv}}\right|_{u=u_a} \\ \vdots & \ddots & \vdots \\ \left.\frac{\partial y_p}{\partial u_1^{1hv}}\right|_{u=u_a} & \cdots & \left.\frac{\partial y_p}{\partial u_{m_v \times m_h}^{1hv}}\right|_{u=u_a} \end{bmatrix} \tag{4.34}$$

Each column of (4.34) is identified by the ramp identification approach of Section 4.2. Hence, for example

$$\begin{bmatrix} \left.\frac{\partial y_1}{\partial u_i^{1hv}}\right|_{u=u_a} \\ \vdots \\ \left.\frac{\partial y_p}{\partial u_i^{1hv}}\right|_{u=u_a} \end{bmatrix} = \left.\frac{\partial y}{\partial u_i^{1hv}}\right|_{u=u_a} \approx \frac{y_{max}^{1hv,i} - y_{min}^{1hv,i}}{u_{i,width}^{1hv}} \tag{4.35}$$

where $y_{max}^{1hv,i}$, $y_{min}^{1hv,i}$ are the joint outputs corresponding to the ramp test applied to the i^{th} element of virtual element $1hv$.

The approach of Section 4.3 is applied unchanged except that

1. the constraints on the input applied experimentally must be referred back to the vector, $\hat{\boldsymbol{u}}$ which is being updated, and
2. having updated $\hat{\boldsymbol{u}}$ the input applied experimentally must be constructed by combining the virtual element solutions.

This requires each virtual element input to be written in terms of the resulting, combined element output. Hence we map the virtual input vectors to the applied stimulation vector component $\hat{u}$ through matrices containing ones and zeros:

$$\begin{aligned}
\hat{\boldsymbol{u}} &= \Phi_{1hv} u^{1hv}, \quad \Phi_{1hv} \in \mathbb{R}^{m\times(m_h\times m_v)} \\
\hat{\boldsymbol{u}} &= \Phi_{2v} u^{2v}, \quad \Phi_{2v} \in \mathbb{R}^{m\times(m_h\times(m_v-1))} \\
\hat{\boldsymbol{u}} &= \Phi_{2h} u^{2h}, \quad \Phi_{2h} \in \mathbb{R}^{m\times((m_h-1)\times m_v)} \\
\hat{\boldsymbol{u}} &= \Phi_{2hv} u^{2hv}, \quad \Phi_{2hv} \in \mathbb{R}^{m\times((m_h-1)\times(m_v-1))}
\end{aligned} \tag{4.36}$$

Hence

$$\hat{\boldsymbol{u}} = \begin{bmatrix} \boldsymbol{\Phi}_{1hv} & \boldsymbol{\Phi}_{2v} & \boldsymbol{\Phi}_{2h} & \boldsymbol{\Phi}_{2hv} \end{bmatrix} \begin{bmatrix} \boldsymbol{u}^{1hv} \\ \boldsymbol{u}^{2v} \\ \boldsymbol{u}^{2h} \\ \boldsymbol{u}^{2hv} \end{bmatrix} = \boldsymbol{\Phi}\boldsymbol{u} \tag{4.37}$$

where

$$\boldsymbol{\Phi} = \begin{bmatrix} \boldsymbol{\Phi}_{1hv} & \boldsymbol{\Phi}_{2v} & \boldsymbol{\Phi}_{2h} & \boldsymbol{\Phi}_{2hv} \end{bmatrix} \tag{4.38}$$

and the constraint (4.22) becomes

$$\hat{\boldsymbol{u}}_{k,i} = \boldsymbol{\Phi}_i \boldsymbol{u}_k \in \mathcal{U}_n \tag{4.39}$$

where Φ_i is the i^{th} row of Φ, so that the constraints on problem (4.19) become

$$v_i \in \{\tilde{u}_1 - \Phi_i u_k,\ \tilde{u}_2 - \Phi_i u_k,\ \ldots\ \tilde{u}_n - \Phi_i u_k\} \tag{4.40}$$

and the problem and solution given by (4.26), (4.27), (4.28), (4.29), (4.30) are identical except for the substitution

$$\tilde{u}_i \Longleftrightarrow \tilde{u}_i - \Phi_i u_k + u_{k,i}. \tag{4.41}$$

Remark 4.1. The form of (4.33) means that the optimization problem (4.26) may be performed sequentially for each virtual element form in turn, before moving onto the next step of minimizing the remaining joint error, whilst transferring the constraints so that the final solution satisfies (4.22). This procedure enables a simple set of uncoupled constraints to be imposed on each sub-problem.

4.4.1 Sparse optimisation for SEA-based control of Hand and Wrist

The control of fingers and wrist using multi-channel SEA-based stimulation in the case when the number of channels available is less than the number of elements in the electrode array can be considered as a sparse optimisation problem with cardinality and minimum threshold constraints. These can be expressed as:

$$\begin{aligned} minimize \;\; f(\boldsymbol{u}) &:= ||\boldsymbol{y}_d - \boldsymbol{g}(\boldsymbol{u})||_2^2 \\ s.t. \;\; ||\boldsymbol{u}||_0 &\leq n \\ u_{min} = 0 \leq u_i \leq u_{max} = 300, \;\; i &= 1, \ldots, m \end{aligned} \tag{4.42}$$

where $f : R^m \rightarrow R$ is assumed to be a continuously differentiable function, $n > 0$ is an integer that denotes the number of channels and $||\boldsymbol{u}||_0$ is equal to the number of non-zero components in $\boldsymbol{u}$. Note, that in general case the f is not assumed to be a convex function, which together with the non-convex constraint function, refers to a general non-linear optimisation problem, which is complex NP-hard. However, assuming linearity of the static model allows the problem to be relaxed to a standard convex optimisation problem as described next.

Static linear model with sparsity

Assume that system is linearized around $\boldsymbol{u_0}$ and $\boldsymbol{g'(u_0)} = \boldsymbol{G}$ and this assumption of linearity then gives rise to the simpler procedure:

$$\begin{aligned} minimize \;\; &||\boldsymbol{y_d} - \boldsymbol{G}\boldsymbol{u}||_2^2 \\ s.t. \;\; &||\boldsymbol{u}||_0 \leq n \\ 0 \leq u_i \leq u_{max}, \;\; &i = 1, \ldots, m \end{aligned} \tag{4.43}$$

where $\boldsymbol{G} \in R^{p \times m}$, $\boldsymbol{y_d} \in R^p$, n is an integer satisfying $1 \leq n \leq m$ and and n denotes the number of channels of the stimulation that are available. The problem (4.43) can be replaced by the following $l_1 - regularized$ least squares problem

$$\begin{aligned} minimize \;\; &||\boldsymbol{y}_d - \boldsymbol{G}\boldsymbol{u}||_2^2 + \tau||\boldsymbol{u}||_1 \\ 0 \leq u_i \leq u_{max}, \;\; &i = 1, \ldots, m \end{aligned} \tag{4.44}$$

where $||\cdot||_1$ denotes the l_1-norm, which equals the sum of the absolute values of the components of $\boldsymbol{u}$. The presence of the l_1 term is used to induce the sparsity in the optimal solution of (4.43). Equivalently, the problem (4.45) can be replaced with the

following minimization problem

$$\begin{aligned} &minimize \;\; ||\boldsymbol{y}_d - \boldsymbol{G}\boldsymbol{u}||_2^2 + \tau \mathbf{1}^{\boldsymbol{T}}\boldsymbol{u} \\ &0 \leq u_i \leq u_{max}, \;\; i = 1, \ldots, m \end{aligned} \tag{4.45}$$

where $\mathbf{1} \in \mathbb{R}^m$ denotes the vector with all entries equal to 1 and $\tau \leq n$ and this problem formulation was used in further analysis.

4.4.2 Proximal Gradient Algorithm

Recently, there has been growing interest in convex optimization techniques for system identification, which is motivated by the success of convex methods for sparse optimization and by the development of new classes of algorithms for large-scale non-differentiable convex optimization, such as proximal gradient methods (Vandenberghe, 2012).

The proximal gradient method is an extension of the gradient algorithm to problems with simple constraints or with simple non-differentiable terms in the cost function, such as $||\boldsymbol{u}||_1$. It is typically a fast method and handles many types of non-differentiable problems that occur in the practice. The proximal gradient algorithm applies to a convex problem in which the cost function J can be split into two components: differentiable function $g(\cdot)$ and non-differentiable term $h(\cdot)$

$$minimize \;\; J(\boldsymbol{u}) = g(\boldsymbol{u}) + h(\boldsymbol{u}) \tag{4.46}$$

In the previously considered sparse problem for SEA, these terms were given by $g(\boldsymbol{u}) = ||\boldsymbol{y}_d - \boldsymbol{G}\boldsymbol{u}||_2^2$ and $h(u) = \tau||\boldsymbol{u}||_1$ respectively.

To solve the composite optimisation problem (4.46), a proximal optimisation problem needs to be solved. The problem can be formulated as follows:

$$\boldsymbol{u}_{k+1} = arg\min_{\boldsymbol{u}} ||\boldsymbol{u} - (\boldsymbol{u}_k - \alpha_k \boldsymbol{g}'(\boldsymbol{u}_k))||_2^2 + \alpha_k h(\boldsymbol{u}) \tag{4.47}$$

where the solution of (4.47) is the proximal gradient algorithm of the form:

$$\boldsymbol{u}_{k+1} = prox_{\alpha_k h}\left[\boldsymbol{u}_k - \alpha_k \boldsymbol{g}'(\boldsymbol{u}_k)\right] \tag{4.48}$$

Each iteration of above proximal-gradient method (4.48) requires the calculation of the proximity operator $prox_{\alpha_k h}$, as described next.

Box-constrained Proximity Operator with l_1-norm

The solution for the box-constrained version of the proximity operation for the considered problem (4.45) can be expressed as:

$$u_i^* = min(max(\hat{u}_i, u_{min}), u_{max}) \tag{4.49}$$

where

$$\hat{u}_i = sgn(u_i)max(|u_i| - \tau\alpha_k, 0) \tag{4.50}$$

is the well known shrinkage or soft-tresholding operator.

The problem 4.46 can be solved using the Accelerated Proximal Gradient (APG) method, which is a one of the fastest methods from the wider group of Proximal Gradient-based approaches (Nesterov, 2004, 2013). The APG method for the considered case of hand and wrist control can be expressed as the following procedure

The Accelerated Proximal Gradient for SEA with cardinality constrained inputs

---

1. Apply $\boldsymbol{u}_k = \boldsymbol{u}_0$ to the system experimentally and record $\boldsymbol{y}_k$. Calculate the postural joint error $\boldsymbol{e}_k = \boldsymbol{y}_d - \boldsymbol{y}_k$
2. Linearize the system about the operating point input u using the approach described in section (4.2)
3. Set $\boldsymbol{v}_0 = \boldsymbol{v}_{-1} = \boldsymbol{0}$, set $t_0 = t_{-1} = 1$ and $L \geq \lambda_{max}(\boldsymbol{G}^T\boldsymbol{G})$, where L denotes the smallest Lipschitz constant and λ_{max} is the maximum eigenvalue.
4. Calculate the new input using APG method with sparse non-negative upper bound constraints and adaptive step size t_k.

$$\begin{aligned}
\boldsymbol{u}_k &:= \boldsymbol{v}_k + \frac{t_{k-1}-1}{t_k}(\boldsymbol{v}_k - \boldsymbol{v}_{k-1}) \\
\boldsymbol{u}_{k+1} &:= \boldsymbol{u}_k - \frac{1}{K}\left[\boldsymbol{G}^T(\boldsymbol{G}\boldsymbol{u}_k - \boldsymbol{y}_d) - \tau\boldsymbol{1}\right] \\
&:= \boldsymbol{u}_k - \frac{1}{L}\left(\boldsymbol{G}\boldsymbol{e_k}^T - \tau\boldsymbol{1}\right) \\
v_{k+1} &:= \min[\max(0, u_{k+1}), u_{max}] \\
t_{k+1} &:= \frac{1}{2}(1 + \sqrt{1 + 4t_k^2})
\end{aligned} \tag{4.51}$$

5. Increment k and go to step 4.

4.4.3 Brute-Force Searching Method

The brute-force searching algorithm selects a combination of electrodes with up to n separate pulse width levels of stimulation to provide the best performance. The main parameters of the algorithm are the input rate u_{rate} and maximal number of elements that can be selected (activated elements) n_{active} and p the number of array elements. Hence the number of possible solutions is equal to

$$s = \frac{p!}{n_{active}!(p - n_{active})!} n_{active}^{n} \frac{(u_{max} - u_{min})}{u_{rate}} \tag{4.52}$$

Let $\mathcal{U}_s$ denotes the set of all possible solutions for chosen parameters. This can be expressed as:

$$\mathcal{U}_s = \{\mathbf{u_1}, \ldots, \mathbf{u_s}\} \tag{4.53}$$

The algorithm finds the best solution, which can be expressed as:

$$\begin{aligned} \min_k \quad & \|\mathbf{G}\mathbf{u_k} - \boldsymbol{y_d}\|_\mathbf{2}^\mathbf{2} \\ & k = 1, \ldots, s \end{aligned} \tag{4.54}$$

and the parameters dictate the speed and accuracy of the searching procedure. Small u_{rate}, can improve the performance of the algorithm, but increases the search space.

Optimal stimulation pattern and sparse input vector

Applying any of the sparse optimisation or discrete optimisation methods introduced previously, results in finding the sparse input vector $\boldsymbol{u}$, which defines the optimal stimulation pattern.

An optimal stimulation pattern, can be defined by sparse input vector $\boldsymbol{u}$, which consists of upto n non-zero electrode elements, i.e. $\boldsymbol{u} = [u_1 = v_1, 0, u_2 = v_2, u_3 = v_2, 0...0, u_n = v_1]$. Each of the elements or group of elements having the same value of input can be treated as a single element of new virtual electrode array, so that $v_1(t)$ is applied to 1 group of elements of the original electrode array , ..., $v_i(t)$ to $i-th$ group of elements and finally the last $n-th$ group is assigned to $v_n(t)$. This results in new vector of $m = n$ inputs $\boldsymbol{v}$, which constitutes the new virtual electrode array that consists of only n pads.

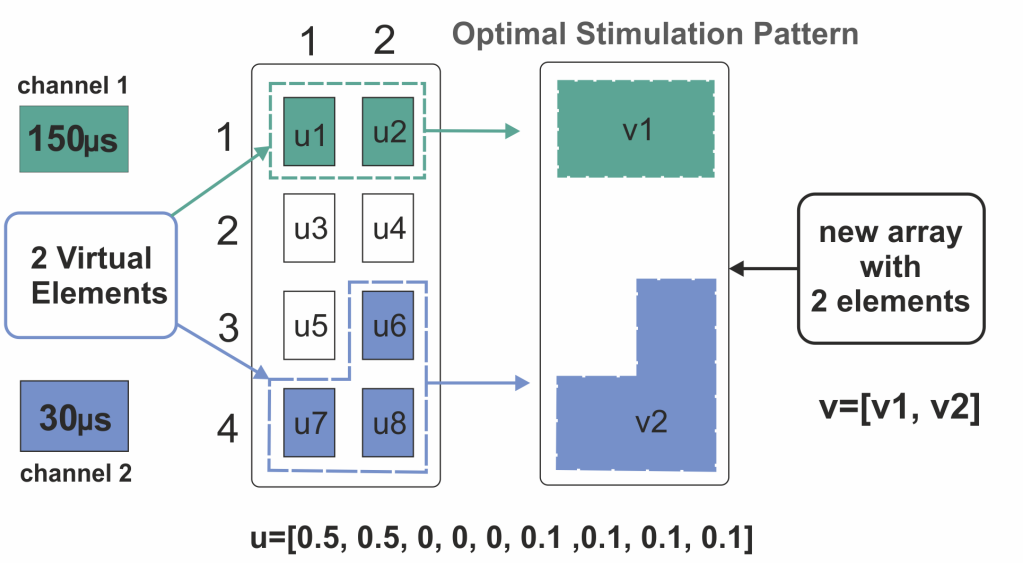

Figure 4.4: Optimal Stimulation Pattern - schematic of mapping array elements $\rightarrow$ input vector $\boldsymbol{u}$

Example: Let the optimal stimulation pattern for the exemplar array (2x4) be represented by the sparse input vector $\boldsymbol{u}$, then the non-negative elements in the sparse vector $\boldsymbol{u}$ constitute a new virtual electrode array that consists of only 2 elements as shown in Figure 4.4

4.4.4 Two-step approach for ILC of SEA

A two-step approach has been developed in which the problem of the tracking of a reference, when having only n stimulation channels is addressed as follows:

Step 1. Select an optimal stimulation pattern that consists of upto n array elements, i.e using previously described penalty function method or sparse optimisation method.

Step 2. Apply ILC-based approach with boundary input constraints for the elements of electrode array selected in Step 1 .

The main concept of this method is preselection of up to n array elements (single or VE) to transform electrode array consisting of m single elements into a new virtual electrode array. This new virtual electrode array consists of only n single elements or eventually n separate groups of single elements (VEs) and hence it can be used with standard ILC algorithms, such as i.e. Gradient ILC with boundary input constraints.

4.5 General ILC-based approach for SEA

A general that has been developed, combines all previously described methods as shown in Figure 4.5. The different parameters and design setting covered by the approach are following:

- k - denotes the number of trials: for single-step approach ($k = 1$) and in the case of multiple-trials approach ($k > 1$)
- m - is the number of single elements in an electrode array.
- Electrode Array Elements included in the procedure are following: standard single electrode array elements, VEs (a group of single elements, which is treated as single array element)
- n denotes the number of channels (number of separate stimulation signals supported by stimulator). In the multi-channel stimulation $n > 1$.
- Optimal Pattern Selection Methods included in the procedure are: penalty method, APG and brute-force method. These methods are incorporated with ILC.
- ILC-based methods included in the procedure are: Gradient ILC, Newton method-based ILC.

Method	**channels**	**trials**
ILC with input boundary constraints	$n \geq m$	$k \geq 1$
ILC with optimisation	$n < m$	$n > k \geq 1$
Optimal Pattern Selection Methods	$n < m$	$k = 1$

Table 4.1: Exemplar methods for selected configuration of different parameters of the general procedure

Electrode array-based technologies can differ in respect to parameters such as: the number of single elements in the electrode array , number of separate stimulation signals supported by the hardware. The general approach developed can be applied to a variety of possible design specification of existing and future SEA-based systems. The exemplar methods used in the general approach for different configuration settings are presented in Table 4.1. The system design with practical considerations and results, including choice of settings of the general procedure applied in experimental trials, are discussed next.

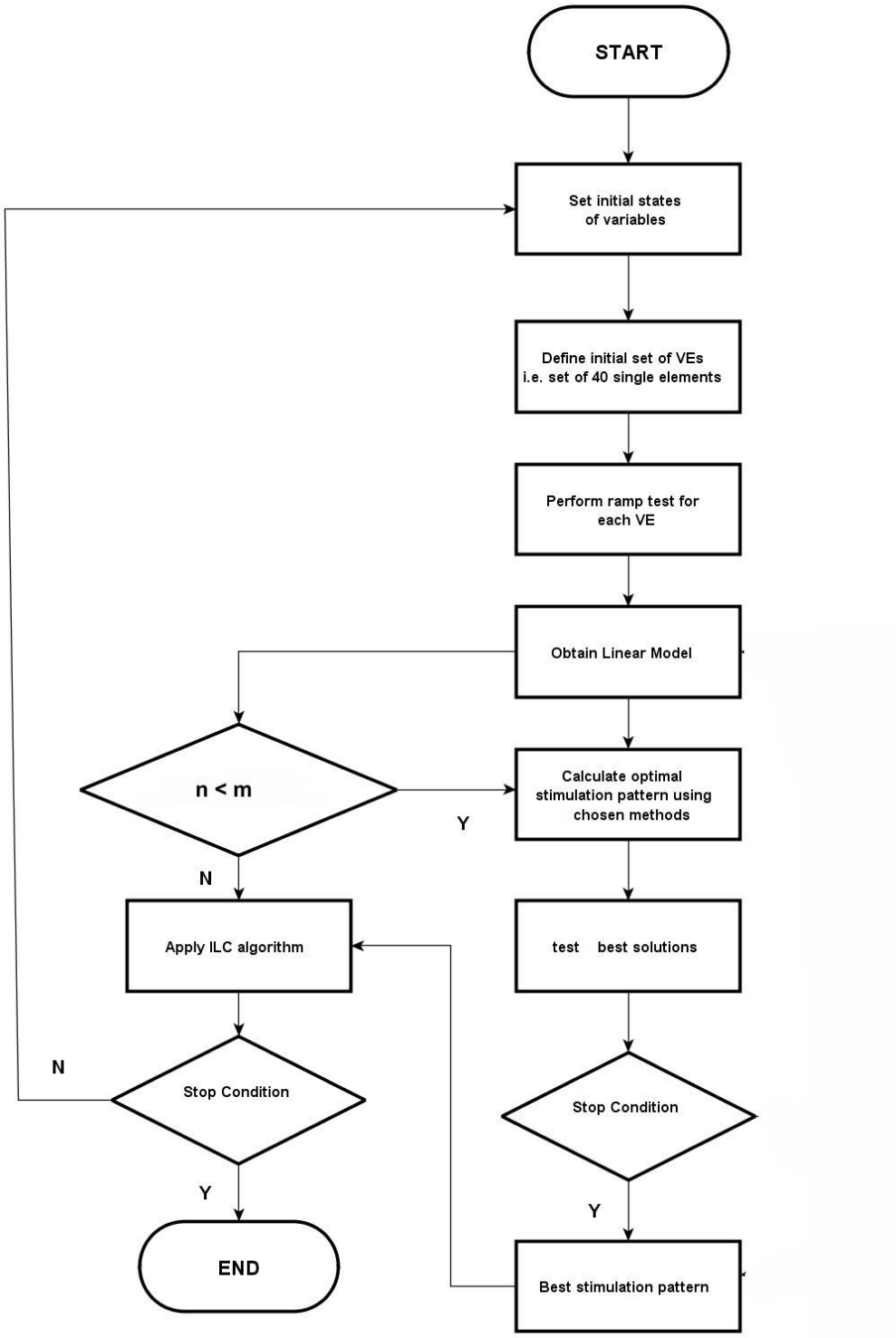

Figure 4.5: General Iterative Approach for control for SEA

Chapter 5

System Design and Experimental Procedure

The Hand Restoration System (HaReS) uses SEA-based stimulation mediated by specifically designed optimisation algorithms, defined within ILC-based framework. The sensors used in the system are two data gloves (model for left and right hand) and goniometers. The hardware is combined with graphical user interface, which allows the patients to interact with a specially designed game-based training environment. The main components of the system are shown in Figure 5.1.

5.1 Electrode Array and Multiplexer

The electrode arrays used in the system, consists of 40 (5x8) elements. The electrode array is controlled by custom made multiplexer, that can access and route two separate stimulation signals to desired array elements. The multiplexer is controlled by Matlab via a dSpace card which outputs a pulse-width modulated signal which is amplified by a commercial Odstock stimulator unit. The Arduino board then uses the information from dSpace to output appropriate signals to control a shift register array Dinh (2012).

To enable control of the stimulation, a commercial stimulator was specially modified. The stimulation parameters, pulse-width, amplitude and frequency have been selected to ensure a smooth muscle contraction. The controller hardware produces a 5V 40Hz square pulse train with variable pulse-width for each channel. This is then fed into the amplification stage of the stimulator, resulting in bi-phasic voltage-amplified stimulation pulses. The amplitude of the pulses for each channel have to be determined manually, whereas the pulse-width is the input parameter, that can be controlled automatically by the Matlab controller. The pulse-width has been safety-limited to be between 0 and 300μs.

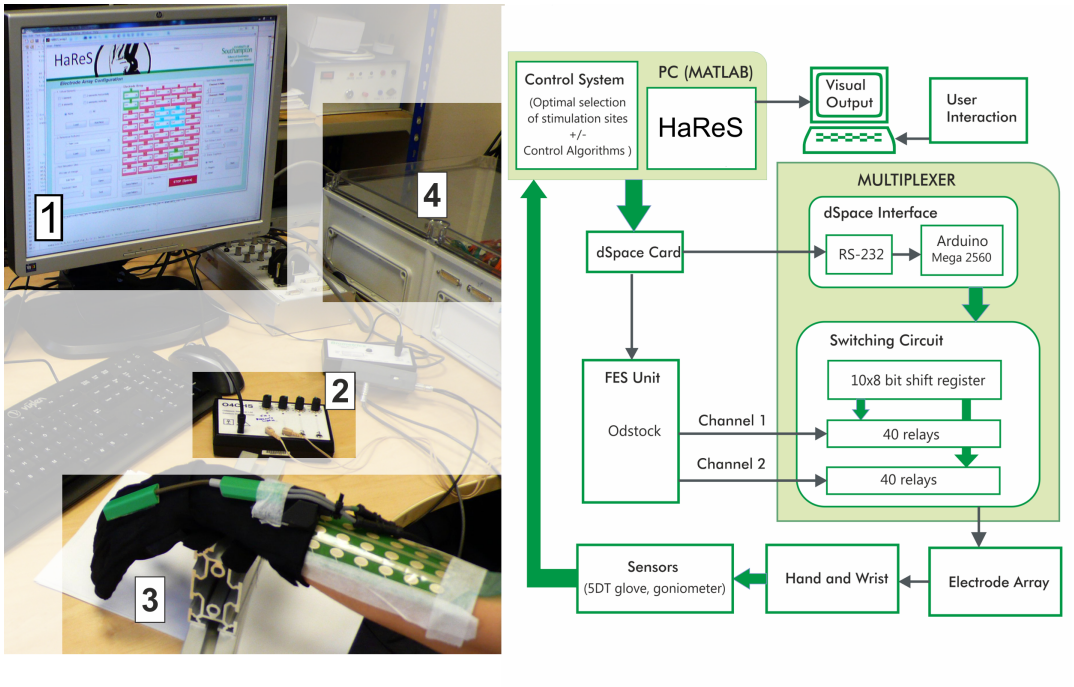

Figure 5.1: **Hardware components:**
(1) Control Module , (2) FES Stimulator (3) Sensors and Electrode Array, (4) Multiplexor

5.2 Sensors

The Biometrics twin axis goniometer SG75 was used to record the movement data of the wrist. The goniometer permits the simultaneous measurement of angles in two planes, e.g. wrist flexion/extension and radial/ulnar deviation. The raw angles of flexion and adduction (or abduction) are calculated using the linear calibration functions provided by the Biometrics Ltd. These are expressed as:

$$\Theta_{flexion} = 90.9091(\Theta_{raw} - 2.5292) \tag{5.1}$$

$$\Theta_{abduction} = 89.2857(\Theta_{raw} - 2.5246) \tag{5.2}$$

To measure finger joint position the 5DT Ultra Glove was used due to its lower cost compared to other commercially available sensing gloves and high accuracy of measurements. The high data quality and data rate make it ideal for realistic real-time applications such as game control and interaction. The glove has two fiber-optic flexion/extension sensors per finger and one abduction sensor between fingers. Each sensor reading represents an integer from 0 to 4095 due to the analog-to-digital conversion electronics embedded in the glove circuitry. The glove has high resolution ans is able to detect changes in fingertip position as small as 0.12 mm. However, the

range of integers corresponding to a full flexion of the glove changes from finger to finger, due to the position of the sensing element within the glove fabric. Therefore, to present the data in degrees it was necessary to determine the relationship between these integers and the finger angles for each finger and each glove.

The relationship between raw integer data values and flexing angle values are found to be close to linear. This linear relationship was confirmed by bending the sensors across the acceptable range of angles in small intervals and obtaining the correlating raw data values. However, the sensors used in the 5DT glove do not measure exact anatomical joint angles (MC,PIP). Mapping from the raw data into the degrees with the assumption that the values represent the real anatomical joint angles leads to a complex non-linear calibration function and to use for example a piece-wise polynomial fitting method. This method of calibration requires lengthy identification experiments. However, the data can be normalised as in (5.3) or represent the approximate values of anatomical flexion/extension angles for each joint. Thus, to enable individual calibration to be performed for each subject before a trial session the sensor outputs were obtained using linear calibration method given by (5.4).

Data Normalisation:

$$out_{norm} = \frac{(raw_{val} - raw_{min})}{(raw_{max} - raw_{min})} \tag{5.3}$$

where raw_{min} and raw_{min} denote the minimal and maximal integer values respectively measured by the 5DT glove sensors.

Linear Calibration:

$$out_{calib} = \frac{(raw_{val} - raw_{min})}{(raw_{max} - raw_{min})} max \tag{5.4}$$

where raw_{min} and raw_{max} denote the maximal/minimal value of hand joint in integer, which was recorded for each participant during the trial and max is the average maximal ROM of a hand joint for the normal functioning hand as in Table 2.1

5.3 Software

The Graphical User Interface (GUI) allows patients to interact with a software, which is used in conjunction with the rehabilitation hardware and SEA-based control methods. A specially designed game provides interactive and motivating training environment with feedback, based on measuring selected quantitative features of hand function such as ROM and tracking error. Additionally GUI provides manual and

automatic configuration methods for the electrode array and control methods described in previous chapter (Chapter 4). The GUI was coded in MATLAB.

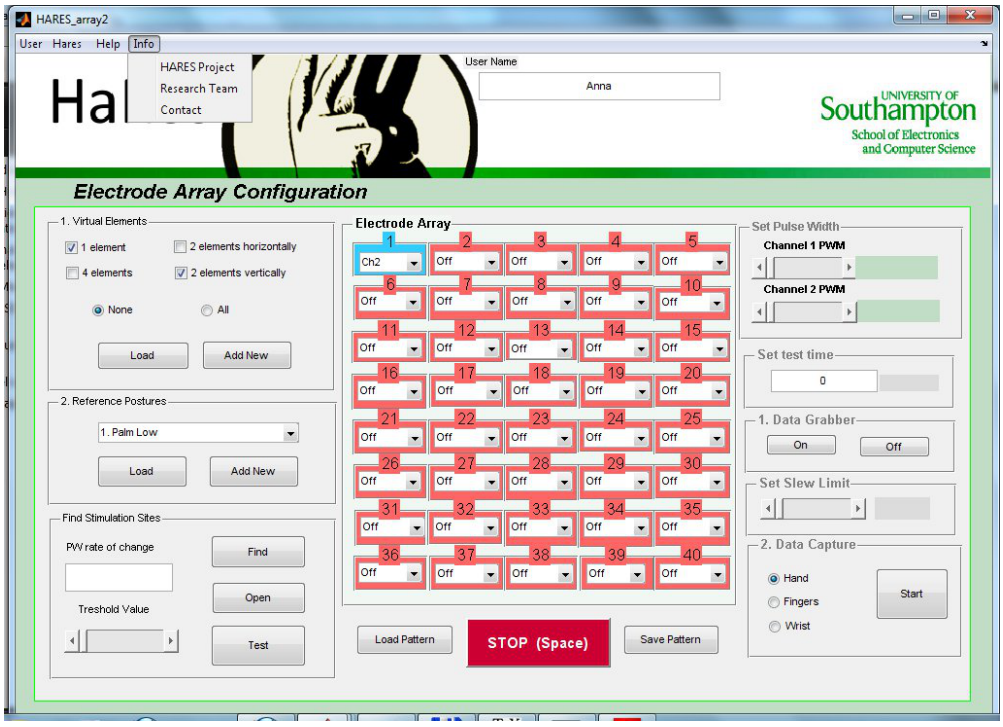

Figure 5.2: Graphical User Interface

5.3.1 Hares Game

Hares is an arcade game designed specifically for the purpose of stroke rehabilitation of patients with hemiplegia and spasticity of hand and wrist. The game was implemented in MATLAB, using image processing toolbox and simple concept of spatial manipulation of hierarchically layered pictures with transparent background property. The cognitive and motor task of the game is to control position of the pad (hat) in such a way that the number of caught objects (hares) is maximized. In the simplest case, the different scenarios of the game and levels of difficulties are defined by three aspects: the number of objects falling, the position of the objects on the screen (including spatial configuration of the objects), the speed of falling. The beta version of the game is shown in Figure 5.3.

While playing a game, patients interact with a virtual universe, which receives their responds and control inputs (hand movements) by changing its status. Information regarding the outcome of the interaction is then conveyed to patients (i.e. scoring), and eventually gathered and used by them to decide what to do next, as shown in Figure 5.4. This cycle is repeated iteratively, until the player wins or loses the game, or

simply decides to suspend temporarily his/her training session. Depending on the predefined movements, used in game control, the exercise can either be focused on a single joint motion such as e.g. wrist flexion or on a multiple-joint movement, such as for example hand opening. In considered case, hand opening/closing movement, performed by the user in the real world is the game control input, which results in the movement of the hat in the game world to the left/right direction along the horizontal axis of the game window, which is displayed on the screen.

Figure 5.3: Hares game

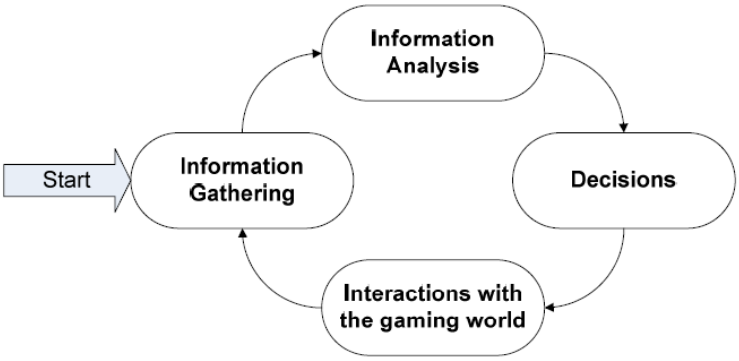

Figure 5.4: Interactive cycle in the playing game experience ((Fabricatore, 2007))

Before running the game, a set of trajectories (i.e. hand opening) for the specified in the game task (movemenent of the pad to the right) have to be defined. A set of

trajectories are stored as the assessment tasks used in Hares Game. Taking into the considerations the level of patient's disability, trajectories are defined with respect to the range of motion capabilities of the participant's hand.

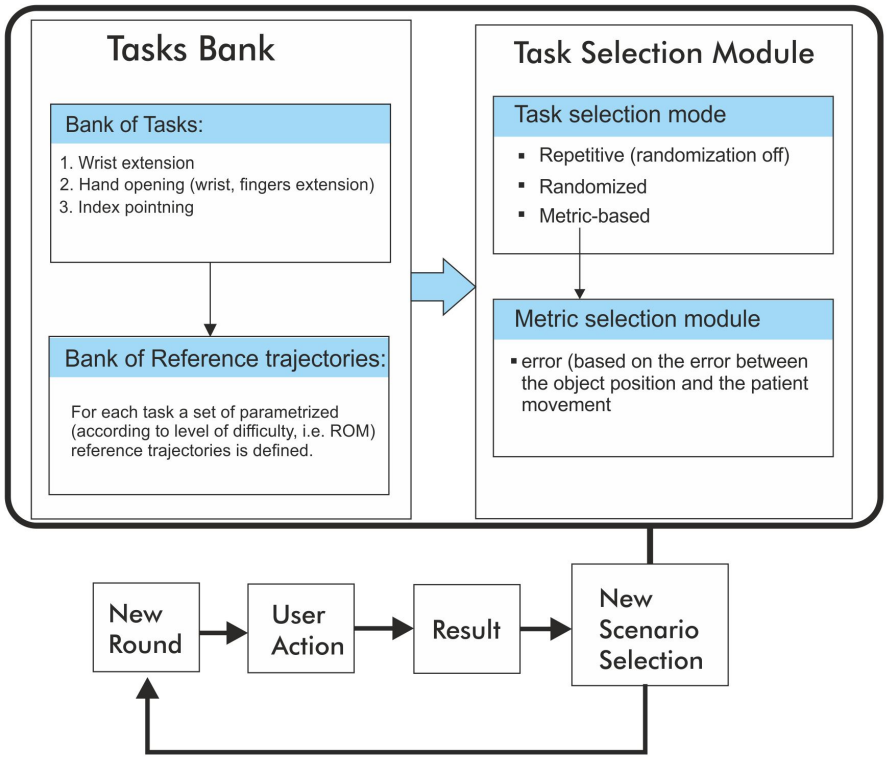

Figure 5.5: Selection of a task

The trajectories are restricted by the game workspace which in the simplest horizontal plane is specified as the (maximal-ROM-of-healthy-person/x-screen-resolution). The trajectories are parametrized and classified according to the difficulty level, which for the simplest case is defined as the normalized value $[0, 1]$. Here, 1 denotes the trajectory with the highest level of difficulty, which in considered case is represented by the maximal horizontal displacement of the hat on the screen.

Trajectories (tasks) can be switched during the training process, or in other words during playing the game by the user. The three modes of switching of the trajectories with respect to the task defined in the game architecture are proposed. These are: Switching Mode off (repeating all the time the same task, tracking the same trajectory), Random Mode (simple random selection from the set of predefined trajectories), Intelligent Mode: a new task/trajectory in the current trial (game scenario) is indicated by the metric and patient performance in previous trial. The three modes of switching tasks are presented in the Figure 5.5.

In the game-based training environment the feedback is provided in form of the

scoring. Generally, the better tracking patients achieve during the training session the higher scores they get. The formula proposed in considered case is following:

$$score = [(1 - normalized\_error) * 100] \tag{5.5}$$

The scoring formula in the simplest case can be determined based on the tracking error. However other parameters such as speed of movement, number of trial, difficulty level in the game (including cognitive and motoric difficulty level) may also be taken into account.

Electrode Array Configuration Module provides interface to manual and/or auto selection of appropriate stimulation patterns for a pre-defined group of reference postures/trajectories, which constitute the set of patients control movements, that can be exercised during the game-based training session. Data collected during configuration of electrode array and during the game-based training session can be stored providing feedback to the patient or to the therapist about the training duration, frequency of training sessions and their effectiveness.

5.4 Design Considerations and Experimental Procedure

The specific character of SEA-based control of the human hand and wrist, makes the design process a difficult task compared with the control of mechanical systems. The main difficulties emerge from the biomechanical nature of the system, which requires a patient-centred approach during system design and implementation. 5 unimpaired participants have volunteered to take part in the experimental tests. Each participant attended 1-4 experimental sessions. Participants anonymity was preserved through use of identifiers P1-P5. The details of each participant are presented in the Table 5.1.

Participant	**Gender**	**Age**	**Hand**
P1	Male	35	Right
P2	Male	27	Right
P3	Male	24	Right
P4	Female	31	Right
P5	Female	26	Right

Table 5.1: Information about the participants, which volunteered to participate in the tests. Participants anonymity was preserved by use of identifiers P1-P5

The experimental procedure was divided into two separate stages. First stage of the experiment was conducted to establish the settings and methods of general procedure to obtain the optimal solutions, which were tested in the 2nd stage of experiments.

Firstly, each participant was invited to the laboratory where after consenting the participant in the study and the equipment, the initial procedure was undertaken to assess whether the participant responded sufficiently to applied stimulation. The electrodes, data glove and goniometer, was put on the participants right hand. The return electrode and active electrode array were attached to the dorsal side of the forearm

The stimulator used in experiments supports 6 levels of stimulation. For each participant the amplitude level had to be set up manually. The criteria of manual selection of amplitude level were following: hand movement could be induced for selected elements of electrode array, there was no discomfort during stimulation with maximal value of pulse-widthinput for these elements. The participants were requested to place their right hand on a specially prepared support and to relax. Participants were further instructed not to apply any voluntary action as the gradually increasing from 0-300 μ input signal was send via randomly selected single elements and group of electrode array elements, whilst the amplitude level was being gradually increased in a safe and careful manner to an appropriate level. During this procedure, it was assesed, that each participant responded well to the 3rd level of the stimulation. Each element was active for 3-5 seconds which for majority of the electrode elements resulted in tetanic muscle contraction and visible hand movements.

5.4.1 Selection of Virtual Elements

During the preliminary tests it was observed that single element stimulation can induce movement of single fingers, i.e. index and little fingers. However, single element stimulation required a higher level of pulse-width to cause visible movement of the hand and wrist. This higher level of stimulation could result in discomfort or even pain sensation. To overcome this problem and increase the practical level of selectivity and accuracy of the optimized stimulation sites, 4 types of elements were considered. These are: standard single element of electrode array (1-element) and 3VEs as follows: 2-elements oriented horizontally, 2-elements oriented vertically and 4 - elements, as shown in Figure 5.6. To collect the data used in optimisation methods, each participant was requested to place the hand on the support, in such a way that the gravitational force was causing flexed position of the wrist with fingers directed down. The participant was advised to relax and not to apply any voluntary movement, whilst the gradually increasing electrical stimulation was passed through every element activated one by one for 3 seconds. There was a varying response to electrical stimulation amongst the participants for different types of the VEs. The factors taken into account during the preliminary selection test were the movement and pain sensation for each element of the electrode array. If during the test with selected

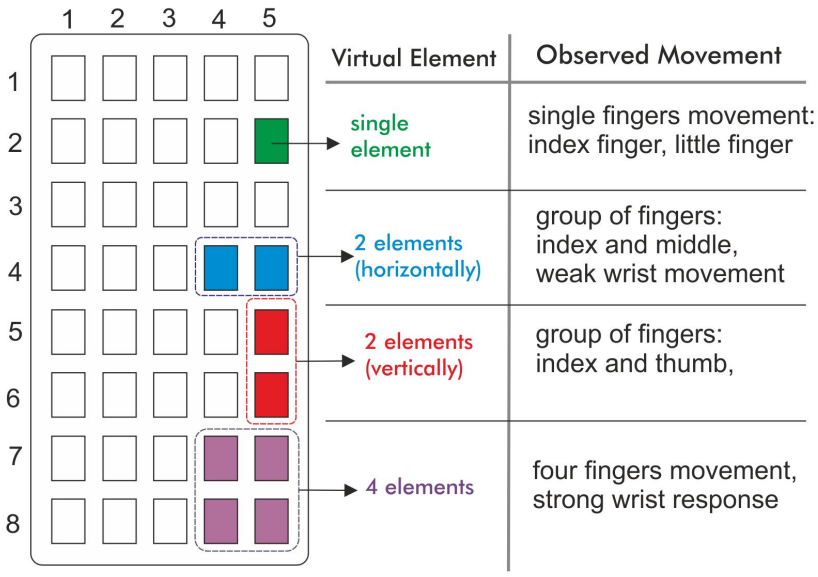

Figure 5.6: Types of virtual elements, tested during electrical practical experiments and the brief characteristic of the movements, that could be observed

element the uncomfortable sensation occurred, the stimulation signal was turned off for safety and comfort of the participant. The elements for which stimulation resulted in unpleasant sensation, were excluded from the final testing. Generally male participant responded well to stimulation for all elements, including single elements. On the other hand, female subjects, showed greater sensitivity in response to the single element stimulation and some array elements had to be excluded from further tests. The excluded elements are shown in Figure 5.7

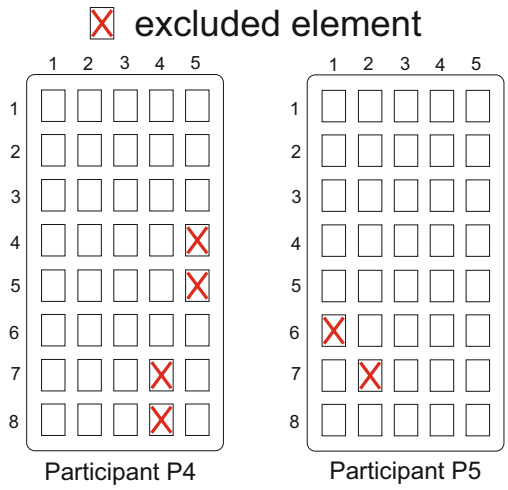

Figure 5.7: The elements which caused unpleasent sensations for P4 and P5 and hence had to be excluded from the general procedure

5.4.2 Choice of reference postures

A set of different reference postures has been chosen, based on practical limitations of the technique, clinical needs and game-based character of the system. The initial and reference postures are listed in Table 5.2.

Posture	**Movement**
Initial Posture	Fingers and wrist flexed
Reference posture	Fingers extended and wrist without flexion and abduction/adduction (Opened hand)

Table 5.2: Initial and reference postures

These postures are used in the optimisation procedures to minimize the norm error between the desired reference posture and that recorded during the trial. These postures was obtained from the participants during, each trial session. To obtain initial posture $\boldsymbol{y_0}$, participants were requested to place the hand on the support with the wrist and fingers directed down, in such a way that the gravitational force was causing maximal wrist flexion, without participants voluntary effort. Participants were requested to keep this posture for 3 seconds, whilst the measured by data glove and goniometer values of all fingers and wrist joints were being recorded by MATLAB software. To obtain the more accurate and reliable data, the initial posture was represented by the average of the recorded over the last second of the measurement process values for each of the 16 joints of the hand and wrist.

Similarly, to obtain the average reference postures $\boldsymbol{y_d}$ for each participant, he or her was requested to simply open the hand and keep this posture for 3 seconds whilst the data from the sensors was being recorded. These postures are used in the optimisation procedures to minimize the difference between the reference postures and those obtained during the test sessions $\boldsymbol{y}$ obtained for optimal stimulation patterns.

The normalised error for an optimal stimulation pattern, was calculated across all 16 joints as follows:

$$\overline{e} = \frac{\|\boldsymbol{y_d} - \boldsymbol{y}\|_2}{\|\boldsymbol{y_d} - \boldsymbol{y_0}\|_2} \tag{5.6}$$

Resulting error is a dimensionless quantity, with 0 indicating perfect fit to the reference posture and 1 indicating maximal error.

5.4.3 Method of optimal pattern selection

The main difficulty in obtaining the appropriate stimulation input is the limitation put on the number of trials that can be performed with patients. The optimal stimulation signal must be identified in a relatively short time, with as few tests performed on patients as possible. The more trials involving stimulation of subject's muscles, the greater the risk of fatigue and the less comfortable the procedure is for the patient. Hence, the methods of finding optimal stimulation pattern for the electrode array have been firstly analysed and compared in numerical studies. The data used in analysis of the optimisation methods were recorded from unimpaired participants during the first stage of the experiments to select optimal stimulation patterns, tested at the final stage of the tests.

Penalty function method

This method limits the number of stimulation levels, but the number of elements that can be made active is unconstrained. The effectiveness of the method depends strongly on the appropriate selection of stimulation level, which is shown in Table 5.3

l	Normalized Error	Non-zero elements of sparse inputs vector **u**
5	0.341	$[u_3 = 0.2, u_4 = 0.2, u_5 = 0.2, u_8 = 0.2]$
8	0.265	$[u_3 = 0.25, u_4 = 0.25, u_5 = 0.25, u_8 = 0.125, u_{39} = 0.125]$
10	0.251	$[u_3 = 0.2, u_4 = 0.3, u_5 = 0.2, u_8 = 0.2, u_{39} = 0.1]$

Table 5.3: Example of numerical results for 5, 8 and 10 stimulation levels for data recorded from the participant on the same trial session.

Accelerated Proximal Gradient

This method selects up to $p = n$ elements from electrode array which can be activated with any pulse width value within the range of stimulation $[0 - 300\mu s]$ (continuous input signal). The effectiveness of the APG algorithm is strongly related to the experimental data. Generally, APG converges monotonically to the sparsest optimal solution as shown in Figure 5.8. Hence, for some experimental data the number of non-zero elements in the optimal solution, may exceeds the number of available stimulation levels. Approximately 60 % of all obtained with APG optimal solutions required more than 2 levels of stimulation. Additionally, in considered case of 2-channel stimulation only up to 2 elements of electrode array can be selected using

APG. Thus the optimal solution in all the cases consisted of single elements stimulated with very high pulse width level, which exceeded $250\mu s$ ($u_i > 0.8$), see Table 5.4. This was increasing a risk of appearing a discomfort during the stimulation. Thus, to overcome these difficulties, a brute-force searching algorithm was developed.

Participant	Active elements	Error $\overline{e}$	Non-zero elements of vector of inputs $\mathbf{u}$
P4	2	0.145	$[u_1 = 0.99, u_{23} = 0.01]$
P5	3	0.151	$[u_1 = 0.897, u_{23} = 0.04, u_{25} = 0.051]$
P3	4	0.221	$[u_2 = 0.551, u_6 = 0.0109, u_7 = 0.121, u_{30} = 0.159]$

Table 5.4: Number of active elements in sparsest solutions of APG for 3 different participants.

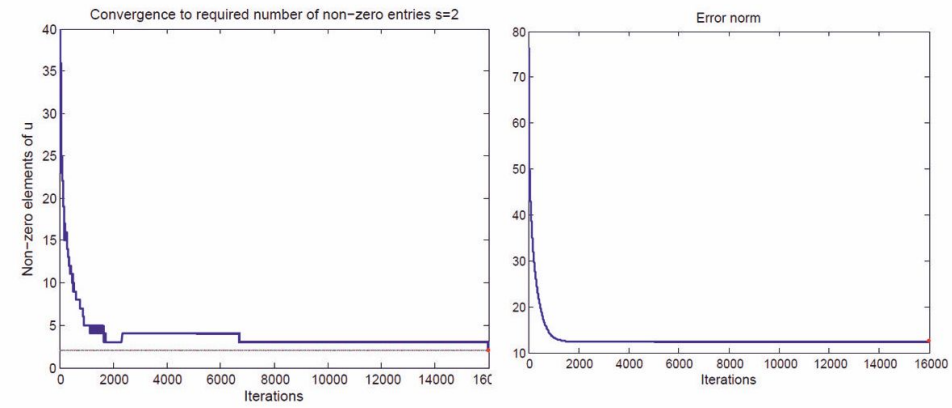

Figure 5.8: Convergence of APG to sparsest solution s = 2 with error norm for 16 joints.

Brute-force Searching Method

Session	u_{rate}	Error $\overline{e}$	Non-zero elements of vector of inputs $\mathbf{u}$
1	0.025	0.213	$[u_2 = 0.375, u_{23} = 0.45]$
1	0.15	0.148	$[u_{11} = 0.3, u_{12} = 0.3, u_{40} = 0.6]$
2	0.025	0.144	$[u_{11} = 0.225, u_{12} = 0.225, u_{39} = 0.675, u_{40} = 0.675]$
2	0.15	0.132	$[u_2 = 0.45, u_3 = 0.45, u_{24} = 0.45, u_{25} = 0.45, u_{29} = 0.45, u_{30} = 0.45]$

Table 5.5: Exemplar results for different values of u_{rate} of brute-force algorithm for data recorded from participant P3 on two different test sessions.

This approach combines the two previously described methods, due to the fact that it constrains both, the number of stimulation levels and the number of activated elements of electrode array.

The parameters of the method dictate the speed and accuracy of the searching procedure. Small u_{rate}, can improve the performance of the algorithm, but increases the search space for the algorithm. The number of elements was predefined based on the average sparsest solution of APG algorithm for different set of data and was set to be $n_{active} \leq 8$. Experimental investigations indicated, that satisfactory results can be obtained using $u_{rate} = 0.15$ as shown in Table 5.5.

Qualitative comparison of methods

Method	**Penalty Method**	**Proximal Gradient**	**Searching Algorithm**
Method	Heuristic	Gradient-based	Greedy
Iterations	Predefined	Data-dependent	Predefined
Elements Number (N)	Unconstrained	N $\geq$ Sparsest Optimum	Predefined
Stimulation Levels	Predefined	Unconstrained	Predefined
Convergence	Parameter-Dependent	Monotonic	Parameter-Dependent
Optimum	Parameter-Dependent	Sparsest Optimal Solution	Parameter-Dependent
Parameter Selection	Ad-hoc	Analytically	Ad-hoc

Table 5.6: Qualitative comparison of methods

The brute-force searching method was used in further experimental tests, due to its simplicity and flexibility in setting the different types of initial constraints as shown in Table 5.6.

5.5 Experimental Results

The clinically relevant task considered during final stage of experimental testing was to move the hand from an initial posture $\boldsymbol{y_0}$, which emulates a spastic hand to a final extended position $\boldsymbol{y}_d$ as shown in Figure 5.9. This represents hand opening movement. The optimal solutions was tested $j = 5$ times and the mean normalized error is given by

$$MNE = \frac{\sum_{i=1}^{j} \overline{e}_i}{j}, \quad j = 5 \tag{5.7}$$

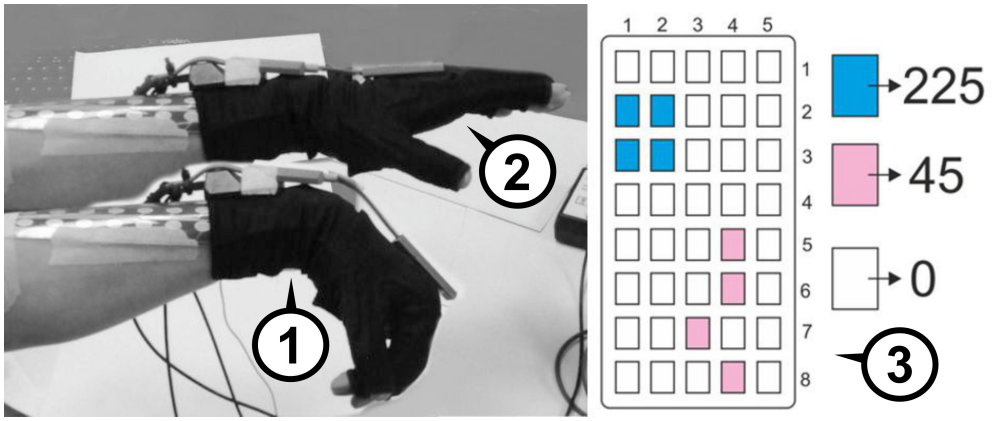

Figure 5.9: FES schematic for hand and wrist control with hardware components: (1) initial posture, (2) reference posture, (3) optimal stimulation pattern, defined by following vector of normalized non-zero elements of vector $\boldsymbol{u} = [u_6 = 0.75, u_7 = 0.75, u_{11} = 0.75, u_{12} = 0.75, u_{24} = 0.15, u_{29} = 0.15, u_{33} = 0.15, u_{39} = 0.15]$ where $u_{max} = 1$ represents the normalized maximal value of pulse-width $= 300\mu s$.

The resulting error (MNE) is a dimensionless quantity, with 0 indicating perfect fit to the reference posture and 1 indicating no improvement from initial posture. The results show that the error was reduced to between 0.24 (for participant P1) and 0.35 (for participant P5) using only two levels of stimulation (see Table 5.7 and Table 5.8.

No.	**Participant**	**NME for all 16 joints**	**Standard deviation**
1	P5.	0.353	0.022
2	P4.	0.338	0.035
3	P3.	0.318	0.041
4	P2.	0.30	0.061
5	P1.	0.24	0.082

Table 5.7: Normalized errors for 5 stimulation patterns listed in Table 5.8.

The results show that the optimal stimulation pattern differs from subject to subject (Table 5.8). Additionally, the test results indicate that there is significant variability in the results for the same participant on different trails (Table 5.9).

No.	Active elements
1.	$[u_1 = 0.15, u_2 = 0.15, u_6 = 0.75, u_7 = 0.75, u_{11} = 0.75, u_{12} = 0.75]$
2.	$[u_3 = 0.6, u_4 = 0.6, u_{14} = 0.3, u_{15} = 0.3]$
3.	$[u_2 = 0.15, u_6 = 0.75, u_{11} = 0.75, u_{12} = 0.75]$
4.	$[u_3 = 0.3, u_8 = 0.6]$
5.	$[u_1 = 0.3, u_2 = 0.3, u_4 = 0.75, u_5 = 0.75]$

Table 5.8: Optimal Stimulation Patterns for 5 participants, where No.1 denotes optimal stimulation pattern obtained for participant P5, No.2 for P4, No.3 for P3, No.4 for P2 and No.5 for P1.

Trial	**Active elements of the array**	Predicted error ($\bar{e}$)	Test error (MNE)
1.	$[u_3 = 0.45, u_4 = 0.45, u_{32} = 0.45, u_{37} = 0.45]$	0.205	0.272
2.	$[u_1 = 0.45, u_2 = 0.45, u_{21} = 0.45]$	0.152	0.253
3.	$[u_2 = 0.3, u_{21} = 0.6]$	0.153	0.257
4.	$[u_1 = 0.3, u_2 = 0.3, u_4 = 0.75, u_5 = 0.75]$	0.238	0.24

Table 5.9: Optimal stimulation patterns for participant P1 on different trials

Average Normalized Error for all test trials	0.36 ± 0.05
Average number of single elements activated n_{active}	5 ± 2
Average size of VE	3 ± 1

Table 5.10: Summary of the results for all participants

The average value of normalized error, calculated for 30 optimal solutions for all participants is equal 0.36 as listed in Table 5.10. The average initial posture $\boldsymbol{y_0}$, reference posture $\boldsymbol{y_d}$ and output posture $\boldsymbol{y}$ defined by all 16 values of the hand and wrist joint measurements expressed in degrees for all 30 tested stimulation patterns are shown in Figure 5.10. The tests have showed, that average number of single array elements in optimal stimulation pattern is equal 5. Average VE consists of 3 single elements of electrode array.

The main factors taken into account in assessing the effectiveness of the approach were: the accuracy of the induced final posture and the participants comfort during the movement. The main objective was to achieve opening of the hand, defined by the extension of the wrist and fingers without wrist abduction and adduction. For each participant, the induced movement was reported to be smooth and comfortable enough and resulted in the final postures fitting from 65 % to 75% the desired ones with all fingers and wrist extended and only minimal abduction and adduction of the wrist (see Figure 5.11, Figure 5.12 and Figure 5.13) for all participants. As it is seen in Figure 5.13 the average range of extension motion (expressed in degrees) for all PIP joints of the four fingers is equal to approximately 15 degrees. This relatively small extension movement is due to the fact that the average flexion of the fingers in the initial posture (see Figure 5.10) was meant to be caused only by the gravitational force to minimize

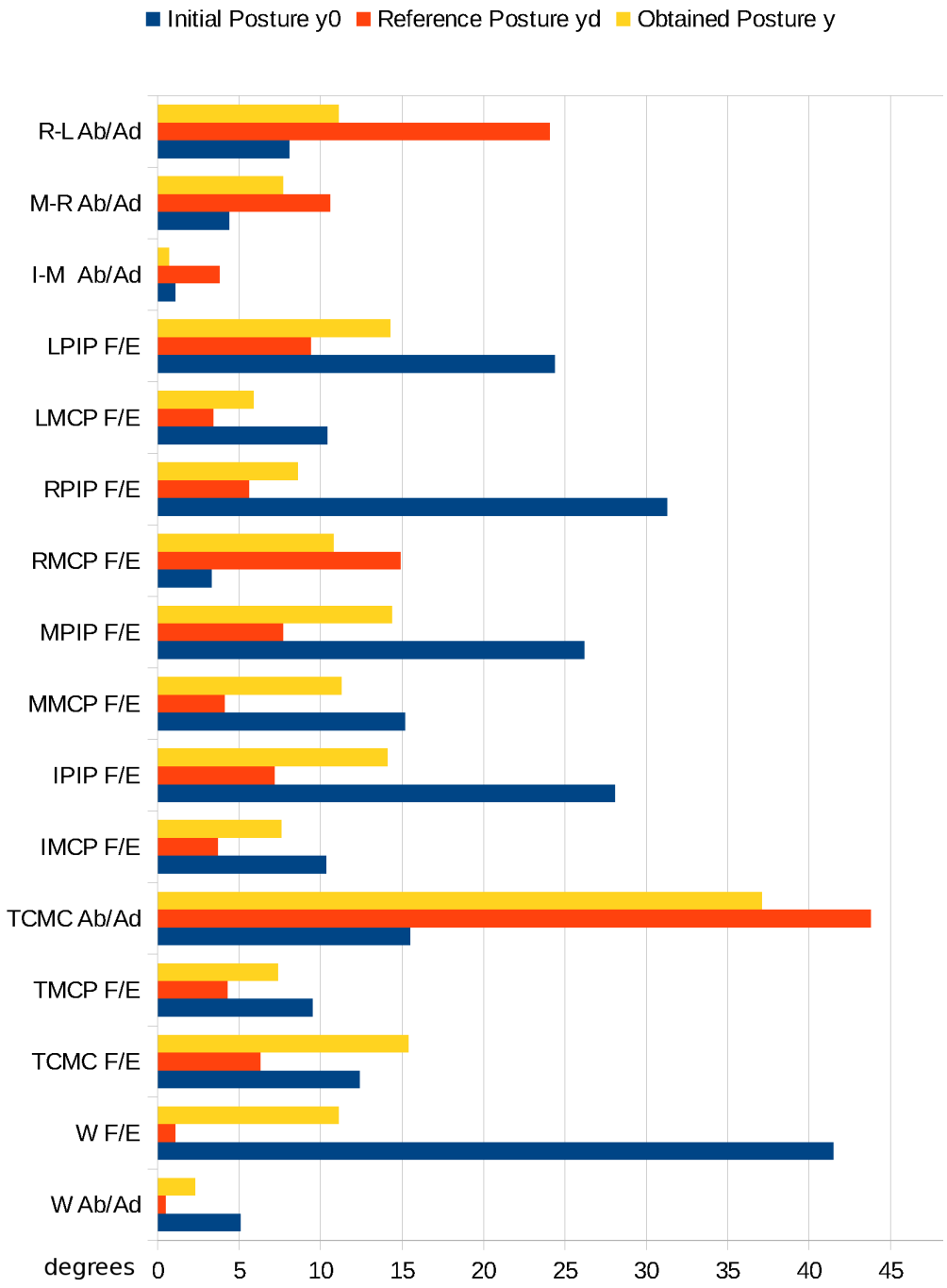

Figure 5.10: Average Error in degrees for each joint Index of the complete 16 DOF Hand and Wrist for all obtained stimulation patterns for participants P1-P5. Here W denotes Wrist, I-Index, M-Middle,R-Ring, L-Little and T-Thumb respectively.

participants voluntary contribution to the movement. However, as it can be observed for example in the Figure 5.13 a for participant P3, the residual voluntary flexion

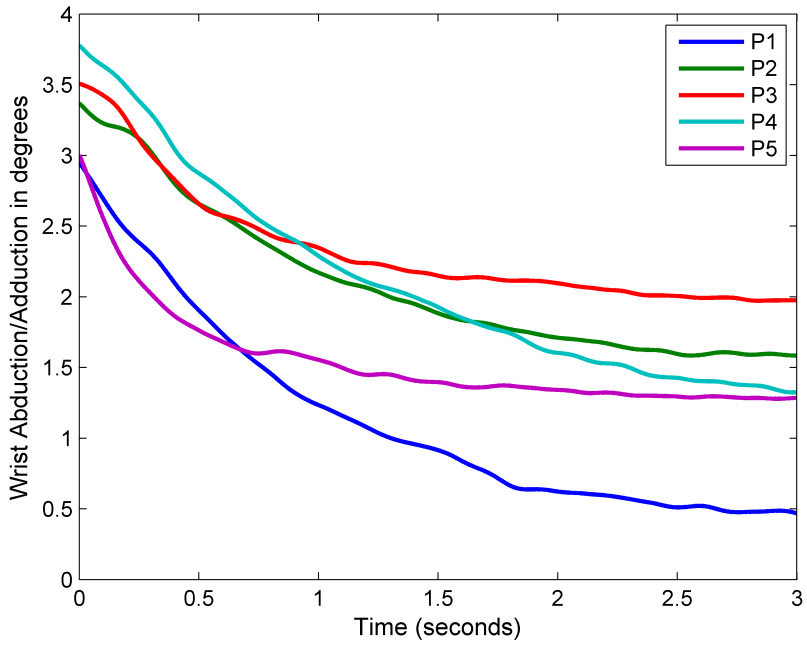

Figure 5.11: Average Wrist Abduction/Adduction for all 5 participants for listed in Table 5.8 optimal stimulation patterns.

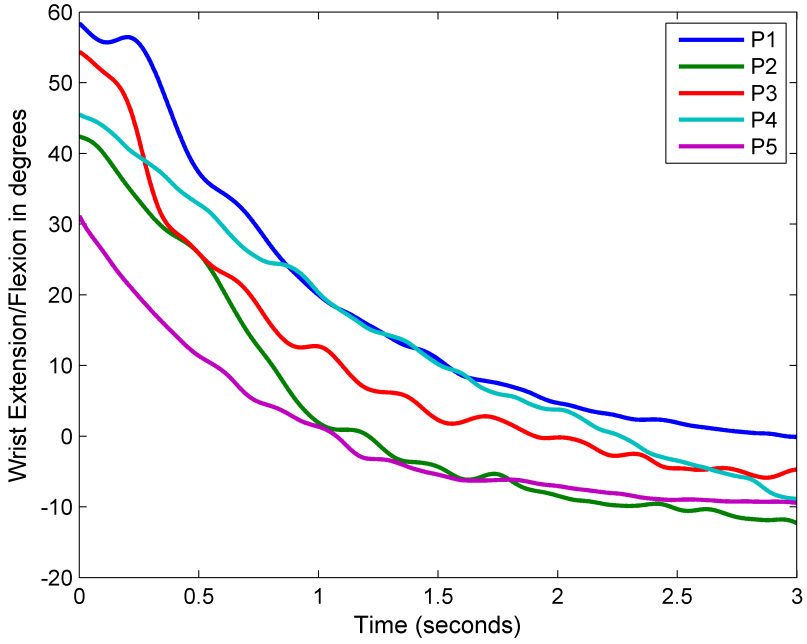

Figure 5.12: Average wrist extension movement (from flexed position) for all participants (P1-P5) induced by the lasting 3 seconds stimulation with listed in 5.8 optimal stimulation patterns.

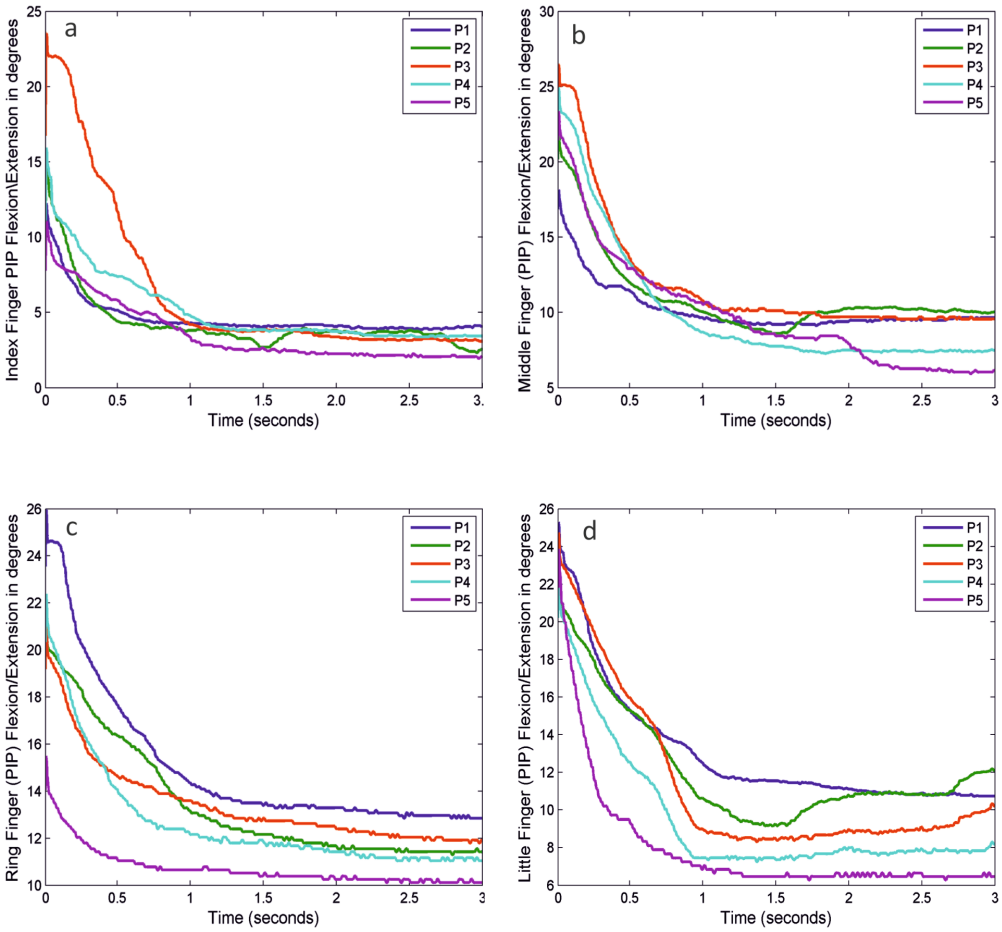

Figure 5.13: a-d Average Index Finger PIP, Middle Finger PIP, Ring Finger PIP and Little Finger PIP extension movements respectively from flexed position for all participants (P1-P5) induced by the lasting 3 seconds stimulation with listed in 5.8 optimal stimulation patterns.

movement was not eliminated in 100%. In addition, the elastic material in combination with sensors included in the 5DT glove can cause additional anti-gravitational effect by lifting the fingers.

In summary, the preliminary trials have confirmed that the developed procedure for automatic selection of appropriate elements of electrode, gives acceptable results for the case of opening the hand with using only two channels of stimulation and single trial optimisation method. The ILC-based approach to give a significant improvement in practical results compared to the previously tested optimisation method requires more than two channels of stimulation. Additionally, for more than two channels tracking of more complex postures such as i.e. postures for which separate stimulation of additional muscles actuating i.e. index finger, thumb or little finger is required. The average number of single elements in the optimal solutions indicated, that at least 3 or

more channels is preferable for the multiple-trial approach. These findings were tested and confirmed in experimental trials by collaborative research team and the results, which can also be find in (Exel et al., 2013b), are presented next.

ILC-based method of selection optimal stimulation pattern

The Newton-based ILC-based approach for SEA-based control of the hand and wrist using 4 channels of stimulation have been tested on 2 unimpaired subjects. Three

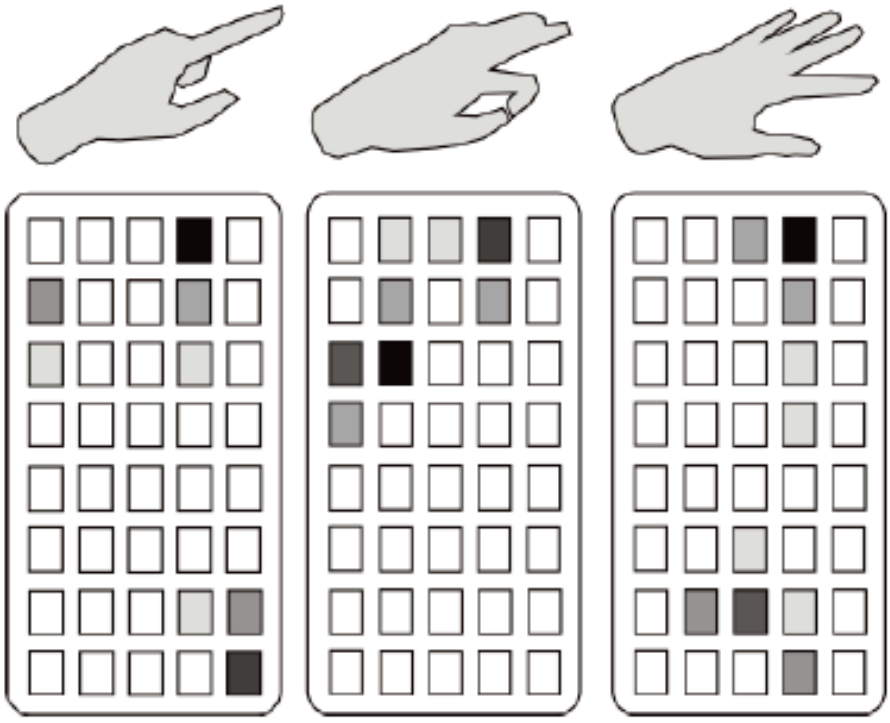

Figure 5.14: Example optimal stimulation patterns identified for subject P1, for the pointing, pinch and open hand postures.

different reference postures, which incorporate specific extension of the fingers and wrist, were selected to verify the optimisation procedure. These are: pointing with the index finger, pinching between thumb and index finger and an open hand posture. Examples of the three hand postures are shown in Figure 5.14. The iterative optimisation procedure was undertaken on two unimpaired participants who each provided no voluntary effort. The optimised solution was tested for the first 3 trials and normalised error was calculated across all joints for each posture. Figure 5.14 shows the optimal stimulation sites identified from Participant 1, for the pointing, pinch and open hand postures. Mean error results for the first 3 optimisation

Trial k	**Subject**	**Pointing**	**Pinching**	**Open**
1	P1	0.297	0.245	0.19
	P2	0.287	0.353	0.221
2	P1	0.112	0.126	0.144
	P2	0.136	0.15	0.13
3	P1	0.036	0.044	0.047
	P2	0.015	0.039	0.034

Table 5.11: The tracking error (NME) for subjects P1 and P2 and 3 different refernce postures on 3 trials

iterations are shown in Table 5.11.

Summary

The proposed general procedure for SEA-based electrical stimulation can identify optimal stimulation patterns in both: single-trial and multi-trail manner. The procedure was successful in selecting optimal stimulation patterns and intensity of stimulation for which the induced postures fit the desired ones in approximately 68-96% for each participant, with NME joint errors significantly reduced on every trial.

Chapter 6

Discussion and Future work

This thesis addresses the use of surface electrode arrays to regulate the stimulation applied to the hand and wrist muscles in order to induce hand movement to desired posture. The developed methods, were presented in the context of the complete design of the hand rehabilitation system to provide both, theoretical and practical indications for future expansion of this rehabilitation technology. Main aspects crucial for practical use of this technology have been established and are discussed in this chapter. These are: problem of the modelling of the hand and wrist, methods of control and optimisation for electrode array, hardware specification of the system and human-computer interface design. SEA-based rehabilitation technology is currently an emerging and promising research area. Most of the existing methods use rule-based selection of suitable elements of electrode array and do not provide a mature mathematical background. Such methods do not use system identification algorithms, have no knowledge about the system and hence, operate in a similar way to clinicians manually repositioning a single electrode to "ad-hoc" find appropriate stimulation sites. Developed in this thesis approach, is the first attempt of remedying these deficiencies. Theoretical and practical considerations were taken into account and the comprehensive mathematical representation for SEA-based technology was provided, including the problem of identification and control of the human hand and wrist using electrical stimulation with electrode array.

To ensure a high-level performance model-based control algorithms require a mathematical model. The model of the controlled system is obtained in the process of system identification. Generally, the more accurate identification of the system and hence the model, the more precise control can be achieved. In case of biological systems, such as those considered in this work, the identification and modelling can be especially difficult task, due to the high-degree complexity, limitations and other factors generated by the special nature of a living organism. These, in case of

identification of neuromuskulotendon model of the human hand include aspects such as:

- a high degree variability and dynamics of the hand system partially due to complexity and uniqueness of every human being
- limited methods of testing and identification of the hand complex anatomical system, mainly due to its alive character, which requires the safety issues to be taken into account during process of system identification and control

To give an overall insight into the level of complexity of the anatomical structure of the hand, together with the mechanisms of the neural control of this highly advanced and sophisticated end effector of a human body, the basic anatomical background was provided. In addition, the simplistic model of the human hand, which included the musculotendon structure of the wrist and finger was developed and analysed in simulation studies. The level of complexity of even this relatively simple model, indicated that there is a need for development other methods of identification of the considered system, which could be applicable for the problem of SEA-based control of the human hand and wrist.

To overcome difficulties associated with complex identification the novel approach for SEA-based control of the hand and wrist has been proposed. The novel approach developed for electrode array is defined as both: optimisation and control problem, by combining the optimisation methods for selection of appropriate elements of the electrode array with ILC. The selection of optimal stimulation pattern of electrode array is defined as optimisation problem of finding sparse input vector $\boldsymbol{u}$. Three different optimisation approaches, which find the sparse input vector have been considered. Each of these methods has been developed, based on a variety of initial constraints which are dictated by the hardware specification, i.e. regarding the number of the channels (n) supported by the stimulator and number of single elements in the electrode array (m). The optimisation methods are following:

- Penalty method: selects a combination of up to $p = m$ electrodes with up to n separate input values $u_i \in \mathcal{U}$, where $\mathcal{U}$ is a set of discrete values of pulse width, which can be defined by the predefined sampling step. For example for the normalized values of input signal, the sampling step equal 0.1 defines the set $\mathcal{U} = [0, 0.1 \dots 1]$
- Proximal Gradient Algorithm: selects up to $p = n$ array elements with the input values $u_i \in [0, 1]$ (continuous values).
- Searching algorithm: selects up to $p = n$ active array elements with the discrete input values $u_i \in \mathcal{U}$ defined by sampling step equal to u_{rate}.

The concept of using the obtained sparse vector $\boldsymbol{u}$ to identify the optimal stimulation pattern, together with indications of using this information to further reduce dimension of the problem for the ILC-based control algorithms is also presented.
The sparse input vector is employed to select only those array elements that are critical to a task completion within iterative learning control framework. The general procedure were tested in practical experiments to assess the performance of developed control approach for control of the entire hand. The normalized error for 16 DOF system of the hand and the wrist showed that the induced movement for obtained optimal stimulations patterns fit the predefined reference postures in approximately 68% on the first trial to 96% on the last one for all participants. The results given confirm the potential of these new approach for the application area but further research and experimental tests are required to confirm general effectiveness of the approach, i.e. for the tracking of more complex postures. In addition, the method was tested on unimpaired participants and hence next step in general validation of proposed control approach within rehabilitation domain, are the clinical tests with patients.

The developed approach is patient-centred as it incorporates the concept of using a group of elements to minimize discomfort of stimulation. Such selected elements are treated as a new single element (Virtual Element (VE)) of the new Virtual Electrode Array. Only three different VEs were considered during preliminary tests (see Figure 5.6). This generates research questions and problems which can be worth of further investigation in the future, such as i.e. the open problem of selecting different types of VEs for more complex postures. Open questions/problems are following:

- Are there VEs or e.v. set of VEs which would be optimal for the specific and more complex postures. Optimal VEs in the sense it would minimize the search space for the optimisation algorithms (for selected postures) and hence speed up the process of electrode array configuration.
- Do there exist optimal VEs, which could be effective (common) for a wider group of patients ?

In addition, the preliminary results give some suggestions about the preferable number of channels, which should be supported by stimulator i.e. for the considered case, when the electrode array is placed on the dorsal side of the forearm and only extensor muscles are stimulated. The advantage of the method is its wide applicability with respect to different electrode array technologies. Proposed procedure supports single-trial and/or multi-trial approaches, which can be applied for a variety of different hardware specifications, including different number of channels, that can be generated by the stimulator, different types of electrode arrays. Some of these findings were tested and confirmed in (Exel et al., 2013b).

The assumptions and simplifications, such as setting a compromise between the high accuracy of the model and the problem of its practical application, make the problem of SEA-based control of the hand and wrist an interesting and open research subject. In considered case only the tracking of simple postures such as an opening the hand or pointing were considered. Thus, the future work should be focused on further testing and improvement of the methods of array optimisation and the control algorithms described in this dissertation for the case of tracking more complex postures where i.e. also flexor muscles are stimulated. The effectiveness of the method, when both types of muscles flexors and extensors can be simultaneously activated is also an open question and needs to be tested in the future. In these cases however, i.e. due to anatomical complexity, coupled and non-linear nature of the mulculotendon system, multi-trial approach such as i.e. considered in this thesis Newton method-based ILC is preferable.

The ILC algorithm is a multi-trial procedure, which requires k times more single tests, compared to single-trial optimisation approaches. For the simple tracking to the final posture it can produce satisfactory results. However, the ILC algorithm have the potential to be more effective approach in case of more complex movements. The ILC approach however, to be effective requires an extended number of stimulation channels. Generally, to track the more complex postures, the larger number of stimulation channels is preferred. The presented iterative approach for finding optimal stimulation levels, must be extended to more general dynamic tracking case, in order to precisely control complex hand movements. This includes development and application of more advanced identification and control methods. All these aspects are still open questions and bring the possibilities for new challenging research projects.

In this work only the stimulation of extensor muscles was considered. To investigate the possibility of control of more complex movements of hand and wrist, a parallel activation of both types of muscles (flexors and extensors) must be supported by the hardware. Additionally to avoid non-convex optimisation problem, stimulator must be capable to produce a number of separate stimulation signals n which is not less than the number of single elements in the electrode array ($n \geq m$).

The stimulation signal was delivered by standard single square electrode (return electrode) in combination with electrode array (active one). This could be extended in the future by replacing the return electrode with an electrode array. This would make the problem of finding an optimal stimulation pattern more complex task, however appropriately selected elements from both electrode arrays, could additionally increase selectivity and hence accuracy of the stimulation. All discussed above aspects, requires the use/development of advance stimulation devices, that would support extended signal routing and larger number of stimulation channels.

Strong Points of the General Approach developed for SEA:

- Adaptable: Electrode array-based technologies can differ in respect to parameters such as: the number of single elements in the electrode array , number of separate stimulation signals supported by the hardware. The general approach developed can be applied to a variety of possible design specification of existing and future SEA-based systems.
- Patient-oriented: Non-invasive, VE-element approach allows adjust individual electrodes in the procedure.
- Does not require complex model identification.
- Uses the concept of VEs, which may be further expand i.e. by selection of different VEs for different muscles/postures.
- Unsupervised: does not require anatomical knowledge to be used and hence, more suitable for home-based systems.

Method weak points:

- Effective for simple movements: such as i.e. hand opening. It requires further investigation to assess whether it is effective for tracking more complex postures. These require a significant modification of the hardware.
- Heuristic: requires appropriate selection of parameters. The effectiveness of the approach is strongly related to the appropriate selection of parameters such as, i.e. amplitude, time of stimulation, type of VEs and u_{rate}.
- Tracking to the posture only: There is no dynamic tracking for which a complex non-linear model is needed and hence more advanced system identification methods have to be developed.
- Valid for the case when there is only one control parameter (in considered case it is pulse width). However, the brute-force searching algorithm could be adjusted to the case where there are more than 1 control parameters: i.e. amplitude and pulse width. This could improve the stimulation outcome and tracking.

Based on the experimental results and the existing literature, a new system for the hand and wrist restoration has been designed. The key element of the system is a game-based task oriented training environment designed for a wide group of patients, including patients with spasticity, hemiplegia and stiffness i.e. following the tendon surgical replacement. The presented in the thesis system, combines SEA-based stimulation mediated by novel optimisation algorithms for automatic calibration of electrode array with game-based virtual training environment. The current prototype

design is very simplistic and requires further development and many significant modifications to be useful in practice. However the core idea of the design was presented to stress the advantages of game-based character of the training and indicate the future directions for the expansion of this approach in rehabilitation domain. Appropriately designed game-based system, can be not only an interesting and motivating environment, it can be also a serious rehabilitation tool of which game is the core element. To make it clear, it is worth to consider the current system design as a starting point leading to further possible expansion and to discuss it in relation to existing rehabilitation interventions.

The greater understanding of the mechanisms of overcoming and adaptation to neurological and motor impairments and the boom in electronic technology has lead to the development of new methods of rehabilitation, such as CIMT, BMT, Robotics, VR and FES. The general aim of these new techniques is to be more effective in delivering rehabilitation, reducing the associated costs and most importantly, in producing greater functional gains in patients than traditional approaches. However, a modern rehabilitation system should be comprehensive, by comprising as many of the new rehabilitation methods as possible into one rehabilitation platform. Currently, the design of the system supports only UMT and CIMT as only one extremity is supported by the game control. These indicates the direction for further modification and development of the system. One future possibility is to extend the current game-based training environment to support other rehabilitation approaches such as, i.e. BMT in which both extremities are performing the same movement. For such case the feedback/performance can be calculated using the data from both extremities.

Another interesting possibility, is to modify the game in such a way, that the extremities are used in a staggered manner. Currently, there is lack of experimental research to support the effectiveness of alternative movements in dealing with motor impairments. This gives the opportunity for testing this approach. This type of movement has one advantage especially when combined with the VR-based system. The alternate character of the movement, can be used in the game design to increase self-motivation in patients. This provides alternative for the complex tele-rehabilitation systems and on-line games, in which users compete with each other, playing in the on-line environment. Instead of playing with another person, patient could play with himself/herself and the competition would be transferred to the scenario in which the left hand of the patient ćompeteświth the right hand. This could be especially beneficial, for the patients with hemiparesis or hemiplegia, which suffer from one extremity impairment. In such a case the healthy hand would be associated with the computer player, whereas the impaired hand would represent the patient. In this setting the self-motivation element, originates from the assumption, that the patient wants to win and hence regain a function in impaired hand. This is also an

interesting example of self-motivating and in some sense interactive feedback.

The system design supports the possibility of collecting a large amount of data. Hence, the final version of the HaReS is meant to serve as a research tool, that can be used for further comparison studies of different rehabilitation interventions such as: unilateral/bilateral movement with/without game-based therapy, with/without SEA-based assistance mediated by ILC. A challenging step into the future, would be an extension of the current version of the system by combining it with the web-based data-center and on-line game environment platform, which would support multi-player on-line mode of the game and could store the patient-specific data online.

A significant research must be also focused on modification and improvement the current version of the hardware. Current sensors used in the system include Bionic goniometers and 5 DT data gloves, which are not suitable for patients with severe hand disabilities. Data glove is made of an elastic material, which makes it difficult to don and doff to even an unimpaired person. Similarly, the goniometer gives precise measurements, however this precision is strongly related to the way of attachment of the goniometer to the hand. One solution to overcome this practical difficulties could be a development of an appropriate custom-made garment, that would combine all the sensors. Another possibility is to use modern sensing technologies such as i.e. Kinect or Leap Motion. These sensors represent the novel and recently emerging type of touchless sensing technology, which can track and recognize the hand motion based on advanced image processing analysis.

Chapter 7

Summary and Conclusions

The main objective of this thesis was to investigate the application of SEA-based control of the hand and wrist. There exsist different stimulation technologies which support different n number of separate stimulation signals (channels). Similarly, there is a variety of different electrode arrays, which can consist of m number of single elements (pads). The general approach developed can be applied to a variety of possible design specification of existing and future SEA-based systems by combining single-trial optimisation methods with multiple-trial ILC (see Table 7.1).

Method	**trials**
ILC with optimisation	$n > k \geq 1$
Single-trial Optimisation Methods	$k = 1$

Table 7.1: The methods tested in experimental sessions, for the considered case when there there is more single elements in the electrode array than stimulation channels ($m > n$)

A number of different optimisation methods for finding the optimal stimulation pattern have been developed based on theoretical and experimental findings. These are: Penalty Method (PM), Brute-Force searching algorithm (BF) and Approximate Gradient Algorithm (APG). A comparison of the methods has been given, taking into account both theoretical and practical constraints. The general algorithm was tested on $2-5$ unimpaired participants using electrode array consisting of $m = 40$ elements and two different stimulation hardwares which supported $n = 2$ and $n = 4$ stimulation channels respectively. The summary of the results achieved during the numerical and experimental tests are shown in Table 7.2.

Preliminary tests with unimpaired participants confirmed the effectiveness of the new algorithm, especially for the multi-trial case. Originally, the ILC-based approach was meant to be use to extend the previously developed system for arm rehabilitation and develop a complete ILC-based system for upper-limb rehabilitation. The first positive results of this project has been already confirmed in (Exel et al., 2013a).

Method	**Test**	**channels**	**trial**	**NME**
BF	N/E1	2	1	0.29/0.36
APG	N	2	1	0.15
PM	N	2	1	0.31
ILC	E2	4	1	0.2
			2	0.15
			3	0.03

Table 7.2: The summary of the general approach developed with the average performace of specific method on each trial for different number of channels. N - method was tested in numerical studies, E1 - Tested on participants P1-P5, E2 - Tested on participants P1-P2

In addition, based on the results in this thesis and the existing literature a separate Hand Rehabilitation System (HaReS) has been designed and is at the stage of development.

Interventions supported	High-intensity and repetitive movements therapy, UMT,CIMT, VR
Muscles included	Extensor muscles of the hand and wrist
Sensors	5DT glove and Biometrics goniometers
Cognitive training	low-level of difficulty visual perception training
Motor training	Trains wrist flexion/extension, wrist stabilisation and alternate hand opening/closing
Feedback	Visual: movement of the object on the screen and scores
Patient Factors	Patient-centred, non-invasive do not require medical skills, increases motivation
Suitable for	extensor muscles weakness, spasticity, overactivity of flexor muscles, hand pain, active stretching the muscle after i.e. tendon injuries or surgical replacement

Table 7.3: The summary of the beta version of the HaReS

The key element of the system is a game-based task oriented training environment designed for a wide group of patients, including those with spasticity and hemiplegia. The platform is being developed especially to increase the motivation with a focus on encouraging patients to perform high number of repetitive movements. The complete

system will be tested in practical trials with unimpaired subjects, however the long-term objective of the work is to test the effectiveness of HaReS in clinical trials with subjects suffering from hand motor impairments due to i.e. spasticity, overactivity of flexor muscles or extensor muscle weakness. The system has been specially designed to collect a large amount of data. Hence it final version is meant to serve as a research tool, that can be used for further comparison studies of different rehabilitation interventions such as: unilateral/bilateral movement with/without game-based therapy, with/without SEA-based assistance mediated by ILC. Summary of the beta version of the system is presented in Table 7.3

Developing an effective rehabilitation system for hand and wrist, that would be beneficial for i.e. stroke or SCI survivors is a challenging and multidisciplinary task. It involves analysis, design, application and comprising many different aspects and methods from different fields of science: such as control, computer science, health science, anatomy, psychology and engineering. The efficacy of the system is strongly related to the accuracy of each of these aspects, however the most important factors which strongly influence the overall effectiveness of any rehabilitation system are those generated by patients themselves. Thus, there is always a need for more research and methods, which would be both effective and patient-centered.

Appendix A

Model and parameters

A.1 The model used in simulation

Note: Step by step developement of the model is described in Chapter 3. MATLAB script with the model is following

```
q1 = x1;
q2 = x2;
q3 = x3;
q1dot = x4;
q2dot = x5;
q3dot = x6;

x = [x1 x2 x3 x4 x5 x6 x7 x8 x9 x10 x11 x12];
u = [u1 u2 u3 u4 u5 u6 u7]';

%*****************************************
% The Moment Arms Matrix
%*****************************************
% Constants (symbolic)
syms w1;
syms w2;
syms w3;
syms rTE;
syms y3_FDP;
syms d3_FDP;
syms rEC1 ;
syms rES ;
syms bRB ;
syms hRB ;
syms bUB ;
syms hUB ;
syms d2_FDS ;
syms y2_FDS ;
syms d2_FDP ;
syms y2_FDP ;
syms d1_FDP ;
syms y1_FDP ;
syms d1_FDS ;
```

```
syms y1_FDS ;
syms rEI  ;
syms bRI  ;
syms hRI ;
syms bUI ;
syms hUI ;
syms bLU ;
syms hLU ;
syms rECR;
syms rECU;
syms rFDP;
syms rEC2

s2 = (sin(x2)-x2)/(2*sin(x2)^2);
s3 = (sin(x3)-x3)/(2*sin(x3)^2);

R_ECR = [-rECR; 0; 0;];

R_ECU = [-rECU; 0; 0;];

R_FDP = [rFDP;
         d1_FDP + y1_FDP *s2;
         d2_FDP + y2_FDP *s3;
         ];

R_RB = [  0;
          0;
         -bRB - 2*hRB*q3;
        ];

R_LU = [0;
        bLU + 2*hLU*q2 - M_FDP(2,1);
        M_RB(2,1) - M_FDP(3,1);
        ];

R_RI = [ 0;
         bRI  + 2*hRI*q2;
         0;
          ];

R_UB = [ 0;
         0;
         -bUB - 2*hUB*q3;
        ];

R_UI = [ 0;
         bUI + 2*hUI*q2;
         M_UB(3,1);
                  ];

c1 = - w2*(bUB +2*hUB*q3) - w3*(bRB + 2*hRB*q3);

R_EC = [ -rEC2
          -rEC1;
          -w1*rES + c1;
        ];

R = [ R_FDP, R_LU, R_UI, R_RI, R_EC, R_ECR, R_ECU];
```

```
f1= x4;

f2= x5;

f3= x6;

f4= (l2^2*m3^2*cos(q3)^2*a3^2-m2*l2^2*m3*a3^2-J4*m3*a3^2-l2^2*m3*J6-l2^2*m3^2*a3
    ^2-m2*l2^2*J6-J4*J6)/(-J2*m2*l2^2*m3*a3^2
-m3*l1^2*J4*J6-m3^2*l1^2*J4*a3^2-m3^2*l1^2*l2^2*J6-m3^3*l1^2*l2^2*a3^2-a1^2*m1*J4
    *J6-m2*l1^2*J4*J6-m2^2*l1^2*l2^2*J6
-J2*J4*m3*a3^2-J2*l2^2*m3*J6-J2*l2^2*m3^2*a3^2-J2*m2*l2^2*J6-J2*J4*J6-2*m3*l1^2*
    m2*l2^2*J6-2*m3^2*l1^2*m2*l2^2*a3^2
-a1^2*m1*J4*m3*a3^2-a1^2*m1*l2^2*m3*J6-a1^2*m1*l2^2*m3^2*a3^2-a1^2*m1*m2*l2^2*J6-
    a1^2*m1*m2*l2^2*m3*a3^2-m2*l1^2*J4*m3*a3^2
-m2^2*l1^2*l2^2*m3*a3^2+m3^3*l1^2*l2^2*cos(q3)^2*a3^2+a1^2*m1*l2^2*m3^2*cos(q3)
    ^2*a3^2
+m2*l1^2*l2^2*m3^2*cos(q3)^2*a3^2+J2*l2^2*m3^2*cos(q3)^2*a3^2+m3^3*l1^2*a3^2*cos(
    q3+q2)^2*l2^2 +m3^2*l1^2*a3^2*cos(q3+q2)^2*m2*l2^2+m3^2*l1^2*a3^2*cos(q3+q2)
    ^2*J4+l2^2*m3^3*l1^2*cos(q2)^2*a3^2 +2*l2^2*m3^2*l1^2*cos(q2)^2*m2*a3^2+l2^2*
    m3^2*l1^2*cos(q2)^2*J6+2*l2^2*m3*l1^2*cos(q2)^2*m2*J6-2*l2^2*m3^3*l1^2*cos(q2
    )*a3^2*cos(q3+q2)*cos(q3)+l2^2*m2^2*l1^2*cos(q2)^2*m3*a3^2+l2^2*m2^2*l1^2*cos
    (q2)^2*J6-2*l2^2*m2*l1^2*cos(q2)*m3^2*a3^2*cos(q3+q2)*cos(q3))*(-k1*(q1-q10)+
    l1*(2*m3*q1dot*a3*sin(q3+q2)+2*m2*q1dot*l2*sin(q2)+2*m3*q1dot*l2*sin(q2)+m3*
    l2*q2dot*sin(q2) +m3*a3*q3dot*sin(q3+q2)+m2*l2*q2dot*sin(q2)+m3*q2dot*a3*sin(
    q3+q2))*q2dot+m3*a3*(2*q1dot*l1*sin(q3+q2)+2*q1dot*l2*sin(q3) +2*l2*q2dot*sin
    (q3)+q3dot*l1*sin(q3+q2)+q3dot*l2*sin(q3)+q2dot*l1*sin(q3+q2))*q3dot+x7-b1*
    q1dot)-(-J4*J6-l2^2*m3^2*a3^2-J4*m3*a3^2-l2^2*m3*J6-m2*l2^2*J6-m2*l2^2*m3*a3
    ^2+l2^2*m3^2*cos(q3)^2*a3^2-l2*m3^2*l1*cos(q2)*a3^2-l2*m2*l1*cos(q2)*m3*a3^2
-l2*m3*l1*cos(q2)*J6-l2*m2*l1*cos(q2)*J6+m3^2*l1*a3^2*cos(q3+q2)*l2*cos(q3))/(-J2
    *m2*l2^2*m3*a3^2-m3*l1^2*J4*J6
-m3^2*l1^2*J4*a3^2-m3^2*l1^2*l2^2*J6-m3^3*l1^2*l2^2*a3^2-a1^2*m1*J4*J6-m2*l1^2*J4
    *J6-m2^2*l1^2*l2^2*J6-J2*J4*m3*a3^2-J2*l2^2*m3*J6-J2*l2^2*m3^2*a3^2-J2*m2*l2
    ^2*J6-J2*J4*J6-2*m3*l1^2*m2*l2^2*J6-2*m3^2*l1^2*m2*l2^2*a3^2-a1^2*m1*J4*m3*a3
    ^2
-a1^2*m1*l2^2*m3*J6-a1^2*m1*l2^2*m3^2*a3^2-a1^2*m1*m2*l2^2*J6-a1^2*m1*m2*l2^2*m3*
    a3^2-m2*l1^2*J4*m3*a3^2-m2^2*l1^2*l2^2*m3*a3^2+m3^3*l1^2*l2^2*cos(q3)^2*a3^2+
    a1^2*m1*l2^2*m3^2*cos(q3)^2*a3^2 +m2*l1^2*l2^2*m3^2*cos(q3)^2*a3^2+J2*l2^2*m3
    ^2*cos(q3)^2*a3^2+m3^3*l1^2*a3^2*cos(q3+q2)^2*l2^2 +m3^2*l1^2*a3^2*cos(q3+q2)
    ^2*m2*l2^2+m3^2*l1^2*a3^2*cos(q3+q2)^2*J4+l2^2*m3^3*l1^2*cos(q2)^2*a3^2 +2*l2
    ^2*m3^2*l1^2*cos(q2)^2*m2*a3^2+l2^2*m3^2*l1^2*cos(q2)^2*J6+2*l2^2*m3*l1^2*cos
    (q2)^2*m2*J6 -2*l2^2*m3^3*l1^2*cos(q2)*a3^2*cos(q3+q2)*cos(q3)+l2^2*m2^2*l1
    ^2*cos(q2)^2*m3*a3^2 +l2^2*m2^2*l1^2*cos(q2)^2*J6-2*l2^2*m2*l1^2*cos(q2)*m3
    ^2*a3^2*cos(q3+q2)*cos(q3))*(-k2*(q2-q20)
-m3*q1dot*l1*l2*q2dot*sin(q2)-m3*q1dot^2*l1*a3*sin(q3+q2)-m3*q1dot*l1*a3*q3dot*
    sin(q3+q2)-m2*q1dot^2*l1*l2*sin(q2)
-m2*q1dot*l1*l2*q2dot*sin(q2)-m3*q1dot^2*l2*l1*sin(q2)
-m3*q1dot*l1*a3*sin(q3+q2)*q2dot+q1dot*l1*(m3*l2*sin(q2)+m3*a3*sin(q3+q2)+m2*l2*
    sin(q2))*q2dot+m3*a3*(q1dot*l1*sin(q3+q2)
+2*q1dot*l2*sin(q3)+q3dot*l2*sin(q3)+2*l2*q2dot*sin(q3))*q3dot+x9-b2*q2dot)+l1*(-
    l2^2*m3^2*cos(q2)*cos(q3)*a3
-l2^2*m2*cos(q2)*m3*cos(q3)*a3+m3^2*a3*cos(q3+q2)*l2^2+m3*a3*cos(q3+q2)*m2*l2^2+
    m3*a3*cos(q3+q2)*J4-l2*m3^2*cos(q2)*a3^2
-l2*m2*cos(q2)*m3*a3^2-l2*m3*cos(q2)*J6-l2*m2*cos(q2)*J6+m3^2*a3^2*cos(q3+q2)*l2*
    cos(q3))/(-J2*m2*l2^2*m3*a3^2
-m3*l1^2*J4*J6-m3^2*l1^2*J4*a3^2-m3^2*l1^2*l2^2*J6-m3^3*l1^2*l2^2*a3^2-a1^2*m1*J4
    *J6-m2*l1^2*J4*J6-m2^2*l1^2*l2^2*J6
-J2*J4*m3*a3^2-J2*l2^2*m3*J6-J2*l2^2*m3^2*a3^2-J2*m2*l2^2*J6-J2*J4*J6-2*m3*l1^2*
    m2*l2^2*J6-2*m3^2*l1^2*m2*l2^2*a3^2
```

```
-a1^2*m1*J4*m3*a3^2-a1^2*m1*l2^2*m3*J6-a1^2*m1*l2^2*m3^2*a3^2-a1^2*m1*m2*l2^2*J6-
    a1^2*m1*m2*l2^2*m3*a3^2-m2*l1^2*J4*m3*a3^2 -m2^2*l1^2*l2^2*m3*a3^2+m3^3*l1^2*
    l2^2*cos(q3)^2*a3^2+a1^2*m1*l2^2*m3^2*cos(q3)^2*a3^2+m2*l1^2*l2^2*m3^2*cos(q3
    )^2*a3^2
+J2*l2^2*m3^2*cos(q3)^2*a3^2+m3^3*l1^2*a3^2*cos(q3+q2)^2*l2^2+m3^2*l1^2*a3^2*cos(
    q3+q2)^2*m2*l2^2 +m3^2*l1^2*a3^2*cos(q3+q2)^2*J4+l2^2*m3^3*l1^2*cos(q2)^2*a3
    ^2+2*l2^2*m3^2*l1^2*cos(q2)^2*m2*a3^2 +l2^2*m3^2*l1^2*cos(q2)^2*J6 +2*l2^2*m3
    *l1^2*cos(q2)^2*m2*J6-2*l2^2*m3^3*l1^2*cos(q2)*a3^2*cos(q3+q2)*cos(q3)+l2^2*
    m2^2*l1^2*cos(q2)^2*m3*a3^2 + l2^2*m2^2*l1^2*cos(q2)^2*J6-2*l2^2*m2*l1^2*cos(
    q2)*m3^2*a3^2*cos(q3+q2)*cos(q3))*(-k3*(q3-q30)-m3*q1dot*l2*a3*q3dot*sin(q3)-
    m3*l2*q2dot^2*a3*sin(q3)-m3*l2*q2dot*a3*q3dot*sin(q3)-m3*q1dot^2*l2*a3*sin(q3
    )
-m3*q1dot^2*l1*a3*sin(q3+q2) -m3*q1dot*l1*a3*q3dot*sin(q3+q2)-2*m3*q1dot*a3*l2*
    q2dot*sin(q3)+m3*a3*(q1dot*l1*sin(q3+q2) +q1dot*l2*sin(q3) +l2*q2dot*sin(q3))
    *q3dot+x12-b3*q3dot);

f5= -(-J4*J6-l2^2*m3^2*a3^2-J4*m3*a3^2-l2^2*m3*J6-m2*l2^2*J6-m2*l2^2*m3*a3^2+l2
    ^2*m3^2*cos(q3)^2*a3^2
-l2*m3^2*l1*cos(q2)*a3^2-l2*m2*l1*cos(q2)*m3*a3^2-l2*m3*l1*cos(q2)*J6
-l2*m2*l1*cos(q2)*J6+m3^2*l1*a3^2*cos(q3+q2)*l2*cos(q3))/(-J2*m2*l2^2*m3*a3^2-m3*
    l1^2*J4*J6-m3^2*l1^2*J4*a3^2
-m3^2*l1^2*l2^2*J6-m3^3*l1^2*l2^2*a3^2-a1^2*m1*J4*J6-m2*l1^2*J4*J6-m2^2*l1^2*l2
    ^2*J6-J2*J4*m3*a3^2-J2*l2^2*m3*J6
-J2*l2^2*m3^2*a3^2-J2*m2*l2^2*J6-J2*J4*J6-2*m3*l1^2*m2*l2^2*J6-2*m3^2*l1^2*m2*l2
    ^2*a3^2-a1^2*m1*J4*m3*a3^2
-a1^2*m1*l2^2*m3*J6-a1^2*m1*l2^2*m3^2*a3^2-a1^2*m1*m2*l2^2*J6-a1^2*m1*m2*l2^2*m3*
    a3^2-m2*l1^2*J4*m3*a3^2
-m2^2*l1^2*l2^2*m3*a3^2+m3^3*l1^2*l2^2*cos(q3)^2*a3^2+a1^2*m1*l2^2*m3^2*cos(q3)
    ^2*a3^2+m2*l1^2*l2^2*m3^2*cos(q3)^2*a3^2
+J2*l2^2*m3^2*cos(q3)^2*a3^2+m3^3*l1^2*a3^2*cos(q3+q2)^2*l2^2+m3^2*l1^2*a3^2*cos(
    q3+q2)^2*m2*l2^2 +m3^2*l1^2*a3^2*cos(q3+q2)^2*J4+l2^2*m3^3*l1^2*cos(q2)^2*a3
    ^2+2*l2^2*m3^2*l1^2*cos(q2)^2*m2*a3^2 +l2^2*m3^2*l1^2*cos(q2)^2*J6+2*l2^2*m3*
    l1^2*cos(q2)^2*m2*J6-2*l2^2*m3^3*l1^2*cos(q2)*a3^2*cos(q3+q2)*cos(q3) +l2^2*
    m2^2*l1^2*cos(q2)^2*m3*a3^2
+l2^2*m2^2*l1^2*cos(q2)^2*J6-2*l2^2*m2*l1^2*cos(q2)*m3^2*a3^2*cos(q3+q2)*cos(q3))
    *(-k1*(q1-q10)
+l1*(2*m3*q1dot*a3*sin(q3+q2)+2*m2*q1dot*l2*sin(q2) +2*m3*q1dot*l2*sin(q2)+m3*l2*
    q2dot*sin(q2)+m3*a3*q3dot*sin(q3+q2) +m2*l2*q2dot*sin(q2)+m3*q2dot*a3*sin(q3+
    q2))*q2dot+m3*a3*(2*q1dot*l1*sin(q3+q2) +2*q1dot*l2*sin(q3)+2*l2*q2dot*sin(q3
    )+q3dot*l1*sin(q3+q2)+q3dot*l2*sin(q3)+q2dot*l1*sin(q3+q2))*q3dot+x7-b1*q1dot
    ) +(-J4*J6-l2^2*m3^2*a3^2-J4*m3*a3^2-l2^2*m3*J6-m2*l2^2*J6-m2*l2^2*m3*a3^2+l2
    ^2*m3^2*cos(q3)^2*a3^2-m3^2*l1^2*a3^2-m3*l1^2*J6-J2*m3*a3^2-a1^2*m1*J6-m2*l1
    ^2*J6-2*l2*m3^2*l1*cos(q2)*a3^2-2*l2*m2*l1*cos(q2)*m3*a3^2-2*l2*m3*l1*cos(q2)
    *J6-2*l2*m2*l1*cos(q2)*J6 +2*m3^2*l1*a3^2*cos(q3+q2)*l2*cos(q3)-a1^2*m1*m3*a3
    ^2-m2*l1^2*m3*a3^2+m3^2*l1^2*a3^2*cos(q3+q2)^2-J2*J6)/(-J2*m2*l2^2*m3*a3^2-m3
    *l1^2*J4*J6-m3^2*l1^2*J4*a3^2-m3^2*l1^2*l2^2*J6-m3^3*l1^2*l2^2*a3^2-a1^2*m1*
    J4*J6-m2*l1^2*J4*J6-m2^2*l1^2*l2^2*J6-J2*J4*m3*a3^2-J2*l2^2*m3*J6-J2*l2^2*m3
    ^2*a3^2-J2*m2*l2^2*J6-J2*J4*J6-2*m3*l1^2*m2*l2^2*J6-2*m3^2*l1^2*m2*l2^2*a3^2-
    a1^2*m1*J4*m3*a3^2-a1^2*m1*l2^2*m3*J6-a1^2*m1*l2^2*m3^2*a3^2-a1^2*m1*m2*l2^2*
    J6-a1^2*m1*m2*l2^2*m3*a3^2-m2*l1^2*J4*m3*a3^2-m2^2*l1^2*l2^2*m3*a3^2+m3^3*l1
    ^2*l2^2*cos(q3)^2*a3^2+a1^2*m1*l2^2*m3^2*cos(q3)^2*a3^2+m2*l1^2*l2^2*m3^2*cos
    (q3)^2*a3^2 +J2*l2^2*m3^2*cos(q3)^2*a3^2+m3^3*l1^2*a3^2*cos(q3+q2)^2*l2^2+m3
    ^2*l1^2*a3^2*cos(q3+q2)^2*m2*l2^2 +m3^2*l1^2*a3^2*cos(q3+q2)^2*J4+l2^2*m3^3*
    l1^2*cos(q2)^2*a3^2+2*l2^2*m3^2*l1^2*cos(q2)^2*m2*a3^2 +l2^2*m3^2*l1^2*cos(q2
    )^2*J6+2*l2^2*m3*l1^2*cos(q2)^2*m2*J6-2*l2^2*m3^3*l1^2*cos(q2)*a3^2*cos(q3+q2
    )*cos(q3) +l2^2*m2^2*l1^2*cos(q2)^2*m3*a3^2+l2^2*m2^2*l1^2*cos(q2)^2*J6- 2*l2
    ^2*m2*l1^2*cos(q2)*m3^2*a3^2*cos(q3+q2)*cos(q3))
*(-k2*(q2-q20)-m3*q1dot*l1*l2*q2dot*sin(q2)-m3*q1dot^2*l1*a3*sin(q3+q2)-m3*q1dot*
    l1*a3*q3dot*sin(q3+q2)
```

```
-m2*q1dot^2*l1*l2*sin(q2)-m2*q1dot*l1*l2*q2dot*sin(q2)-m3*q1dot^2*l2*l1*sin(q2)
-m3*q1dot*l1*a3*sin(q3+q2)*q2dot+q1dot*l1*(m3*l2*sin(q2)+m3*a3*sin(q3+q2)+m2*l2*
    sin(q2))*q2dot+m3*a3*(q1dot*l1*sin(q3+q2) +2*q1dot*l2*sin(q3)+q3dot*l2*sin(q3
    )+2*l2*q2dot*sin(q3))*q3dot+x9-b2*q2dot)-(-l2*m2*l1*cos(q2)*J6-l2^2*m3^2*l1*
    cos(q2)*cos(q3)*a3-l2^2*m2*l1*cos(q2)*m3*cos(q3)*a3+m3^2*l1*a3*cos(q3+q2)*l2
    ^2+m3*l1*a3*cos(q3+q2)*m2*l2^2 +m3*l1*a3*cos(q3+q2)*J4-m3^2*l1^2*a3^2-m3*l1
    ^2*J6-J2*m3*a3^2-a1^2*m1*J6-m2*l1^2*J6-l2*m3^2*l1*cos(q2)*a3^2
-l2*m2*l1*cos(q2)*m3*a3^2-l2*m3*l1*cos(q2)*J6+m3^2*l1*a3^2*cos(q3+q2)*l2*cos(q3)-
    a1^2*m1*m3*a3^2
-m2*l1^2*m3*a3^2+m3^2*l1^2*a3^2*cos(q3+q2)^2-J2*J6-m3^2*l1^2*l2*cos(q3)*a3-a1^2*
    m1*l2*m3*cos(q3)*a3
-m2*l1^2*l2*m3*cos(q3)*a3-J2*l2*m3*cos(q3)*a3+l2*m3^2*l1^2*cos(q2)*a3*cos(q3+q2)
+l2*m2*l1^2*cos(q2)*m3*a3*cos(q3+q2))/(-J2*m2*l2^2*m3*a3^2-m3*l1^2*J4*J6-m3^2*l1
    ^2*J4*a3^2-m3^2*l1^2*l2^2*J6
-m3^3*l1^2*l2^2*a3^2 -a1^2*m1*J4*J6-m2*l1^2*J4*J6-m2^2*l1^2*l2^2*J6-J2*J4*m3*a3
    ^2-J2*l2^2*m3*J6-J2*l2^2*m3^2*a3^2
-J2*m2*l2^2*J6-J2*J4*J6-2*m3*l1^2*m2*l2^2*J6-2*m3^2*l1^2*m2*l2^2*a3^2-a1^2*m1*J4*
    m3*a3^2-a1^2*m1*l2^2*m3*J6
-a1^2*m1*l2^2*m3^2*a3^2-a1^2*m1*m2*l2^2*J6-a1^2*m1*m2*l2^2*m3*a3^2-m2*l1^2*J4*m3*
    a3^2
-m2^2*l1^2*l2^2*m3*a3^2+m3^3*l1^2*l2^2*cos(q3)^2*a3^2+a1^2*m1*l2^2*m3^2*cos(q3)
    ^2*a3^2+m2*l1^2*l2^2*m3^2*cos(q3)^2*a3^2 +J2*l2^2*m3^2*cos(q3)^2*a3^2+m3^3*l1
    ^2*a3^2*cos(q3+q2)^2*l2^2+m3^2*l1^2*a3^2*cos(q3+q2)^2*m2*l2^2 +m3^2*l1^2*a3
    ^2*cos(q3+q2)^2*J4+l2^2*m3^3*l1^2*cos(q2)^2*a3^2+2*l2^2*m3^2*l1^2*cos(q2)^2*
    m2*a3^2 +l2^2*m3^2*l1^2*cos(q2)^2*J6+2*l2^2*m3*l1^2*cos(q2)^2*m2*J6-2*l2^2*m3
    ^3*l1^2*cos(q2)*a3^2*cos(q3+q2)*cos(q3) +l2^2*m2^2*l1^2*cos(q2)^2*m3*a3^2
+l2^2*m2^2*l1^2*cos(q2)^2*J6-2*l2^2*m2*l1^2*cos(q2)*m3^2*a3^2*cos(q3+q2)*cos(q3))
    *(-k3*(q3-q30)
-m3*q1dot*l2*a3*q3dot*sin(q3)-m3*l2*q2dot^2*a3*sin(q3)-m3*l2*q2dot*a3*q3dot*sin(
    q3)-m3*q1dot^2*l2*a3*sin(q3)
-m3*q1dot^2*l1*a3*sin(q3+q2)-m3*q1dot*l1*a3*q3dot*sin(q3+q2)
-2*m3*q1dot*a3*l2*q2dot*sin(q3)+m3*a3*(q1dot*l1*sin(q3+q2)+q1dot*l2*sin(q3)+l2*
    q2dot*sin(q3))*q3dot+x12-b3*q3dot);

f6= l1*(-l2^2*m3^2*cos(q2)*cos(q3)*a3
-l2^2*m2*cos(q2)*m3*cos(q3)*a3+m3^2*a3*cos(q3+q2)*l2^2+m3*a3*cos(q3+q2)*m2*l2^2+
    m3*a3*cos(q3+q2)*J4-l2*m3^2*cos(q2)*a3^2
-l2*m2*cos(q2)*m3*a3^2-l2*m3*cos(q2)*J6-l2*m2*cos(q2)*J6+m3^2*a3^2*cos(q3+q2)*l2*
    cos(q3))/(-J2*m2*l2^2*m3*a3^2
-m3*l1^2*J4*J6-m3^2*l1^2*J4*a3^2-m3^2*l1^2*l2^2*J6-m3^3*l1^2*l2^2*a3^2-a1^2*m1*J4
    *J6-m2*l1^2*J4*J6-m2^2*l1^2*l2^2*J6
-J2*J4*m3*a3^2-J2*l2^2*m3*J6-J2*l2^2*m3^2*a3^2-J2*m2*l2^2*J6-J2*J4*J6-2*m3*l1^2*
    m2*l2^2*J6-2*m3^2*l1^2*m2*l2^2*a3^2
-a1^2*m1*J4*m3*a3^2-a1^2*m1*l2^2*m3*J6-a1^2*m1*l2^2*m3^2*a3^2-a1^2*m1*m2*l2^2*J6-
    a1^2*m1*m2*l2^2*m3*a3^2
```

```
-m2*l1^2*J4*m3*a3^2-m2^2*l1^2*l2^2*m3*a3^2+m3^3*l1^2*l2^2*cos(q3)^2*a3^2+a1^2*m1*
    l2^2*m3^2*cos(q3)^2*a3^2 +m2*l1^2*l2^2*m3^2*cos(q3)^2*a3^2+J2*l2^2*m3^2*cos(
    q3)^2*a3^2 +m3^3*l1^2*a3^2*cos(q3+q2)^2*l2^2 +m3^2*l1^2*a3^2*cos(q3+q2)^2*m2*
    l2^2+m3^2*l1^2*a3^2*cos(q3+q2)^2*J4+l2^2*m3^3*l1^2*cos(q2)^2*a3^2 +2*l2^2*m3
    ^2*l1^2*cos(q2)^2*m2*a3^2+l2^2*m3^2*l1^2*cos(q2)^2*J6 +2*l2^2*m3*l1^2*cos(q2)
    ^2*m2*J6-2*l2^2*m3^3*l1^2*cos(q2)*a3^2*cos(q3+q2)*cos(q3)+l2^2*m2^2*l1^2*cos(
    q2)^2*m3*a3^2 +l2^2*m2^2*l1^2*cos(q2)^2*J6-2*l2^2*m2*l1^2*cos(q2)*m3^2*a3^2*
    cos(q3+q2)*cos(q3))*(-k1*(q1-q10) +l1*(2*m3*q1dot*a3*sin(q3+q2)+2*m2*q1dot*l2
    *sin(q2)+2*m3*q1dot*l2*sin(q2)+m3*l2*q2dot*sin(q2)+m3*a3*q3dot*sin(q3+q2) +m2
    *l2*q2dot*sin(q2)+m3*q2dot*a3*sin(q3+q2))*q2dot+m3*a3*(2*q1dot*l1*sin(q3+q2)
    +2*q1dot*l2*sin(q3)+2*l2*q2dot*sin(q3) +q3dot*l1*sin(q3+q2)+q3dot*l2*sin(q3)+
    q2dot*l1*sin(q3+q2))*q3dot+x7-b1*q1dot)-(-l2*m2*l1*cos(q2)*J6-l2^2*m3^2*l1*
    cos(q2)*cos(q3)*a3-l2^2*m2*l1*cos(q2)*m3*cos(q3)*a3 +m3^2*l1*a3*cos(q3+q2)*l2
    ^2+m3*l1*a3*cos(q3+q2)*m2*l2^2+m3*l1*a3*cos(q3+q2)*J4-m3^2*l1^2*a3^2-m3*l1^2*
    J6-J2*m3*a3^2
-a1^2*m1*J6-m2*l1^2*J6-l2*m3^2*l1*cos(q2)*a3^2-l2*m2*l1*cos(q2)*m3*a3^2
-l2*m3*l1*cos(q2)*J6+m3^2*l1*a3^2*cos(q3+q2)*l2*cos(q3)-a1^2*m1*m3*a3^2-m2*l1^2*
    m3*a3^2
+m3^2*l1^2*a3^2*cos(q3+q2)^2-J2*J6-m3^2*l1^2*l2*cos(q3)*a3-a1^2*m1*l2*m3*cos(q3)*
    a3-m2*l1^2*l2*m3*cos(q3)*a3
-J2*l2*m3*cos(q3)*a3+l2*m3^2*l1^2*cos(q2)*a3*cos(q3+q2)+l2*m2*l1^2*cos(q2)*m3*a3*
    cos(q3+q2))/(-J2*m2*l2^2*m3*a3^2
-m3*l1^2*J4*J6-m3^2*l1^2*J4*a3^2-m3^2*l1^2*l2^2*J6-m3^3*l1^2*l2^2*a3^2-a1^2*m1*J4
    *J6-m2*l1^2*J4*J6-m2^2*l1^2*l2^2*J6
-J2*J4*m3*a3^2-J2*l2^2*m3*J6-J2*l2^2*m3^2*a3^2-J2*m2*l2^2*J6-J2*J4*J6-2*m3*l1^2*
    m2*l2^2*J6-2*m3^2*l1^2*m2*l2^2*a3^2
-a1^2*m1*J4*m3*a3^2-a1^2*m1*l2^2*m3*J6-a1^2*m1*l2^2*m3^2*a3^2-a1^2*m1*m2*l2^2*J6-
    a1^2*m1*m2*l2^2*m3*a3^2
-m2*l1^2*J4*m3*a3^2-m2^2*l1^2*l2^2*m3*a3^2+m3^3*l1^2*l2^2*cos(q3)^2*a3^2+a1^2*m1*
    l2^2*m3^2*cos(q3)^2*a3^2 +m2*l1^2*l2^2*m3^2*cos(q3)^2*a3^2 +J2*l2^2*m3^2*cos(
    q3)^2*a3^2+m3^3*l1^2*a3^2*cos(q3+q2)^2*l2^2 +m3^2*l1^2*a3^2*cos(q3+q2)^2*m2*
    l2^2 +m3^2*l1^2*a3^2*cos(q3+q2)^2*J4 +l2^2*m3^3*l1^2*cos(q2)^2*a3^2+2*l2^2*m3
    ^2*l1^2*cos(q2)^2*m2*a3^2 +l2^2*m3^2*l1^2*cos(q2)^2*J6+2*l2^2*m3*l1^2*cos(q2)
    ^2*m2*J6-2*l2^2*m3^3*l1^2*cos(q2)*a3^2*cos(q3+q2)*cos(q3) +l2^2*m2^2*l1^2*cos
    (q2)^2*m3*a3^2
+l2^2*m2^2*l1^2*cos(q2)^2*J6
-2*l2^2*m2*l1^2*cos(q2)*m3^2*a3^2*cos(q3+q2)*cos(q3))*(-k2*(q2-q20)-m3*q1dot*l1*
    l2*q2dot*sin(q2)
-m3*q1dot^2*l1*a3*sin(q3+q2)-m3*q1dot*l1*a3*q3dot*sin(q3+q2)-m2*q1dot^2*l1*l2*sin
    (q2)-m2*q1dot*l1*l2*q2dot*sin(q2)
-m3*q1dot^2*l2*l1*sin(q2)
-m3*q1dot*l1*a3*sin(q3+q2)*q2dot+q1dot*l1*(m3*l2*sin(q2)+m3*a3*sin(q3+q2)+m2*l2*
    sin(q2))*q2dot+m3*a3*(q1dot*l1*sin(q3+q2) +2*q1dot*l2*sin(q3)+q3dot*l2*sin(q3
    )+2*l2*q2dot*sin(q3))*q3dot+x9-b2*q2dot)+(-m3*l1^2*J4-m2^2*l1^2*l2^2-m3^2*l1
    ^2*l2^2
-m2*l1^2*J4-a1^2*m1*J4-J2*m2*l2^2-J2*l2^2*m3-2*m3*l1^2*m2*l2^2-a1^2*m1*m2*l2^2
-a1^2*m1*l2^2*m3+l2^2*m2^2*l1^2*cos(q2)^2+l2^2*m3^2*l1^2*cos(q2)^2-J2*J4+2*l2^2*
    m3*l1^2*cos(q2)^2*m2-m3^2*l1^2*a3^2
-m3*l1^2*J6-J2*m3*a3^2-a1^2*m1*J6-m2*l1^2*J6-a1^2*m1*m3*a3^2-m2*l1^2*m3*a3^2+m3
    ^2*l1^2*a3^2*cos(q3+q2)^2
-J2*J6-2*m3^2*l1^2*l2*cos(q3)*a3-2*a1^2*m1*l2*m3*cos(q3)*a3-2*m2*l1^2*l2*m3*cos(
    q3)*a3
-2*J2*l2*m3*cos(q3)*a3+2*l2*m3^2*l1^2*cos(q2)*a3*cos(q3+q2)+2*l2*m2*l1^2*cos(q2)*
    m3*a3*cos(q3+q2))/(-J2*m2*l2^2*m3*a3^2
-m3*l1^2*J4*J6-m3^2*l1^2*J4*a3^2-m3^2*l1^2*l2^2*J6-m3^3*l1^2*l2^2*a3^2-a1^2*m1*J4
    *J6-m2*l1^2*J4*J6-m2^2*l1^2*l2^2*J6
-J2*J4*m3*a3^2-J2*l2^2*m3*J6-J2*l2^2*m3^2*a3^2-J2*m2*l2^2*J6-J2*J4*J6-2*m3*l1^2*
    m2*l2^2*J6-2*m3^2*l1^2*m2*l2^2*a3^2
```

```
-a1^2*m1*J4*m3*a3^2-a1^2*m1*l2^2*m3*J6-a1^2*m1*l2^2*m3^2*a3^2-a1^2*m1*m2*l2^2*J6-
    a1^2*m1*m2*l2^2*m3*a3^2-m2*l1^2*J4*m3*a3^2
-m2^2*l1^2*l2^2*m3*a3^2+m3^3*l1^2*l2^2*cos(q3)^2*a3^2+a1^2*m1*l2^2*m3^2*cos(q3)
    ^2*a3^2+m2*l1^2*l2^2*m3^2*cos(q3)^2*a3^2
+J2*l2^2*m3^2*cos(q3)^2*a3^2+m3^3*l1^2*a3^2*cos(q3+q2)^2*l2^2+m3^2*l1^2*a3^2*cos(
    q3+q2)^2*m2*l2^2
+m3^2*l1^2*a3^2*cos(q3+q2)^2*J4+l2^2*m3^3*l1^2*cos(q2)^2*a3^2+2*l2^2*m3^2*l1^2*
    cos(q2)^2*m2*a3^2 +l2^2*m3^2*l1^2*cos(q2)^2*J6+2*l2^2*m3*l1^2*cos(q2)^2*m2*J6
    -2*l2^2*m3^3*l1^2*cos(q2)*a3^2*cos(q3+q2)*cos(q3) +l2^2*m2^2*l1^2*cos(q2)^2*
    m3*a3^2+l2^2*m2^2*l1^2*cos(q2)^2*J6-2*l2^2*m2*l1^2*cos(q2)*m3^2*a3^2*cos(q3+
    q2)*cos(q3))
*(-k3*(q3-q30)-m3*q1dot*l2*a3*q3dot*sin(q3)-m3*l2*q2dot^2*a3*sin(q3)-m3*l2*q2dot*
    a3*q3dot*sin(q3)-m3*q1dot^2*l2*a3*sin(q3)
-m3*q1dot^2*l1*a3*sin(q3+q2)-m3*q1dot*l1*a3*q3dot*sin(q3+q2)-2*m3*q1dot*a3*l2*
    q2dot*sin(q3) +m3*a3*(q1dot*l1*sin(q3+q2)+q1dot*l2*sin(q3)+l2*q2dot*sin(q3))*
    q3dot+x12-b3*q3dot);

f7 = x8;

f8 = -2*wn*x8   - wn^2*x7  + wn^2*(R(1,1)*u1+M(1,2)*u2+R(1,3)*u3+R(1,4)*u4+R(1,5)
    *u5+R(1,6)*u6+R(1,7)*u7);

f9 = x10;

f10 = -2*wn*x10 - wn^2*x9  + wn^2*(R(2,1)*u1+R(2,2)*u2+R(2,3)*u3+R(2,4)*u4+R(2,5)
    *u5+R(2,6)*u6+R(2,7)*u7);

f11 = x12;

f12 = -2*wn*x12 - wn^2*x11 + wn^2*(R(3,1)*u1+R(3,2)*u2+R(3,3)*u3+M(3,4)*u4+R(3,5)
    *u5+R(3,6)*u6+R(3,7)*u7);

f=[f1 ; f2 ; f3 ; f4 ; f5 ; f6 ; f7 ; f8 ; f9 ; f10 ; f11 ; f12];

fid = fopen('matrices2.m','w');

A = jacobian(f,x);
[sm sn] = size(A);
fprintf(fid,'A = zeros(%d,%d);\n',sm,sn);
save 'A' A;
 for i =1:sm
   for j=1:sn
    fprintf('A(%d,%d)=',i,j);
    disp(A(i,j));
    fprintf('\b\b\b;\n');
    fprintf(fid,'A(%d,%d)=%s;\n\n',i,j,char(A(i,j)));
   end
 end

B = jacobian(f,[u1 u2 u3 u4 u5 u6 u7]);
[sm sn] = size(B);
fprintf(fid,'B = zeros(%d,%d);\n\n',sm,sn);
save 'B' B;
 for i=1:sm
  for j=1:sn
    fprintf('B(%d,%d)=',i,j);
    disp(B(i,j));
    fprintf('\b\b\b;\n');
     fprintf(fid,'B(%d,%d)=%s;\n\n',i,j,char(B(i,j)));
```

```
  end
end
```

A.2 Parameters of the finger model used in simulation

Tendon - type (joint)	d	y	r	h	b
EC - extrinsic (wrist)	-	-	14.12	-	-
ECR - extrinsic (wrist)	-	-	-	-11.72	1.14
ECU - extrinsic (wrist)	-	-	-	-8.51	1.55
FDP - extrinsic (MCP)	8.32	8.32	-	-	-
RI - intrinsic (MCP)	-	-	-	-1.29	5.62
UI - intrinsic (MCP)	-	-	-	-8.16	18.76
LU - intrinsic (MCP)	-	-	-	-2.17	12.53
EC (MCP)	-	-	8.3	-	-
FDP (PIP)	5.76	7.5	-	-	-
ES - intrinsic (PIP)	-	-	2.92	-	-
RB - intrinsic (PIP)	-	-	-	-0.47	2.54
UB - intrinsic (PIP)	-	-	-	0.57	1.7

```
m1 = 0.4;          % mass of the metacarpus [kg]
m2 = 0.25;          % mass of the proximal phalangeals [kg]
m3 = 0.2;          % mass of the intermediate + distal phalangeals [kg]
l1 = 0.1;          % length of the metacarpus [m]
l2 = 0.05;          % length of the proximal phalangeal in [m]
l3 = 0.04;          % length of the intermediate + distal phalangeal in [m]
c1 = 0.05;         % distance from wrist joint to the mass centre
                    % of the metacarpal bone in [m]
c2 = 0.025;          % distance from MCP joint to the mass centre
                    % of the proximal phalangeal [m]
c3 = 0.02;          % distance from PIP joint to the mass centre
                    % of the middle + distal phalangeals [m]
b1 = 0.4;           % viscous friction parameter in kg m s^-2
b2 = 0.4;           % viscous friction parameter in kg m s^-2
b3 = 0.4;           % viscous friction parameter in kg m s^-2
k1 = 0.8;           % torsional spring constant in Nm/rad
k2 = 0.8;           % torsional spring constant in Nm/rad
k3 = 0.8;           % torsional spring constant in Nm/rad
theta0_1 = (2/3)*pi;
theta0_2 = pi/2;
theta0_3 = pi/3;
J2 = 1e-4;
J4 = 1e-4;
J6 = 1e-4;
```

The parameters were taken from Brook et al. (1995), Theodorou et al. (2011).

References

H.S. Ahn, Y.Q. Chen, and K.L. Moore. Iterative learning control: brief survey and categorization. *IEEE Transactions on Systems, Man and Cybernetics, Part C*, 37(6):1109–1121, 2007.

H. Aizawa, M. Inase, H Mushiake, K. Shima, and J. Tanji. Reorganization of activity in the supplementary motor area associated with motor learning and functional recovery. *Experimental Brain Research*, 84(3):668–671, 1991.

I. Albrecht, J. Haber, and H. Seidel. Construction and animation of anatomically based human hand models. In *SIGGRAPH Symposium for Computer Animation*, volume 22, pages 98–109. ACM SIGGRAPH, 2003.

K. D. Anderson. Targeting recovery: priorities of the spinal cord-injured population. *Journal of Neurotrauma*, 21:1371–1383, 2004.

N. Angarita-Jaimes, O. P. Dewhirst, D.M. Simpson, Y. Kondoh, R. Allen, and P. A. L. Newland. The dynamics of analogue signalling in local networks controlling limb movement. *The European Journal of Neuroscience*, 36(9):3269–3282, 2012.

S. Arimoto, S. Kawamura, and F. Miyazaki. Bettering operations of robots by learning. *Journal of Robotic Systems*, 1:123–140, 1984a.

S. Arimoto, F. Miyazaki, and S. Kawamura. Bettering operation of dynamical systems by learning: a new control theory for servomechanism or mechatronics systems. In *Proceedings of the 23rd Conference on Decision and Control*, pages 1064–1069, Las Vegas, Nevada, 1984b.

T. J. Armstrong and D. B. Chaffin. An investigation of the relationship between displacements of the finger and wrist joints and the extrinsic finger flexor tendons. *Journal of Biomechanics*, 11(3):119–128, 1978.

L. L. Baker, D. R. McNeal, L. A. Barton, B. R. Bowman, and R. L. Waters. *Neuromuscular electrical stimulation: A practical guide*. Los Amigos Research and Education Institute, 2000.

J. Biggs, K. Horch, and F. J. Clark. Extrinsic muscles of the hand signal fingertip location more precisely than they signal the angles of individual finger joints. *Experimental Brain Research*, 125(3):221–230, 1999.

B. Brewer, S. McDowell, and L. Worthen-Chaudhari. Poststroke Upper Extremity Rehabilitation: A Review of Robotic Systems and Clinical Results. *Topics in Stroke Rehabilitation*, 14(16):22–44, 2007.

B. R. Brewer, R. Klatzky R, and Y. Matsuoka. Visual feedback distortion in a robotic environment for hand rehabilitation. *Brain Research Bulletin*, 75(6):804–813, 2008.

D. Bristow, M. Tharayil, and A. Alleyne. A survey of Iterative Learning Control. *IEEE Control Systems Magazine*, 26(3):96–114, 2006.

J. Broeren, A. Bjorkdahl, and L. Claesson. Virtual rehabilitation after stroke. *Studies in Health Technology and Informatics*, 136:77–82, 2008.

J. Broeren, M. Rydmark, A. Bjorkdahl, and K. S. Sunnerhagen. Assessment and training in a 3-dimensional virtual environment with haptics: a report on 5 cases of motor rehabilitation in the chronic stage after stroke. *Neurorehabilitation and Neural Repair*, 21:180–189, 2007.

N. Brook, J. Mizrahi, M. Shoham, and J. Dayan. A biomechanical model of index finger dynamics. *Medical Engineering & Physics*, 17(1):54–63, 1995.

G. Burdea. Virtual Rehabilitation: Benefits and Challenges. *Schattauer Journal of Methods Information in Medicine*, 42(5):519–523, 2003.

J. Burke, M. McNeill, D. Charles, P. Morrow, J. Crosbie, and S. McDonough. Serious games for upper-limb rehabilitation following stroke. In *1st IEEE International Conference in Games and Virtual Worlds for Serious Applications, VS-GAMES '09, Coventry*, pages 103–111, 2009.

Z. Cai, D. Tong, C. Freeman, and E. Rogers. Application of newton-method based ilc to 3d stroke rehabilitation. In *18th IFAC World Congress*, pages 4851–4856, Milano,Italy, August 28 - September 2 2011.

J. Cauraugh, N. Lodha, S. K. Naik, and J. J. Summers. Bilateral movement training and stroke motor recovery progress: A structured review and meta-analysis. *Hum Mov Sci*, 29(5):853–870, 2010.

E. Y. Chao, J. D. Opgrande, and F. E. Axmear. Three dimensional force analysis of finger joints in selected isometric hand functions. *Journal of Biomechanics*, 9:387–396, 1976.

S. Cobos, R. Aracil, and M. Ferre. Low dimensionality space for controlling human hand models. In *Proceedings of the 2010 3rd IEEE RAS & EMBS, International Conference on Biomedical Robotics and Biomechatronics*, pages 203–208, Tokyo, Japan, 2010a.

S. Cobos, M. Ferre, and R. Aracil. Simplified human hand models based on grasping analysis. In *International Conference on Intelligent Robots and Systems (IROS)*, pages 610–615, 2010b.

S. Cobos, M. Ferre, M. A. Sànchez-Uràn, and J. Ortego. Constraints for realistic hand manipulation. In *The 10th Annual International Workshop on Presence. PRESENCE*, pages 369–370, 2007.

S. Cobos, M. Ferre, S. Uran, J. Ortego, and C. Pena. Efficient Human Hand Kinematics for Manipulation Tasks. In *IEEE/RSJ International Conference on Intelligent Robots and Systems*, pages 2246–2250, 2008.

R. Colombo, F. Pisano, and A. Mazzone. Design strategies to improve patient motivation during robotaided rehabilitation. *Journal of Neuroengineering and Rehabilitation*, 3(4):1196–1207, 2007.

M. R. Cutkosky. On grasp choice, grasp models, and the design of hands for manufacturing tasks. *IEEE Transactions on Robotics and Automation*, 5(3):269–279, 1989.

M.S. Dennis, J. P. Burn, P. A. Sandercock, J. M. Bamford, D. T. Wade, and C. P. Warlow. Long-term survival after first-ever stroke: The oxfordshire community stroke project. *Stroke*, 24:987–993, 1993.

A. D. Deshpande, J. Ko, D. Fox, and Y. Matsuoka. Anatomically correct testbed hand control: muscle and joint control strategies. In *Robotics and Automation,ICRA'09.*, pages 4416–4422, 2009.

J. E. Deutsch, M.Borbely, J. Filler, K. Huhn, and P. Guarrera-Bowlby. Use of a low-cost, commercially available gaming console (wii) for rehabilitation of an adolescent with cerebral palsy. *Physical Therapy*, 10(88):1196–1207, 2008.

P. Le Dinh. FES-based stroke rehabilitation of the hand and wrist using a multi-electrode array, 2012.

K. K. Dou, K. Tan, T. H. Lee, and Z. Zhou. Iterative learning feedback control of human limbs via functional electrical stimulation. *Control Engineering Practice*, 7(3):315–325, 1999.

P. W. Duncan, S. M. Lai, and J. Keighley. Defining post-stroke recovery: implications for design and interpretation of drug trials. *Neuropharmacology*, 39:835–841, 2000.

A. Esteki and J. M Mansour. A dynamic model of the hand with application in functional neuromuscular stimulation. *Annals of Biomedical Engineering*, 25(3):440–451, 1997.

T. Exel, C. T. Freeman, K. Meadmore, M. Kutlu, E. Hallewell, A. M. Hughes, J. H. Burridge, and E. Rogers. Goal orientated stroke rehabilitation utilising electrical stimulation, iterative learning and microsoft kinect. *International Conference on Rehabilitation Robotics 2013, 24 - 26 Jun 2013. Seattle, US*, 2013a.

T. Exel, C. T. Freeman, K. L. Meadmore, A. M. Hughes, E. Hallewell, and J. H. Burridge. Optimisation of hand posture stimulation using an electrode array and iterative learning control. *Journal of Automatic Control*, 21(1):1–5, 2013b.

C. Fabricatore. Gameplay and game mechanics design: a key to quality in videogames. In *OECD-CERI Expert Meeting on Videogames and Education, Santiago de Chile, Chile, 2007*, 2007.

S. Flynn, P. P. Palma, and A. Bender. Feasibility of using the Sony PlayStation 2 gaming platform for an individual poststroke: a case report. *IEEE Control Systems Magazine*, 4(31):180–189, 2007.

C. Freeman, Z. Cai, E. Rogers, and P. Lewin. Iterative Learning Control for Multiple Point-to-Point Tracking Application. *IEEE Transactions on Control Systems Technology*, 19(3):590–600, 2011a.

C. T. Freeman. Constrained point-to-point iterative learning control with experimental verification. *Control Engineering Practice*, 23(2):32–42, 2012.

C. T. Freeman, I. Davies, P. Lewin, and E. Rogers. Iterative learning control of upper limb reaching using functional electrical stimulation. In *the 17th IFAC World Congress*, pages 13444–13449, Seoul, Korea, 2008.

C. T. Freeman, A. M. Hughes, J. Burridge, P. Chappell, P. Lewin, and E. Rogers. Design and control of an upper arm FES workstation for rehabilitation. In *IEEE 11th International Conference on Rehabilitation Robotics (ICORR 2009), Kyoto, Japan*, pages 66–72, 2009a.

C. T. Freeman, A. M. Hughes, J. Burridge, P. Chappell, P. Lewin, and E. Rogers. Iterative learning control of FES applied to the upper extremity for rehabilitation. *Control Engineering Practice*, 26 (3):368–381, 2009b.

C. T. Freeman, E. Rogers, A.-M. Hughes, J. H. Burridge, and K. L. Meadmore. Iterative learning control in healthcare electrical stimulation and robotic-assisted upper limb stroke rehabilitation. *IEEE Control Systems Magazine*, 1(32):18–43, 2012.

C. T. Freeman, Y. Tan, and Z. Cai. Point-to-point iterative learning control with mixed constraints. In *2011 American Control Conference, June 29 - July 1, 2011, San Francisco, California, USA*, 2011b.

K. Fujita, K. Shiga, and H. Takahashi. Learning control of hand posture with neural network in fes for hemiplegics. In *20th Annual International Conference of IEEE Engineering in Medicine and Biology Society*, volume 20, pages 2588–2589, 1998.

A. Gaggioli, F. Morganti, R. Walker, A. Meneghini, M. Alcaniz, J. A. Lozano, J. Montesa, J. A. Gil, and G. Riva. Training with computersupported motor imagery in post-stroke rehabilitation. *Cyberpsychology and Behavior*, 7:327–332, 2004.

K. L. Gao, S. S. Ng, J. W. Kwok, R. T. Chow, and W. W. Tsang. Eye-hand coordination and its relationship with sensori-motor impairments in stroke survivors. *Journal of Rehabilitation Medicine*, 42(4):368–373, 2010.

M. Giroud, A. Jacquin, and Y. Bèjot. The worldwide landscape of stroke in the 21st century. *The Lancet*, 383(9913):195–197, 2014.

R. Hart, K. Kilgore, and P. Hunter. A comparison between control methods for implanted FES hand-grasp systems. *IEEE Transactions on Rehabilitation Engineering*, 6(2):208–218, 1998.

L. Harvey. *Management of Spinal Cord Injuries: A Guide for Physiotherapists.* Elsevier, 2008.

H. Hendricks, M. Ljzerman, J. Kroon, and G. Zilvold. Functional electrical stimulation by means of the ness handmaster orthosis in chronic stroke patients: an exploratory study. *Clinical Rehabilitation*, 15 (2):217–220, 2001.

T. Hill. The heat of shortening and the dynamic constants of muscle. *Proceedings of the Royal Society of London. Series B, Biological Sciences*, 126:135–195, 1938.

M. D. Holden and T. Dyar. Virtual environment training: a new tool for neurorehabilitation. *Journal of Neurologic Physical Therapy*, 26(2):62–71, 2002.

M. K. Holden. Virtual environments for motor rehabilitation: review. *Cyberpsychology and Behavior*, 8 (3):187–211, 2005. discussion 212-219.

M. Huber, B. Rabin, C. Docan, G. Burdea, M.E. Nwosu, M. AbdelBaky, and M.R. Golomb. PlayStation 3-based tele-rehabilitation for children with hemiplegia. In *Virtual Rehabilitation, 2008*, pages 105–112, 2008.

A.-M. Hughes, C. T. Freeman, J. H. Burridge, P. H. Chappel, P. L. Lewin, and E. Rogers. Feasibility of Iterative Learning Control mediated by Functional Electrical Stimulation for reaching after Stroke. *Journal of Neurorehabilitation and Neural Repair*, 6(23):559–568, 2009a.

A. M. Hughes, C. T. Freeman, J. H. Burridge, P. H. Chappell, P. Lewin, and E. Rogers. Feasibility of iterative learning control mediated by functional electrical stimulation for reaching after stroke. *Journal of Neurorehabilitation and Neural Repair*, 23(6):559–568, 2009b.

M. Hund-Georgiadis and D. Y. von Cramon. Motor-learning-related changes in piano players and non-musicians revealed by functional magneticresonance signals. *Experimental Brain Research*, 125(4): 417–425, 1999.

J. N. Ingram, K. P. Körding, I. S. Howard, and D. M. Wolpert. The statistics of natural hand movements. *Experimental Brain Research*, 188(2):223–236, March 2008. ISSN 0014-4819.

X. Jing, D. M. Simpson, R. Allen, and P. L. Newland. Understanding neuronal systems in movement control using wiener/volterra kernels: A dominant feature analysis. *Journal of Neuroscience Methods*, 203:220–232, 2012.

L. Kalra and R. Ratan. Recent advances in stroke rehabilitation. *Stroke*, 38:235–237, 2007.

D. G. Kamper, R. L. Harvey, S. Suresh, and W. Z. Rymer. Relative contributions of neural mechanisms versus muscle mechanics in promoting finger extension deficits following stroke. *Muscle and Nerve*, 28(3):309–318, 2003.

D. G. Kamper and W. Z. Rymer. Impairment of voluntary control of finger motion following stroke: role of inappropriate muscle coactivation. *Muscle and Nerve*, 24(5):673–681, 2001.

E. R. Kandel, J. H. Schwartz, T. M. Jessel, S. Siegelbaum, and A. J. Hudspeth. *Principles of Neural Science*. McGraw-Hill Professional, 2012.

A. Karni, G. Meyer, P. Jezzard, M. M. Adams, R. Turner, and L. G. Ungerleider. Functional mri evidence for adult motor cortex plasticity during motor skill learning. *Nature*, 377(6545):155–158, 1995.

J. Kowalczewski. Upper extremity neurorehabilitation. Doctoral Thesis, Medicine Department of Alberta University, 2009.

H. I. Krebs, L. Dipietro, S. Levy-Tzedek, S. E. Fasoli, A. Rykman-Berland, J. Zipse, J. A. Fawcett, J. Stein, H. Poizner, A. C. Lo, B. T. Volpe, and N. Hogan. A paradigm shift for rehabilitation robotics. therapeutic robots enhance clinician productivity in facilitating patient recovery. *Engineering in Medicine and Biology Magazine, IEEE*, 27(4):61–70, 2008.

J. Landsmeer. Anatomical and functional investigations on the articulation of the human fingers. *Acta Anatomica 24*, 2(25):1–69, 1955.

C. E. Lang, J. R. MacDonald, and C. Gnip. Counting repetitions: an observational study of outpatient therapy for people with hemiparesis post-stroke. *Neurologic Physical Therapy*, 1(31):3–10, 2007.

P. Langhorne, F. Coupar, and A. Pollock. A motor recovery after stroke: a systematic review. *The Lancet Neurology*, 8(8):741–754, 2009.

F. Le, I. Markovsky, C. T. Freeman, and E. Rogers. Identification of electrically stimulated muscle models of stroke patients. *Control Engineering Practice*, 18:396–407, 2010.

T. Lin, D. H. Owens, and J. Hďż″tďż″nen. Newton method based iterative learning control for discrete non-linear systems. *International Journal of Control*, 79(10):1263–1276, 2006a.

T. Lin, D. H. Owens, and J. J. Hďż″tďż″nen. Newton method based iterative learning control for discrete non-linear systems. *International Journal of Control*, 79(10):1263–1276, 2006b.

R. C. V. Loureiro, W. S. Harwin, R. Lamperd, and C. Collin. Evaluation of reach and grasp robot-assisted therapy suggests similar functional recovery patterns on proximal and distal arm segments in sub-acute hemiplegia. *Neural Systems and Rehabilitation Engineering, IEEE Transactions on*, 22 (3):593–602, 2013.

R. C. V. Loureiro, B. Lamperd, C. Collin, and W.S. Harwin. Reach & grasp therapy: Effects of the gentle/g system assessing sub-acute stroke whole-arm rehabilitation. In *Rehabilitation Robotics, 2009. ICORR 2009. IEEE International Conference on*, pages 755–760, 2009.

R. C. V. Loureiro, D. Valentine, B. Lamperd, C. Collin, and W. S. Harwin. Gaming and social interactions in the rehabilitation of brain injuries: A pilot study with the nintendo wii console. *Designing Inclusive Interactions. Springer*, pages 219–228, 2010.

R.C.V. Loureiro, W.S. Harwin, K. Nagai, and M. Johnson. Advances in upper limb stroke rehabilitation: a technology push. *Medical and Biological Engineering and Computing,*, 49:1103–118, 2011.

P. S. Lum, C. G. Burgar, M. Van der Loos, P. C. Shor, M. Majmundar, and R. Yap. The MIME robotic system for upper-limb neuro-rehabilitation: results from a clinical trial in subacute stroke. In *Rehabilitation Robotics, 2005. ICORR 2005. 9th International Conference on*, pages 511–514, 2005.

C. L. Lynch and M. R. Popovic. Functional electrical stimulation. *IEEE Control Systems Magazine*, 28 (2):40–50, 2008.

G. M. Lyons, G. E. Leane, M. Clarke-Moloney, J. V. O'Brien, and P. A. Grace. An investigation of the effect of electrode size and electrode location on comfort during stimulation of the gastrocnemius muscle. *Medical Engineering & Physics*, 10(26):873–878, 2004.

N. Malešević and L. Popović. Classification of muscle twitch response using ann: Application in multi-pad electrode optimization. In *Neural Network Applications in Electrical Engineering (NEUREL), 2010 10th Symposium on*, pages 11–13, 2010.

N. Malešević and L. Popović. Muscle twitch responses for shaping the multi-pad electrode for functional electrical stimulation. *Journal Of Automatic Control*, 20:53–57, 2010.

L. Masia, H. I. Krebs, P. Cappa, and N. Hogan. Whole-arm rehabilitation following stroke: Hand module. In *In Biomedical Robotics and Biomechatronics, 2006. BioRob 2006. The First IEEE/RAS-EMBS International Conference on*, pages 1085–1089, 2006.

K. L. Meadmore, A.-M. Hughes, C. T. Freeman, C. Z. Tong, D. Tong, J. H. Burridge, and E. Rogers. Functional Electrical Stimulation mediated by Iterative Learning Control and 3D robotics reduces motor impairment in chronic stroke. *Journal of Neuroengineering and Rehabilitation*, 9(32), 2012.

A. S. Merians, E. Tunik, and S. V. Adamovich. Virtual reality to maximize function for hand and arm rehabilitation: exploration of neural mechanisms. *Studies in Health Technology and Informatics*, 145: 109–125, 2009a.

A. S. Merians, E. Tunik, and G. G. Fluet. Innovative approaches to the rehabilitation of upper extremity hemiparesis using virtual environments. *European Journal of Physical and Rehabilitation Medicine*, 45(1):123–133, 2009b.

A. Miller, P. Allen, V. Santos, and F. Valero-Cuevas. From robotic hands to human hands: a visualization and simulation engine for grasping research. *Industrial Robot: An International Journal*, 32(1):55–63, 2005. ISSN 0143–991X.

L. J Miltner, W. H. Bauder, M. Sommer, C. Dettmers, E. Taub, and C. Weiller. Motor cortex plasticity during constraint induced movement therapy in stroke patients. *Neuroscience Letters*, 250(1):58, 1998.

D.W. Moran and A.B. Schwartz. Motor cortical representation of speed and direction during reaching. *Journal of Neurophysiology*, 82(5):2676–2692, 1999.

J. R. Napier. The prehensile movements of the human hand. *The Journal of Bone and Joint Surgery*, 38-B(4):902–913, 1956.

T. Nef, M. Mihelj, and R. Riener. Armin: a robot for patient-cooperative arm therapy. *Medical and Biological Engineering and Computing*, 45(9):887–900, 2007.

Y. Nesterov. *Introductory Lectures on Convex Optimization.* Kluwer Academic Publisher, Dordrecht, The Netherlands, 2004.

Y. Nesterov. Gradient methods for minimizing composite functions. *Mathematical Programming*, 140 (1):125–161, 2013.

R. J. Nudo. Adaptive plasticity in motor cortex: Implicationsfor rehabilitation after brain injury. *Rehabilitation Medicine*, (41):7–10, 2003.

R. J. Nudo. Recovery after brain injury: Mechanisms and principles. *Frontiers in Human Neuroscience*, 7(887), 2013.

S. B. O'Dwyer, D. T. O'Keeffe, S. Coote, and G. M. Lyons. An electrode configuration technique using an electrode matrix arrangement for fes-based upper arm rehabilitation systems. *Medical Engineering & Physics*, 28:166–176, 2006.

S. B. O'Dwyer, D. T. O'Keeffe, S. Coote, and G. M. Lyons. An electrode configuration technique using an electrode matrix arrangement for FES-based upper arm rehabilitation systems. *Medical Engineering & Physics*, 28(2):166–176, 2006.

J. M. Ortega and W. C. Rheinboldt. *Iterative Solution Of Nonlinear EquationsIn Several Variables*. Academic Press, New York, 1 edition, 1970.

L. Piron, T. Paolo, F. Piccione, V. Laia, E. Trivello, and M. Dam. Virtual environment training therapy for arm motor rehabilitation. *Presence*, 14:732–740, 2005.

E. P. Pitarch. *Virtual Human Hand: Grasping Strategy and Simulation*. PhD thesis, Universitat Politècnica de Catalunya (UPC), 2007.

V. M. Pomeroy, L. M. King, A. Pollock, A. Baily-Hallam, and P. Langhorne. Electrostimulation for promoting recovery of movement or functional ability after stroke: a review. *Cochrane Database of Systematic Reviews*, 2006.

D. Popovic. Clinical evaluation of the bionic glove. *Archives of Physical Medicine & Rehabilitation*, 80: 299–304, 1999.

D. B. Popovìc and M. B. Popovìc. Automatic determination of the optimal shape of a surface electrode: Selective stimulation. *Journal of Neuroscience Methods*, 178(1):174–181, 2009.

A. Prochazka. The bionic glove: an electrical stimulator garment that provides controlled grasp and hand opening in quadriplegia. *Archives of Physical Medicine & Rehabilitation*, 78(6):608–614, 1997.

P. Raghavan. The nature of hand motor impairments after stroke and its treatment. *Current Treatment Options in Cardiovascular Medicine*, 9(3):221–228, 2007.

R. Riener, T. Nef, , and G. Colombo. Robot-aided neurorehabilitation of the upper extremities. *Medical and Biological Engineering and Computing*, 43(1):2–10, 2005.

I. Roloff, V. R. Schoffl, L. Vigouroux, and F. Quaine. Biomechanical model for the determination of the forces acting on the finger pulley system. *Journal of Biomechanics*, 39:915–923, 2006.

F. D. Rose, B. M. Brooks, and A. A. Rizzo. Virtual reality in brain damage rehabilitation: review. *Cyberpsychology and Behavior*, 8:241–262, 2005.

P. M. Rossini, C. Calautti, F. Pauri, and J.-C. Baron. Post-stroke plastic reorganisation in the adult brain. *Lancet Neurology*, 2(8):493–502, 2003.

D. N. Rushton. Functional electrical stimulation and rehabilitation: an hypothesis. *Medical Engineering & Physics*, 25(1):75–78, 2003.

R. J. Sanchez, J. Liu, S. Rao, P. Shah, R. Smith, T. Rahman, S.C. Cramer, J.E. Bobrow, and D. J. Reinkensmeyer. Automating arm movement training following severe stroke: Functional exercises with quantitative feedback in a gravity-reduced environment. *IEEE Transactions on Neural Systems and Rehabilitation Engineering,*, 14(3):378–389, 2006.

J. L. Sancho-Bru, A. Perez-Gonzalez, M. Vergara-Monedero, and D. Giurintano. A 3-D dynamic model of human finger for studying free movements. *Journal of Biomechanics*, 34(11):1491–1500, 2001.

G. Saposnik and M. Levin. Virtual reality in stroke rehabilitation: a meta-analysis and implications for clinicians. *Stroke*, 42(5):1380–1386, 2011.

O. Schill, R. Rupp, C. Pylatiuk, S. Schulz, and M. Reischl. Automatic adaptation of a self-adhesive multi-electrode array for active wrist joint stabilization in tetraplegic sci individuals. In *Science and Technology for Humanity (TIC-STH), 2009 IEEE Toronto International Conference*, pages 708–713, 2009.

G. Schlesinger. *Der mechanische Aufbau der künstlichen Glieder*. Springer Berlin Heidelberg, 1919.

L. H. Sekhon and M. G. Feblings. Epidemiology, demographics and patophysiology of acute spinal cord injury. *Spine*, 26:2–12, 2001.

M. Selzer, S. Clarke, P. Duncan, and F. Gage. *Textbook of Neural Repair and Rehabilitation*. Cambridge University Press, Cambridge, UK, 2006.

A. B. Sghaier, L. Romdhane, F. B. Ouezdou, and F. Vèlizy. Biomechanical analysis of the normal and reconstructed human hand: Prediction of muscle forces in pinch and grasp. In *12th IFToMM World Congress*, 2007.

D. K. Shin, Z. Gurdal, and O. H. Griffin Jr. A penalty approach for nonlinear optimization with discrete design variables. *Engineering Optimization*, 16:29–42, 1990.

G. J. Snoek, H. J. Hermens, D. Maxwell, and F. Biering-Sorensen. Survey of the needs of patients with spinal cord injury: impact and priority for improvement in hand function in tetraplegics. *Spinal Cord*, 42:526–532, 2004.

American Society for Surgery of The Hand. *The Hand: Examination and Diagnosis*. Churchill Livingstone, 3 edition, 1990.

M. W. Spong and M. Vidyasagar. *Robot Dynamics and Control*. John Wiley and Sons, New York, 1989. 1st edition.

S. Sueda, A. Kaufman, and D. K. Pai. Musculotendon simulation for hand animation. In *ACM SIGGRAPH 2008 papers*, pages 1–8, 2008.

T. Szturm, J. F. Peters, and C. Otto. Task-specific rehabilitation of finger-hand function using interactive computer gaming. *Archives of Physical Medicine and Rehabilitation*, 89(11):2213–2217, 2008.

R. Tabak and P. Plummer-D'Amato. Bilateral movement therapy post-stroke: underlying mechanisms and review. *International Journal of Therapy and Rehabilitation*, 17(1):15–23, 2010.

E. Taub. Overcoming learned nonuse: a new behavioral medicine approach to physical medicine. *Clinical Applied Psychophysiology*, pages 185–220, 1994.

E. Taub, J. E. Crago, and G. Uswatte. Constraint-induced movement therapy: A new approach to treatment in physical rehabilitation. *Rehabilitation Psychology*, 43(2):152–170, 1998.

E. Taub and G. Uswatte. *Constraint-induced movement therapy: A paradigm for translating advances in behavioral neuroscience into rehabilitation treatments; Handbook of neuroscience for the behavioral sciences*, volume 2. Wiley, 2009.

P. Taylor, J. Esnouf, and J. Hobby. The functional impact of the freehand system on tetraplegic hand function, clinical results. *International Spinal Cord Society*, 40:560–566, 2002.

E. Theodorou, E. Todorov, and F. J. Valero-Cuevas. Neuromuscular stochastic optimal control of a tendon driven index finger model. In *American Control Conference*, pages 348–355, 2011.

G.J. Tortora and B. Derrickson. *Principles of Anatomy and Physiology*. John Wiley & Sons, 2007.

W. Tsang, K. Singh, and E. Fiume. Helping hand: an anatomically accurate inverse dynamics solution for unconstrained hand motion. In *Proceedings of the 2005 ACM SIGGRAPH/Eurographics symposium on Computer animation*, pages 319–328, 2005.

R. Tubiana, J.-M. Thomine, and E. Mackin. *Examination of the hand and wrist*. Martin Dunitz Ltd. The Livery House, 2 edition, 1996.

F. J. Valero-Cuevas. A mathematical approach to the mechanical capabilities of limbs and fingers. *Advances in Experimental Medicine & Biology*, 629:619–633, 2009.

F. J. Valero-Cuevas, V. V. Anand, A. Saxena, and H. Lipson. Beyond parameter estimation: Extending biomechanical modeling by the explicit exploration of model topology. *IEEE Transactions on Biomedical Engineering*, 54(11):1951–1964, nov 2007.

F. J. Valero-Cuevas, M. E. Johanson, and J. D. Towles and towards a realistic biomechanical model of the thumb: The choice of kinematic description is more critical than the solution method or the variability/uncertainty of musculoskeletal parameters. *Journal of Biomechanics*, 36(7):1019–1030, 2003.

L. Vandenberghe. Convex optimization techniques in System Identification. *Proceedings in IFAC Symposium on System Identification*, 16:71–76, 2012.

L. Vigouroux, F. Quaine, A. Labarre-Vila, and F. Moutet. Estimation of finger muscle tendon tensions and pulley forces during specific sport-climbing grip techniques. *Journal of Biomechanics*, 39(14): 2583–2592, 2006.

M. L. De Vivo, I. S. Richards, S. L. Stover, and B. K Go. Spinal cord injury. rehabilitation adds life to years. *The Western Journal of Medicine*, 154(5):602–606, 1991.

Y. Wang, F. Gao, and F.J. Doyle. Survey on Iterative Learning Control, Repetitive Control, and Run-to-Run Control. *Journal of Process Control*, 19(10):1589–1600, 2009.

T. Watanabe. A method of multichannel pid control of two-degree-of-freedom wrist joint movements by functional electrical stimulation. *Systems and Computers in Japan*, 34(5):25–36, 2003.

A. J. Westerveld, A. C. Schouten, P. H. Veltink, and H. van der Kooij. Selectivity and resolution of surface electrical stimulation for grasp and release. *IEEE Transaction on Neural Systems & Rehabilitation Engineering*, 20(1):94–101, 2012.

D. L. Wilson, Q. Zhu, J. L. Duerk, J. M Mansour, K. Kilgore, and P. E. Crago. Estimation of tendon moment arms from three-dimensional magnetic resonance images. *Annals of Biomedical Engineering*, 27(2):247–256, 1999.

G.F. Wittenberg. Experience, cortical remapping, and recovery in brain disease. *Neurobiological Disorders*, 37(2):252–258, 2010.

S. Wood, N. Murillo, and P. Bach y Rita. Motivating, game-based stroke rehabilitation: a brief report. *Topics in Stroke Rehabilitation*, 10(2):134–140, 2003.

D. Yin, Y. Luo, F. Song, D. Xu, B.S. Peterson, L. Sun, W. Men, X. Yan, and M. Fan. Functional reorganization associated with outcome in hand function after stroke revealed by regional homogeneity,. *Neuroradiology*, 2013.

J. Z. Zheng, S. De La Rosa, and A. M. Dollar. An investigation of grasp type and frequency in daily household and machine shop tasks. In *2011 IEEE International Conference on Robotics and Automation Shanghai International Conference Center*, 2011.